1961

Transport Phenomena in a Single Crystal of Bismuth at Liquid Helium Temperatures.

Jimmy Ray Sybert
Louisiana State University and Agricultural & Mechanical College

TRANSPORT PHENOMENA IN A SINGLE CRYSTAL OF BISMUTH AT LIQUID HELIUM TEMPERATURES

A Dissertation

Submitted to the Graduate Faculty of the
Louisiana State University and
Agricultural and Mechanical College
in partial fulfillment of the
requirements for the degree of
Doctor of Philosophy

in

The Department of Physics and Astronomy

by
Jimmy R. Sybert
M.A., North Texas State College, 1956

ACKNOWLEDGMENT

The author wishes to express his profound gratitude to Prof. Claude G. Grenier for his constant guidance, advice and assistance throughout the course of this study. He is also indebted to Prof. J. M. Reynolds for his supervision, advice, and assistance in the various facets of the problem. He wishes to thank Mr. G. N. Rao for his assistance in the crystal growing and taking some of the measurements, and Dr. N. H. Zebouni for enlightening discussions and assistance in making the measurements. He is very grateful to all the members of the low temperature group for their various contributions which have made this work possible.

He is also indebted to the Southern Fellowships Fund and the National Science Foundation for fellowships granted.

TABLE OF CONTENTS

Page

LIST OF TABLES

LIST OF FIGURES

Figure | Page

ABSTRACT

Galvanomagnetic and thermomagnetic potentials have been measured on a single crystal of bismuth in magnetic fields ranging from zero to sixteen kilogauss as a means of studying the energy band structure of bismuth. The potentials measured were a) the magnetoresistance and Hall effect, and b) the corresponding potentials with a heat current substituted for the electric current (thermoelectric power and Nernst-Ettingshausen effect respectively). Also, measurements were made of the thermal conductivity of the bismuth. No transverse thermal effect (Righi-Leduc effect) was detected in the temperature range of 2.1°K to 4.3°K investigated. The other magnetic field dependent transport effects, the Peltier effect and Ettingshausen effect, were not measured directly but may be calculated from the measured quantities by the Onsager reciprocity theorem.

A study of the oscillations observed in the galvanomagnetic potentials for different orientations of the magnetic field has led to the mapping of a high mobility hole band. This pocket has the form (in momentum space) of an ellipsoid of revolution with the major axis oriented along the trigonal axis of the crystal. The ratio of major to minor axis is $3.\bar{6}$. An analysis of the electrical conductivity data, with emphasis on the Hall conductivity, by the quasi-classical Sondheimer-Wilson theory has indicated that there are energy bands in bismuth besides the previously discovered high

mobility electron band(s) and the hole ellipsoid band mentioned above. In particular, the presence of a low mobility hole band, with effective mass in the neighborhood of the free electron mass m_o, has been discovered. Measurements of the oscillatory effects at high magnetic fields have substantuated the existence of this low mobility hole band.

Measurements of the oscillatory effects are in general agreement with the theory of Lifshitz and Kosevich for oscillations in the electrical conductivities. The Lifshitz-Kosevich theory, when modified with the quasi-classical expressions for the thermomagnetic effects at high magnetic fields, agrees in some respects (such as the phase of the oscillations) with the experimental data. However, it fails to predict the temperature dependence of the effects, and agrees with the size of the effects only in order of magnitude.

The thermal conductivity measurements have demonstrated that less than one per cent of the heat current is carried by the electrons.

CHAPTER I

INTRODUCTION

The Transport Effects

The study of transport in a system concerns the problem of rates of real physical processes. A treatment of such phenomena necessarily falls into the realm of irreversible thermodynamics. In other words, the transport processes we wish to consider are such that they cannot be thought of as quasi-static processes which must occur extremely slowly. The quasi-static processes are the only processes which can be treated in terms of equilibrium thermodynamics. We will not attempt a general discussion of the irreversible thermodynamics and statistical mechanics, but detail will be given to certain of the results which are applicable to the transport processes in a metal.

Processes in irreversible thermodynamics are described in terms of a "force" parameter which drives the process and an additional parameter to describe the response to this force. The "driving force" for the process is referred to as the affinity, and the response parameter is called the flux. In many practical cases--including the one we wish to consider--the processes do not deviate radically from equilibrium, and the relation between the affinities

and fluxes can be represented by a simple linear relationship. This very good approximation is written

$$J_k = \sum_j L_{jk} F_j \qquad (1)$$

where the affinities are given by the F_j, J_k is the flux, and the L_{jk} are the linear factors relating the different affinities and their fractional contribution to the total flux. The L_{jk} are called kinetic coefficients and are functions of the local intensive parameters. An additional assumption is that at a given instant, the fluxes depend only on the values of the affinities at that instant. A process having the properties we have described is formally called a linear Markoff process. These processes are carefully considered in the text by Callen.[1]

Although we will not attempt to give the exact mathematical formulation for the affinities F_j, we will investigate the physical quantities which give rise to them. With these quantities available we will be able to write Eq. (1) for the case at hand, without explicitly identifying the F_j and the L_{jk}. The exact identity of these two quantities is necessary, however, for the case we will present; they can be found in the text by Callen. We will draw freely from the results of Callen when they are needed in the description of these effects.

In the transport processes in a crystal, the fluxes are a) the electric current density J, and b) the heat current density w. The

---

[1] Callen, H. B., Thermodynamics, John Wiley and Sons, Inc., New York, 1960.

affinities are due to the temperature gradient (we use the negative of the gradient $G = -\nabla T$) and the electric field E. Actually there is another field due to the chemical potential of the electrons. For convenience this is combined with the electric field due to the electrostatic potential and the resulting field is written

$$E^* = E - \frac{1}{e}\frac{\partial \xi}{\partial x} \tag{2}$$

where e is the electronic charge, x is the space variable, and ξ is the chemical potential. A term involving the chemical potential also contributes to the heat current density w, so for convenience we incorporate this term in a manner similar to that expressed by Eq. (2) and use a modified heat current w^*.[2] Then, w^* is the total energy current less that part of the heat current which is due to the electrochemical potential Λ.

$$\Lambda = \xi + e\phi \tag{3}$$

where ϕ is the electrostatic potential. This gives for the modified electric field

$$E^* = -\frac{1}{e}\frac{\partial \Lambda}{\partial x} \quad . \tag{4}$$

Since the flux w is given by

$$w = u - \phi J \tag{5}$$

where u is the total energy current, the modified form of the heat flux which we shall use in further discussion is

$$w^* = u - \frac{\Lambda}{e} J = w - \frac{\xi}{e} J. \tag{6}$$

---

[2] H. B. Callen, Phys. Rev. 85, 16 (1952).

In view of the linear relationship between fluxes and affinities, we can now write the dynamical equations which apply to a two-dimensional transport problem.

$$\begin{aligned} J_1 &= \sigma_{11}E^*_1 + \sigma_{12}E^*_2 - \epsilon''_{11}G_1 - \epsilon''_{12}G_2 \\ J_2 &= \sigma_{21}E^*_1 + \sigma_{22}E^*_2 - \epsilon''_{21}G_1 - \epsilon''_{22}G_2 \\ w^*_1 &= -\pi''_{11}E^*_1 - \pi''_{12}E^*_2 + \lambda''_{11}G_1 + \lambda''_{12}G_2 \\ w^*_2 &= -\pi''_{21}E^*_1 - \pi''_{22}E^*_2 + \lambda''_{21}G_1 + \lambda''_{22}G_2 \end{aligned} \tag{7a}$$

The Eq. (7a) applies to effects which occur when electric and heat currents are permitted to flow in a plane perpendicular to an applied magnetic field, as is the case we will consider experimentally. For convenience we write Eq. (7a) in the matrix notation

$$\begin{aligned} \vec{J} &= \hat{\sigma}\vec{E}^* - \hat{\epsilon}''\vec{G} \\ \vec{w}^* &= -\hat{\pi}''\vec{E}^* + \hat{\lambda}''\vec{G} \end{aligned} \tag{7b}$$

From the thermodynamics which apply in the discussion of the processes under consideration, it is important to call attention to a theorem which expresses a certain symmetry in the response of two simultaneously occurring processes. This is the Onsager reciprocity theorem. It states a symmetry between the linear effect of the j^{th} affinity on the k^{th} flux and the linear effect of the k^{th} affinity on the j^{th} flux, when these effects are measured in opposite magnetic fields. Specifically, Onsager has demonstrated that the value of the kinetic coefficient L_{jk} measured in a magnetic field H is identical to the kinetic coefficient L_{kj} measured in the reversed magnetic field -H; that is,

$$L_{jk}(H) = L_{kj}(-H). \tag{8}$$

In order to apply this powerful theorem to the case at hand one must a) determine the exact relation between the coefficients $\hat{\sigma}$, $\hat{\epsilon}''$, $\hat{\pi}''$ and $\hat{\lambda}''$ and the kinetic coefficients, and b) take note of certain symmetry relations which exist between the $\hat{\sigma}$, $\hat{\epsilon}''$, $\hat{\pi}''$ and $\hat{\lambda}''$: For the case of the magnetic field parallel to the 3-axis, Onsager[3] has shown that physical isotropy exists in the 1-2 plane if the symmetry of the crystal about the 3-axis is 3-, 4- or 6-fold and the fluxes and affinities are confined to the 1-2 plane. Notice that we have adopted the convention of referring to the axis attached to the crystal with the numbers 1, 2, and 3. The letters x, y, and z will be used to designate directions in space (see Fig. 1). We now take the case of a crystal with a 3-fold axis of symmetry (bismuth), where the crystal is in the form of a thin plate with the 3-fold symmetry axis (the 3-axis) perpendicular to the face of the plate. Then the tensor of coefficients will be 2 x 2 and of the form

$$\hat{a} = \begin{vmatrix} a_{11} & a_{12} \\ a_{21} & a_{22} \end{vmatrix} \tag{9}$$

where $\hat{a}$ is to be replaced by $\hat{\sigma}$, $\hat{\epsilon}''$, $\hat{\pi}''$ or $\hat{\lambda}''$. The isotropy in the plane gives the relation

$$\begin{aligned} a_{21} &= -a_{12} \\ a_{11} &= a_{22}. \end{aligned} \tag{10}$$

A consideration of these coefficients in the magnetic field yields

---

[3] L. Onsager, Phys. Rev. 37, 405 (1931); 38, 2265 (1931).

the result that the diagonal terms are even functions of the field H, and the off-diagonal terms are odd functions of the field H. These symmetry relations, together with the proper identification of the affinities, yield Onsager's relations between the coefficients. We state them without further proof:

$$\begin{aligned} T\epsilon'_{11}(H) &= \pi'_{11}(H) \\ T\epsilon'_{12}(H) &= \pi'_{12}(H) \end{aligned} \tag{11}$$

or, more simply in tensor notation,

$$T\hat{\epsilon}' = \hat{\pi}' \tag{12}$$

It has been shown[4] that the algebra involved in analysis is greatly simplified if the dynamical equations (Eq. 7) are written such that the electric current $\vec{J}$ and the temperature gradient $\vec{G}$ appear on the right hand side of the equations as independent variables. Thus, the representation

$$\begin{aligned} \vec{E}^* &= \hat{\rho}\vec{J} + \hat{\epsilon}\vec{G} \\ \vec{W}^* &= -\hat{\pi}\vec{J} + \hat{\lambda}\vec{G} \end{aligned} \tag{13}$$

is often used. From the viewpoint of the experimentalist, a third representation is desired, where the experimentally controllable quantities, $\vec{J}$ and $\vec{W}^*$, are the independent variables. This representation is

$$\begin{aligned} \vec{E}^* &= \hat{\rho}'\vec{J} + \hat{\epsilon}'\vec{W}^* \\ \vec{G} &= \hat{\pi}'\vec{J} + \hat{\gamma}\vec{W}^*. \end{aligned} \tag{14}$$

---

[4] P. Mazur and I. Prigogine. J. Phys. Radium 12, 612 (1951).

The coefficients in $\hat{\rho}$, $\hat{\epsilon}'$, $\hat{\pi}'$, and $\hat{\gamma}$ are those which are measured directly in the laboratory. The relations between these "measurable quantities" and the coefficients in the other representations can be found quite easily. We demonstrate the method and at the same time give the names applying to the different effects: Consider first the isothermal galvanomagnetic effects. With $\vec{G} = 0$, Eq. (13) gives

$$\vec{E}^* = \hat{\rho}\vec{J}. \tag{15}$$

If we further impose the condition $J_x = J$, $J_y = 0$, the coefficient

$$\rho_{11} = E_x/J_x \tag{16}$$

is called the magnetoresistivity, and

$$\rho_{21} = E_y/J_x \tag{17}$$

is the Hall resistivity. With zero heat current ($\vec{W}^* = 0$), Eq. (14) gives

$$\vec{G} = \hat{\pi}'\vec{J}. \tag{18}$$

In the case $J_x = J$, $J_y = 0$, we have

$$\pi'_{11} = G_x/J_x \tag{19}$$

where π'_{11} is the Peltier coefficient and

$$\pi'_{21} = G_y/J_x \tag{20}$$

where π'_{21} is the Ettingshausen coefficient. These are the four basic galvanomagnetic effects. For the thermomagnetic effects, take $\vec{J} = 0$, and restrict the heat current $\vec{W}^*$ to the x-direction. Then Eq. (14) gives

$$\vec{G} = \hat{\gamma}\vec{W}^* \tag{21}$$

where the coefficient

$$\gamma_{11} = G_x/w^*_x \tag{22}$$

is the thermal magnetoresistivity, and the coefficient

$$\gamma_{21} = G_y/w^*_x \tag{23}$$

is the Righi-Leduc coefficient (resistivity). Finally, with $\vec{J} = 0$, and $\vec{w}^*$ directed along the x-axis, Eq. (14) gives

$$\vec{E}^* = \hat{\epsilon}'\vec{w}^* \tag{24}$$

where

$$\epsilon'_{11} = E_x/w^*_x \tag{25}$$

is the thermoelectric coefficient and

$$\epsilon'_{21} = E_y/w^*_x \tag{26}$$

is the Nernst-Ettingshausen coefficient. Thus there are eight basic effects involved in the transport processes we are considering.

These algebraic processes in which we have indulged can be continued to show the relationship between the various coefficients we have defined in Eqs. (7), (13), and (14). The more important ones are given at this point for future reference:

$$\begin{aligned}
&\hat{\epsilon}'' = \hat{\sigma}\hat{\lambda}\hat{\epsilon}' = \hat{\sigma}\hat{\epsilon} \\
&\hat{\pi}'' = \hat{\sigma}\hat{\lambda}\hat{\pi}' = \hat{\sigma}\hat{\pi} \\
&\hat{\gamma} = 1/\hat{\lambda} = \hat{\lambda}^{-1} \\
&\hat{\sigma} = 1/\hat{\rho} = \hat{\rho}^{-1} \\
&\hat{\pi}''\hat{\rho}' = \hat{\pi}'\hat{\lambda}'' \\
&\hat{\rho}' = \hat{\rho} + \hat{\epsilon}\hat{\pi}\hat{\lambda}^{-1}
\end{aligned} \tag{27}$$

It can be shown that each of these quantities has the properties given by Eqs. (9) and (10).

The basic transport effects previously outlined will be the basis of this experimental study. An analysis of the experimental findings will be presented in Chapter IV.

The Oscillatory Phenomena

The galvanomagnetic effects can be used quite effectively as a tool for studying the energy structure of the electrons in metals such as bismuth.[5] These effects are characterized by a periodic dependence of the Hall effect and magnetoresistance in metal single crystals upon reciprocal magnetic field at low temperatures. The oscillatory phenomena was first observed in bismuth by Shubnikov and de Haas[6] in 1930. Similar oscillations in the magnetic susceptibility were discovered by de Haas and van Alphen[7] shortly thereafter. Both effects have subsequently been observed in other substances. The explanation of the behavior of the susceptibility was provided by Landau[8] and Peierls[9] in their papers on the quantum theory of electrons in solids in the presence of external magnetic fields. The theory is not so well established for the galvanomagnetic effects as for the de Haas-van Alphen effect. However, detailed analyses have appeared in the last few years from several investigators[10] including important contributions

---

[5] J. M. Reynolds, H. W. Hemstreet, T. E. Leinhardt, and D. D. Triantos, Phys. Rev. 96, 1203 (1954).

[6] L. Shubnikov and W. J. de Haas, Leiden Comm. 207a, 207c, 207d, 210a (1930).

[7] W. J. de Haas and P. M. van Alphen, Leiden Comm. 208d, 212a (1930).

[8] L. D. Landau, Z. Physik 64, 629 (1930).

[9] R. Peierls, Z. Physik 80, 763 (1933).

[10] A. H. Kahn and H. P. R. Frederikse, Solid State Physics 9, 258 (1959).

of Zil'berman[11] and Lifshitz and Kosevich.[12] Briefly, it is known that for electrons in magnetic fields the energy levels coalesce into quantized levels of field dependent spacing and degeneracy. As the field is varied, the electrons redistribute among these levels in such a way as to give rise to the oscillations. For an understanding of the conductivity processes in which we are most interested at this point, one must be able to explain the scattering mechanisms and their magnetic field dependence. In Chapter IV, experimental results for the oscillatory components of the conductivity tensor will be compared with the theory of Lifshitz and Kosevich.

The anisotropy of the periodic electric field of the crystalline lattice can be taken into account by considering the carriers (electrons or holes) to have anisotropic effective masses. The Fermi surface for a group of carriers is then no longer spherical as would be expected for free electrons, but instead has a topology determined by the interaction of the electrons with the lattice in each direction in space. In bismuth, as in many cases, surfaces of constant energy in momentum space may be approximated by a quadratic dependence on momentum p, i.e., ellipsoids. These approximately ellipsoidal pockets of electrons (or holes) exist where the Fermi surface overlaps (or underlaps) Brillouin zone boundaries. An extensive experimental study of the Fermi surface of bismuth has been done by Schoenberg[13]

---

[11] G. E. Zil'berman, Soviet Physics JETP 2, 650 (1956).

[12] I. M. Lifshitz and L. M. Kosevich, Soviet Physics JETP 6, 67 (1958).

[13] D. Schoenberg, Phil. Trans. A 245, 1 (1952).

by measurements on the oscillations in the magnetic susceptibility at low temperatures. His experiments have established that the portion of the Fermi surface he was able to measure can be represented in momentum space by the superposition of three ellipsoids. These are ellipsoids of electrons, with each ellipsoid having its major axis oriented approximately along one of the three binary axes of the crystal. Since Schoenberg's experiments, proposals of models of the band structure have been made by Jones,[14] Blackman,[15] Heine[16] and others. The physical properties of bismuth indicate that in this metal there is a small overlap of the conduction band and valence band, and that electrical conductivity is due to a small number of electrons at the bottom of the conduction band and an equal number of holes at the top of the valence band. The models are consistent with these properties. The galvanomagnetic effects, then, are determined by the detailed structure of the bottom of the conduction band and the top of the valence band. The model for the energy surfaces which is most generally accepted has the following characteristics: The Fermi surface for electrons consists of three sets of two ellipsoids each (after Schoenberg). The three sets are interrelated by 120° rotations around the z-axis (the 3-axis). The doubling of each set arises from inversion symmetry. One of the

---

[14] H. Jones, Proc. Roy. Soc. A147, 369 (1934); A155, 653 (1936).

[15] M. Blackman, Proc. Roy. Soc. A166, 1 (1936).

[16] V. Heine, Proc. Phys. Soc. A69, 513 (1956).

principal axes of each ellipsoid is parallel to a binary axis. The particular set of ellipsoids with principal axis along the x-axis is given by

$$2m_o\zeta^e = \alpha_{11}p_x^2 + \alpha_{22}p_y^2 + \alpha_{33}p_z^2 + 2\alpha_{23}p_yp_z \tag{28}$$

where $\vec{p} = \hbar\vec{k}$ and $\vec{k}$ is measured with respect to the center of the ellipse. The Fermi energy of the electrons is ζ^e, m_o is the mass of a free electron, and the α_{ij} are the components of the reciprocal mass tensor in units of $1/m_o$. The Fermi surface for the holes consists of two ellipsoids of revolution centered on the z-axis and described by

$$2m_o\zeta^H = \beta_{11}(p_x^2 + p_y^2) + \beta_{33}p_z^2 \tag{29}$$

where ζ^H is the Fermi energy of the holes, and the β_{ij} are the components of the reciprocal mass tensor. Again $\vec{p} = \hbar\vec{k}$ with $\vec{k}$ measured from the center of the hole ellipsoid.

The areas of intersection of the ellipsoids (in momentum space) with a plane perpendicular to the magnetic field have been related to the periods of oscillation of the galvanomagnetic effects by Lifshitz and Kosevich.[17] They have demonstrated that the periodicity of the oscillations in the conductivity and resistivity tensor elements is identical to that of the oscillations in the magnetic susceptibility. Specifically, the period is given by

$$\Delta\left(\frac{1}{H}\right) = \frac{eh}{cS_m(\zeta_o)} \tag{30}$$

where $S_m(\zeta_o)$ is the extremal area of intersection of the Fermi

---

[17] I. M. Lifshitz and L. M. Kosevich, op. cit.

ellipsoid with a plane perpendicular to the magnetic field H. A different frequency of oscillation is superimposed on the gross effect for each different ellipsoid seen by the field. In this same treatment of the "Shubnikov-de Haas effect," Lifshitz and Kosevich have arrived at an expression for the amplitude of the oscillations. We will make mention of their theory in relation to the experimental results in Chapter IV.

The ellipsoid of holes has not previously been observed with galvanomagnetic measurements, although measurements of Abeles and Meiboom[18] have given an indication of its asymmetry. However, certain other types of measurements have yielded information concerning this "pocket" of holes. These approaches to the problem include measurements from cycletron resonance,[19] anamolous skin effect,[20] ultrasonic attenuation,[21] and some recent measurements of the de Haas-van Alphen effect at extremely low temperatures.[22] A comparison of the results of various techniques will be given in tabular form in Chapter IV.

In 1954, Reynolds, et al.[23] measured the oscillatory Hall effect in a single crystal of bismuth at liquid helium temperatures. An

---

[18] B. Abeles and S. Meiboom, Phys. Rev. 101, 544 (1956).

[19] J. K. Galt, W. A. Yager, F. R. Merritt, B. B. Celtin, and A. D. Brailsford, Phys. Rev. 114, 1396 (1959).

[20] George E. Smith, Phys. Rev. 115, 1561 (1959).

[21] Darrell H. Reneker, Phys. Rev. 115, 303 (1959).

[22] N. B. Brandt, JETP (U.S.S.R.) 38, 1355 (1960).

[23] J. M. Reynolds, H. W. Hemstreet, T. E. Leinhardt, and D. D. Triantos, op. cit.

analysis of their data for the magnetic field oriented along the trigonal axis of the crystal showed a marked deviation from the results of Schoenberg. At that time, the galvanomagnetic theory was in such preliminary form it was thought that perhaps the descrepancy might stem from inadequacies in the theory. It has since come to mind that the ellipsoids of holes are mainly responsible for these low temperature oscillations, and that the measurements of Reynolds, et al., were on the hole ellipsoid and not the electron ellipsoids of Schoenberg. Therefore, at the suggestion of Prof. Reynolds, an orientation study of the galvanomagnetic effects in bismuth was initiated to map the Fermi surface and determine the parameters of the hole ellipsoid. The results of these measurements will be described in Chapter IV.

The theory of the oscillatory thermoelectric effects is not at all well established, although some insight into the problem of the longitudinal effect (thermoelectric power) is given by Zil'berman.[24] No quantum theory of the transverse effect (Nernst-Ettingshausen effect) has been given. However, the classical asymptotic considerations of these phenomena by Bychkov, Gurevich, and Nedlin[25] can be used to compare with experimental results. In light of these theories, an attempt will be made in Chapter IV to examine the amplitude, magnetic field, and temperature dependence of the experimental data for these

---

[24] Zil'berman, op.cit.

[25] Yu. A. Bychkov, L. E. Gurevich, and G. M. Nedlin, Soviet Physics JETP 37, 377 (1960).

effects. In addition, a comparison of the oscillatory components of the longitudinal conductivity and thermoelectric effect (we use the notation $\tilde{\sigma}_{11}$ and $\tilde{\epsilon}'_{11}$) will be made through the work of Zil'berman. The corresponding transverse quantities, $\tilde{\sigma}_{12}$ and $\tilde{\epsilon}'_{12}$, can be exmained using the theories of Bychkov, et al., and Lifshitz and Kosevich.[26]

The Sondheimer-Wilson Theory

A simpler, quasi-classical consideration of the galvanomagnetic effects has been given by Sondheimer and Wilson.[27] For a single band, the σ_{12} tensor element is given by

$$\sigma_{12} = \frac{e^2}{3\pi^2\hbar^4}(2m_1)^{3/2}\alpha \int_0^\infty \frac{E^{3/2}}{\alpha^2+(\frac{m_1}{\hbar\tau_1})^2} \frac{\partial f_o}{\partial E} dE \qquad (31)$$

where f_o is the distribution function for the charge carriers, E is the energy of the carriers of effective mass m_1 and charge e (a negative number), h is Planck's constant, and τ is the effective relaxation time. The quantity α is given by

$$\alpha = \frac{eH}{\hbar c}$$

where H is the external magnetic field. For the Fermi distribution of electrons (or holes) the integral is easily evaluated (to a good approximation) and the final expression is

$$\sigma_{12} = \frac{ec}{H}\left[\frac{n_1}{1+\frac{H_1^2}{H^2}}\right] \qquad (32)$$

---

[26] Lifshitz and Kosevich, op.cit.

[27] A. H. Wilson, The Theory of Metals, Cambridge University Press, (1954) p. 212ff.

where n_1 is the number of carriers per unit volume and is found from

$$n_1 = \frac{(2m_1\zeta_1)^{3/2}}{3\pi^2\hbar^3} \tag{33}$$

where ζ_1 is the Fermi energy; H_1 is defined by

$$H_1 = \frac{cm_1}{e\tau_1} \tag{34}$$

and is thus a "saturation field," inversely proportional to the mobility of the carriers. For more than one band, Eq. (32) becomes simply

$$\sigma_{12} = \sum_j \frac{c}{H}\left[\frac{e_j n_j}{1+\frac{H_j^2}{H^2}}\right] \tag{35}$$

where the sign of e_j depends upon the nature of the charge carriers (it is negative for electrons and positive for holes).

In an analogous manner, the longitudinal conductivity tensor, σ_{11}, can be obtained from

$$\sigma_{11} = -\frac{e^2}{3\pi^2\hbar^4}(2m)^{3/2}\frac{m}{\hbar}\int_0^\infty \frac{E^{3/2}}{\tau\left[\alpha^2+\left(\frac{m}{h\tau}\right)^2\right]}\frac{\partial f_0}{\partial E}\,dE \tag{36}$$

which reduces finally to

$$\sigma_{11} = -ec\sum_j n_j \frac{H_j}{H_j^2+H^2}\,. \tag{37}$$

From a measure of the concentration of holes in the ellipsoidal "pocket" discussed in the previous section and an indication of the average mobility of these holes as compared to those of the electron ellipsoids of Schoenberg,* one can have some insight into the behavior of the Hall effect. It is seen that the "saturation fields," H_j,

*See "The Fermi Hole Ellipsoid," Chapter IV.

corresponding to each type of carriers (see Eq. (35)), have the same ratio as do the average mobilities of the carriers. Thus one may expect a reversal of sign of the Hall effect at some value of the magnetic field. The experimentally observed σ_{ik} are discussed in terms of the Sondheimer-Wilson Theory in Chapter IV.

CHAPTER II

THE BISMUTH CRYSTAL AND EXPERIMENTAL APPARATUS

The Bismuth Crystal

The single crystal of bismuth was grown from spectroscopically pure bismuth metal purchased from Johnson, Matthey and Co., Ltd., London.

A crystal in the form of a cylindrical ingot was grown by causing a mold containing molten bismuth to emerge slowly from a specially constructed furnace. This furnace was built and described by Hemstreet.[28] The furnace was moved vertically upward by a motor driven screw at a constant rate of approximately 3 centimeters per hour with respect to the stationary mold. The mold was simply a 75 centimeter length of 18 millimeter cylindrical pyrex tubing which had been closed at the lower end by pulling it to a point. Prior to the closing of the lower end the glass was cleaned by passing various cleaning solutions through the tube: First, the tube was flushed with concentrated nitric acid, then concentrated potassium hydroxide, and finally a 5 per cent solution of hydrofluoric acid. The tube was rinsed thoroughly with distilled water after each application of cleaning solution.

---

[28] H. W. Hemstreet, Dissertation, Louisiana State University, 1956.

The bulk bismuth was cleaned first with acetone and then etched with a dilute solution of nitric acid. After the etching process the bismuth was placed inside the tube along with a few cubic centimeters of silicone fluid (Dow-Corning 550). The purpose of the silicone fluid was two fold: it served to prevent oxidation of the molten bismuth, and it wet the glass and thus inhibited any secondary seeding of the ingot after the original seed (at the tip) had begun to grow. It may be pointed out that the silicone fluid is not absolutely essential as many successful crystals have been grown by evacuating the mold to prevent oxidation. However, it was found that the presence of the fluid made the process much simpler and produced more satisfactory results. That is to say, the secondary seeding of the ingot ceased to be a great problem after the introduction of the silicone fluid into the process. Nevertheless, several attempts were necessary to grow a satisfactory ingot.

The crystal structure of bismuth is rhombohedral.* The unit cell of bismuth then can be thought of as a slightly distorted cube. An axis of three fold symmetry coincides with the direction of one of the cube body diagonals. In addition to this trigonal axis there are two other types of symmetry. There are three two-fold axes of symmetry (Binary axes) aligned at 120 degrees to each other and all lying in a plane perpendicular to the trigonal axis. Also, there is the so-called bisectrix axis of symmetry. The bismuth structure has three of these lying in the same plane as the binary axes and bisecting the angles between them.

---

*See Appendix 1.

For this study it was desired to construct a single crystal in the form of a right parallelepiped with the axes of the crystal oriented as shown in Fig. 1. The trigonal axis is parallel to the small dimension and the bisectrix is parallel to the large dimension of the crystal. It may be noted that, for simplicity, the crystal was designed to approximate a flat rectangular plate.

The desired crystal was achieved in the following manner: the ingot was removed from the glass mold by attacking the glass with concentrated hydrofluoric acid for a period of several hours. Then the ingot was etched in a dilute solution of nitric acid. After etching it was possible to determine visually whether or not the ingot was a single crystal. This is true because the reflectivity of the surface depends rather strongly on the angle the incident light makes with the crystal. Thus a visual examination of the surface reveals quite clearly the presence of secondary crystals ingrown into the ingot. After obtaining a single crystal, the orientation of the axes was easily determined by cleaving the ingot with a sharp blade while holding it immersed in a bath of liquid nitrogen. The principal clevage plane in bismuth is the plane in which the binary axes lie. That is to say, the principal clevage plane is perpendicular to the principal (trigonal) axis. There are also secondary clevage planes which lie in the directions of the binary axes and perpendicular to the principal clevage plane. Therefore when the ingot is cleaved the directions of the three binary axes show up as lines on the clevage surface if the clevage is not perfectly smooth. It is therefore

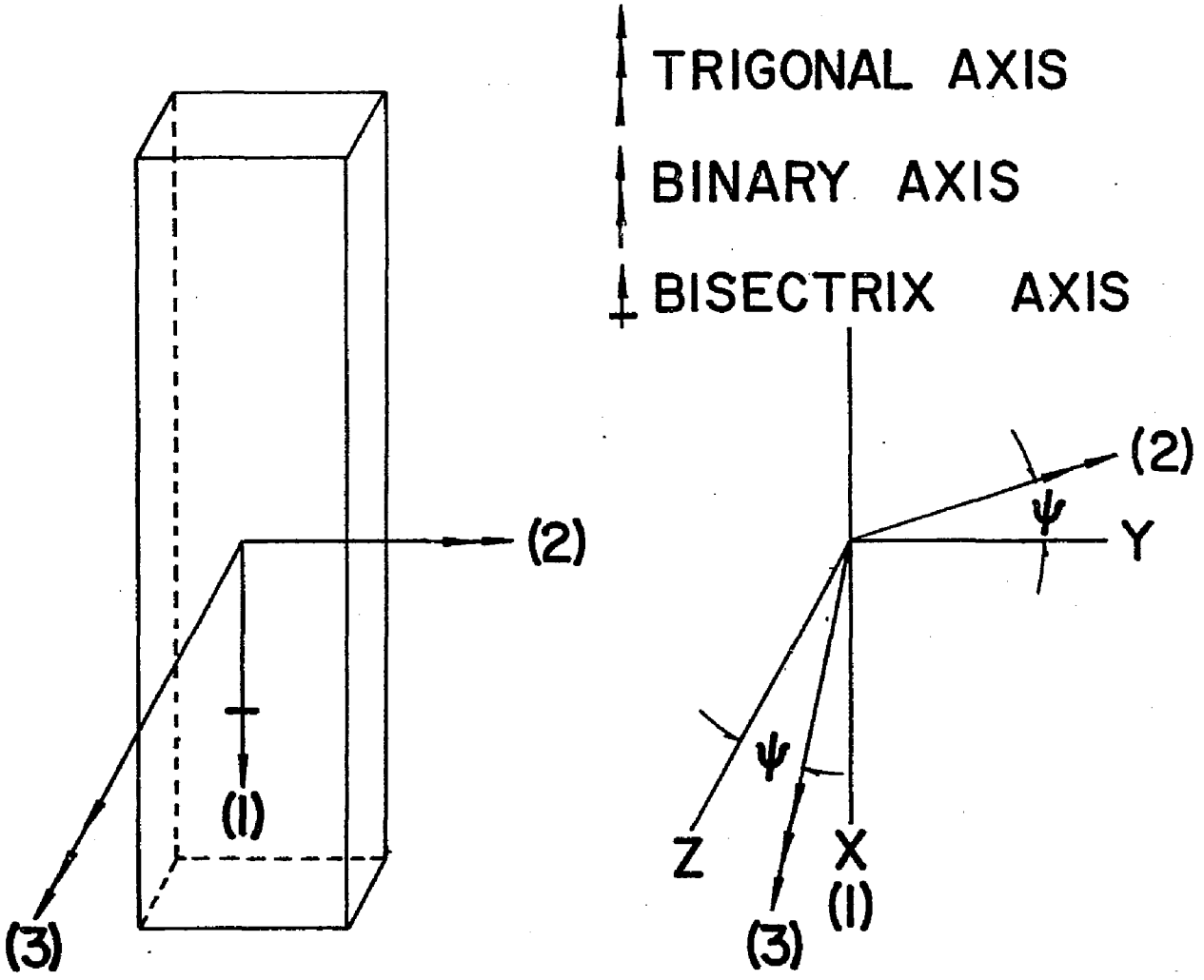

Fig. 1

THE SYMMETRY AXES OF THE BISMUTH CRYSTAL

possible to determine the orientations of all the symmetry axes of the crystal by visual inspection. In practice, the principal clevage plane was found by trial and error, and the single crystal ingot was cleaved into two approximately equal parts. Then, guided by the lines of secondary clevage, the rectangular cross section of the desired crystal was determined and marked on the flat clevage face of the half ingot. Then the four sides of the crystal perpendicular to the clevage face were cut with a water-cooled carborundum saw. The sixth and final face of the crystal was then obtained by beginning at the point most remote from the initial face and repeatedly cleaving small thicknesses away until the desired specimen was achieved. The obvious purpose of this last step was to avoid any possible strain in the finished specimen. Finally, the specimen was etched in dilute nitric acid and subjected to an X-ray examination. The purpose of the Laue photographs was two fold: the finished crystal was examined for possible strain and the orientation of the crystalline axes was confirmed.

In the specimen chosen for this series of experiments the dimensions were 24.3 x 6.9 x 2.5 millimeters.

Suspension of the Crystal

In order to maintain the bismuth crystal at liquid helium temperatures, a crystal chamber of the design shown in Fig. 2 was constructed. The crystal was attached at one end to the copper holder by a copper clamp held by two brass screws. Thermal contact was enhanced by a light layer of silicone vacuum grease between copper

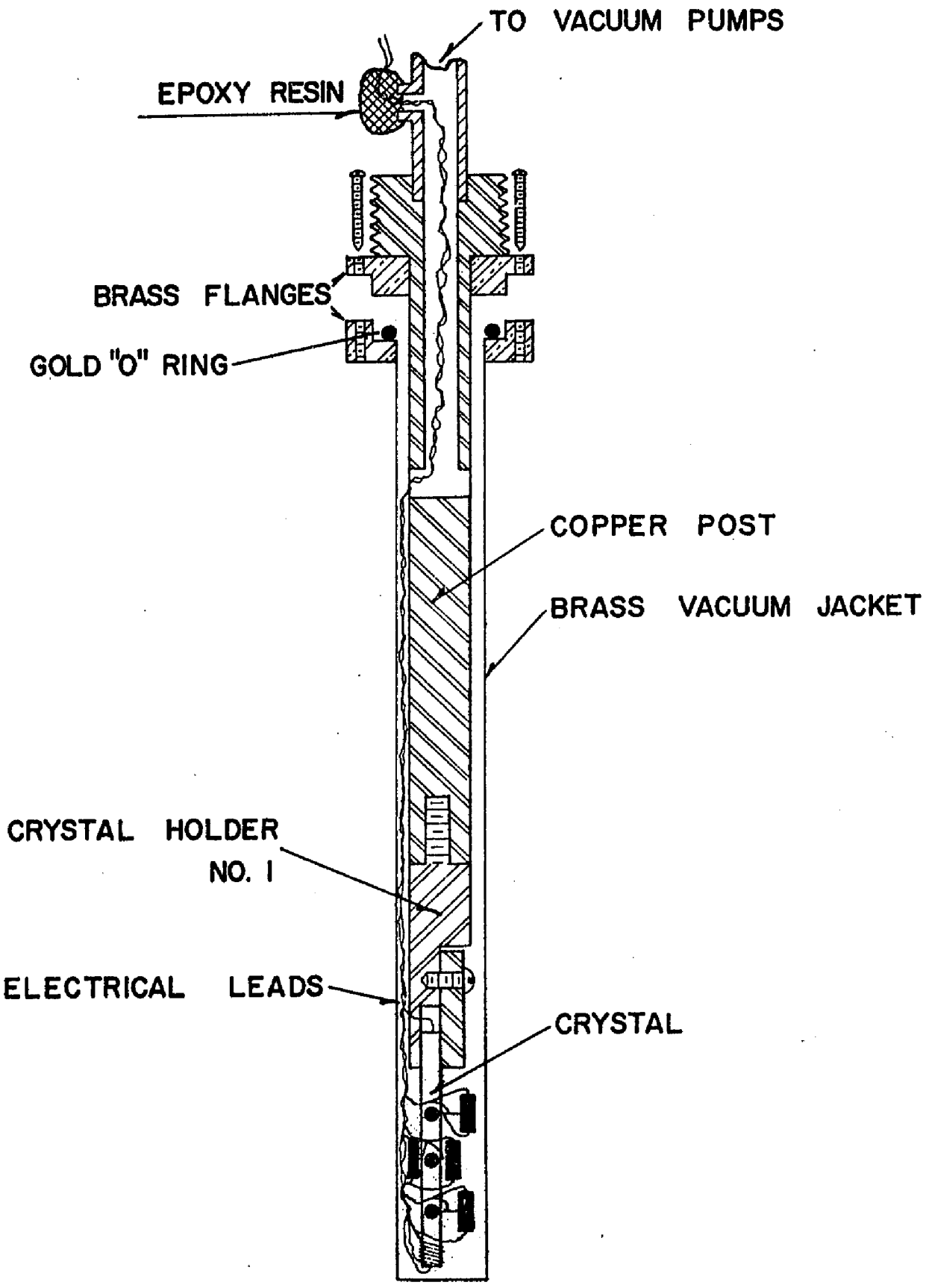

THE CRYSTAL CHAMBER

Fig. 2

and bismuth. Electric isolation of the crystal was effected by insulating the portion of the crystal to be clamped with cigarette paper. The upper end of the crystal holder was reduced in cross section, threaded, and screwed firmly into the lower end of the supporting copper post. With this arrangement it was possible to use a variety of crystal holders with the one suspension system, although the holder shown in the Fig. 4 was the only one needed for this series of experiments. A brass tube with an opening in the cylinder wall was soldered to the upper end of the copper post. To the top of this tube was attached a radiation trap and finally a thin walled stainless steel tube. The electric leads from the crystal were brought through an axial bore in the copper post into the brass tube and finally out into the surrounding liquid helium bath through a short length of 3/16-inch copper tubing which was soldered to the side opening of the tube. The vacuum seal was made at this point by closing with epoxy resin (Stycast 2850 GT). This vacuum seal was previously proven satisfactory and described in detail in the article of Balain and Bergeron.[29] A cylindrical brass jacket supplied the outer wall for the crystal chamber. It was attached by the flange at its upper end to another flange which was soldered around the circumference of the copper post near its upper end. Note in Fig. 2 that a portion of the copper post extends outside the chamber and is in contact with the liquid helium. A 24 carat 24 gauge gold "O" ring was used to make the vacuum seal between the two flanges. It is seen that the axial bore in the

---

[29] K. S. Balain and C. J. Bergeron, Rev. Sci. Instr. 30, 1058 (1959).

copper post served the dual role of a vacuum line from the crystal chamber and a passage for electric leads from the crystal chamber into the liquid helium bath.

The vacuum in the crystal chamber was achieved by a fore pump and diffusion pump flange connected to the upper end of the stainless steel tube. The elctric leads emerging from the expoxy seal were taped to the out wall of the stainless steel tube and brought to the cap of the liquid helium bath. They were then passed into the atmosphere through a short length of 3/8" copper tubing and finally a short length of rubber vacuum hose which was clamped at the upper end. A small quantity of silicone vacuum grease inside the rubber tube in the region of clamping was sufficient for the vacuum seal. The leads were then passed through a plastic spaghetti inside a flexible metallic shield to the measuring apparatus. This suspension system is included in Fig. 3.

The Helium Chamber

The basic features of the helium system used for these experiments are illustrated in Fig. 3. Temperatures of liquid helium lower than 4.2°K were obtained by pumping on the helium bath with a Kinney high capacity vacuum pump. The pumping rate, and hence the pressure in the chamber, was controlled by squeezing the rubber evacuation tube with a vise. For convenience, the vise was driven by a pair of Selsyn motors, one connected through a gear arrangement to the vise, the other located near the manometers. With this arrangement the temperature stability was adequate for experiments under discussion. The pressure in the

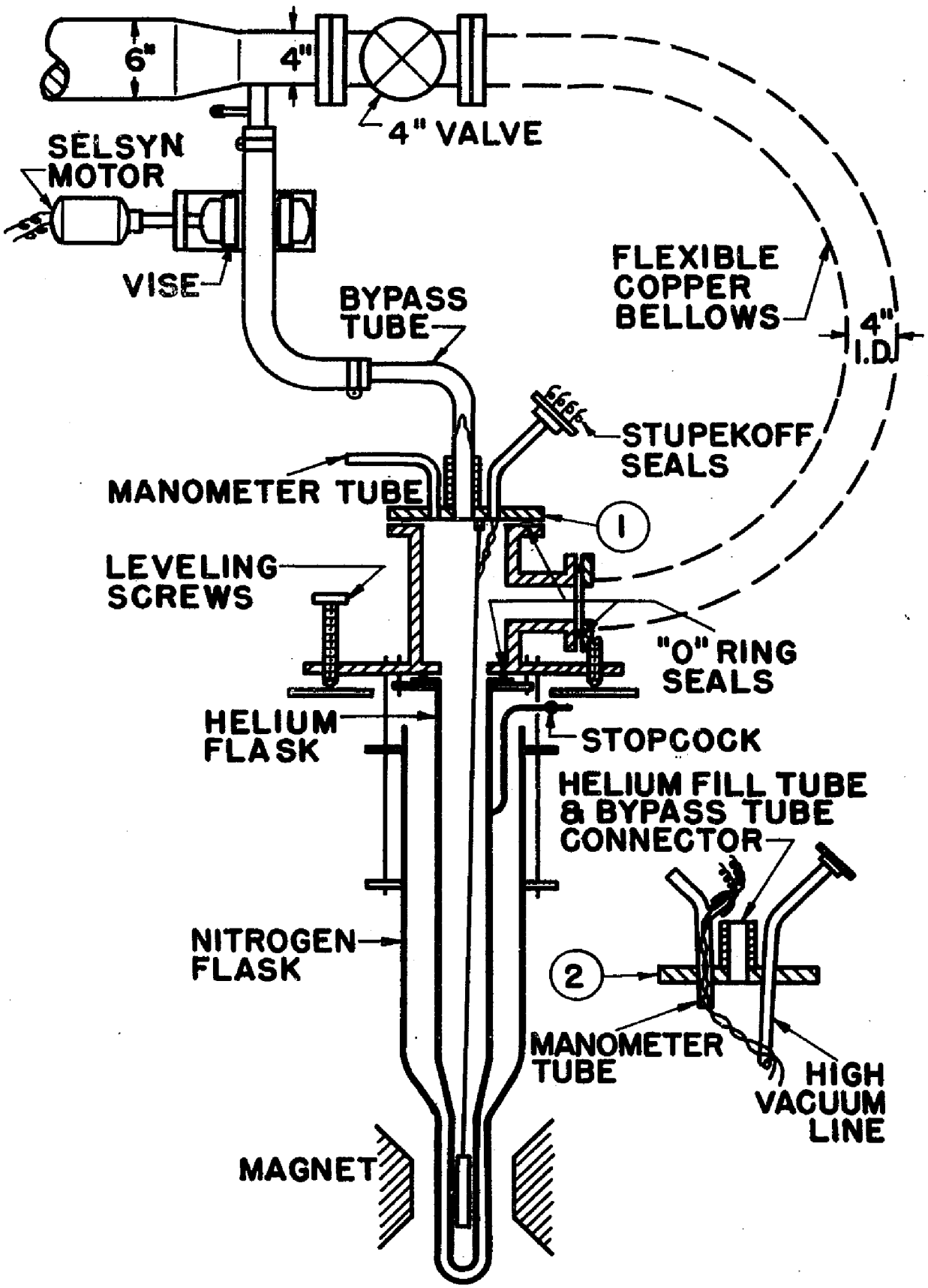
6"
4"
4" VALVE
SELSYN MOTOR
VISE
BYPASS TUBE
FLEXIBLE COPPER BELLOWS
4" I.D.
STUPEKOFF SEALS
MANOMETER TUBE
1
LEVELING SCREWS
"O" RING SEALS
HELIUM FLASK
STOPCOCK
HELIUM FILL TUBE & BYPASS TUBE CONNECTOR
NITROGEN FLASK
2
MANOMETER TUBE
HIGH VACUUM LINE
MAGNET

Fig. 3

helium chamber was monitored by oil and mercury manometers; connection was made to the helium system through a T-section in the same 3/8 inch copper tube that was used to bring the electrical leads into the atmosphere (see assembly number 2 in Fig. 3). The helium chamber and pumping system described here were installed and first used by Bergeron.[30]

The Thermometers and Heater

The carbon resistance thermometers and associated measuring circuit are essentially the same as those used by Zebouni and described in his thesis.[31] Further information on the use of the carbon resistors for thermometers can be had in the article of Clement and Quinnel.[32] Two pairs of 50 ohm (room temperature resistance), 1/10 watt Allen-Bradley resistors were selected by noting the temperature characteristics in the liquid helium range of a group of these resistors. These radio type resistors have properties which render them quite useful as temperature measuring devices in experiments such as those under discussion: Their resistance varies rapidly with temperature in the liquid helium range, they are relatively insensitive to the measuring current and external magnetic fields, and they have a small thermal capacity.

The four resistors selected were coated with an electric insulating compound (Sherwin-Williams Co., Newark, N.J.) and inserted into snug fitting copper jackets. To each jacket was soldered a short length of

---

[30] C. J. Bergeron, Dissertation, Louisiana State University, 1959.

[31] N. H. Zebouni, Dissertation, Louisiana State University, 1961.

[32] J. R. Clement and E. H. Quinnell, Rev. Sci. Instr. 23, 213 (1952).

number 28 copper wire which provided a thermal lead from the jacket to the bismuth crystal. The thermal leads were joined to the crystal with a specially prepared bismuth solder composed of 50 per cent bismuth, 25 per cent tin and 25 per cent lead. The melting point of this solder is approximately 110°C, and thus could be safely used against the bismuth crystal. This mounting provided good thermal contact and electric insulation between the thermometers and the crystal. Two electric leads of Advance number 40 resistance wire were then connected to each end of the resistor; one pair of leads was used to pass a current through the resistor, the other pair being for measurement of the potential across the resistor.

The source of heat current through the crystal was provided by winding approximately 12 inches of number 40 Advance silk-cotton insulated resistance wire around the lower end of the bismuth crystal. The heater was held in close contact with the crystal by a solution of Dupont Duco Cement thinned with acetone. Two leads were then attached to either end of the heating coil; one pair for passing current, and the other pair for voltage measurements. The heater and thermometers are shown attached to the crystal in Fig. 4.

Magnets

The magnetic fields required for this series of experiments ranged from zero continuously to 16 kilogauss. These fields were achieved by using three different magnets.

In the range from zero to 25 gauss the fields were produced by Helmholtz coils of 33 centimeter radius. Calibration of the coils gave 1.96 gauss per ampere.

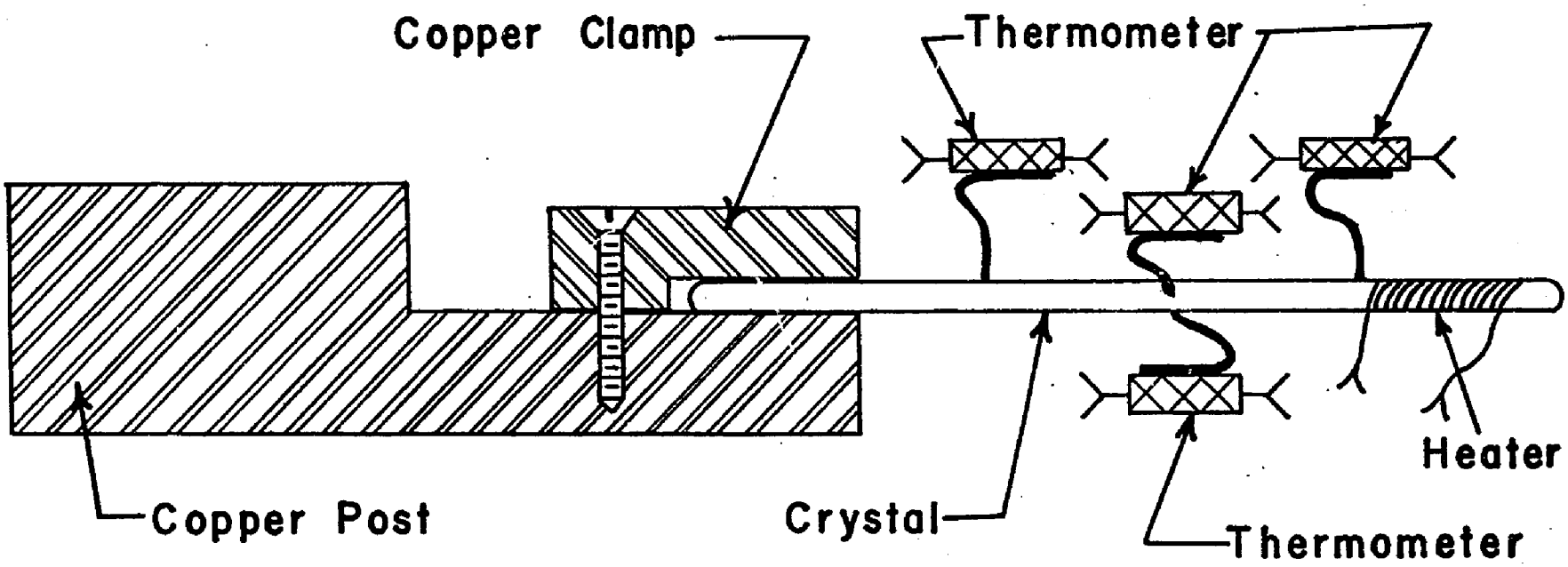

CRYSTAL HOLDER NUMBER I

Fig. 4

For the range of 25 to 2500 gauss a small portable iron core magnet with 3 5/8 inch pole pieces and a 2 inch air gap was used. As no cooling facility was built into this magnet, the current was limited to 1.5 amperes. Calibration of this "intermediate range" magnet with a nuclear resonance fluxmeter gave an approximately linear dependence of field on current, with 1765 gauss for one ampere of current. The residual magnetism was estimated at 25 gauss (hence the need for the Helmholtzcoils).

The high field measurements were made in the 1 5/8 inch air gap of an iron core Weiss magnet with 8 inch pole pieces. The magnet was free to rotate about a vertical axis, and could be positioned with approximately 1/4 degree accuracy. A calibration was made toward the beginning of the series of measurements using the nuclear resonance flux meter. Fig. 5 is a plot of this calibration. It is seen that the field is linear with current (2.97 kilogauss per ampere) up to approximately 33 amperes. The residual magnetism is in the neighborhood of 50 gauss. A schematic and description of the control circuit is given by Ali.[33] With this control circuit the magnet could be ranged from approximately 1 to 18 kilogauss.

A continuous field sweep was possible for each of the two iron core magnets by driving a variable helipot in the control circuit with a clock motor. The magnet currents were monitored by observing the voltage across a 0.01 ohm standard resistor with a Rhodes voltmeter-potentiometer (Sensitive Research Instrument Corp., New York).

---

[33] S. A. Ali, Dissertation, Louisiana State University, 1958.

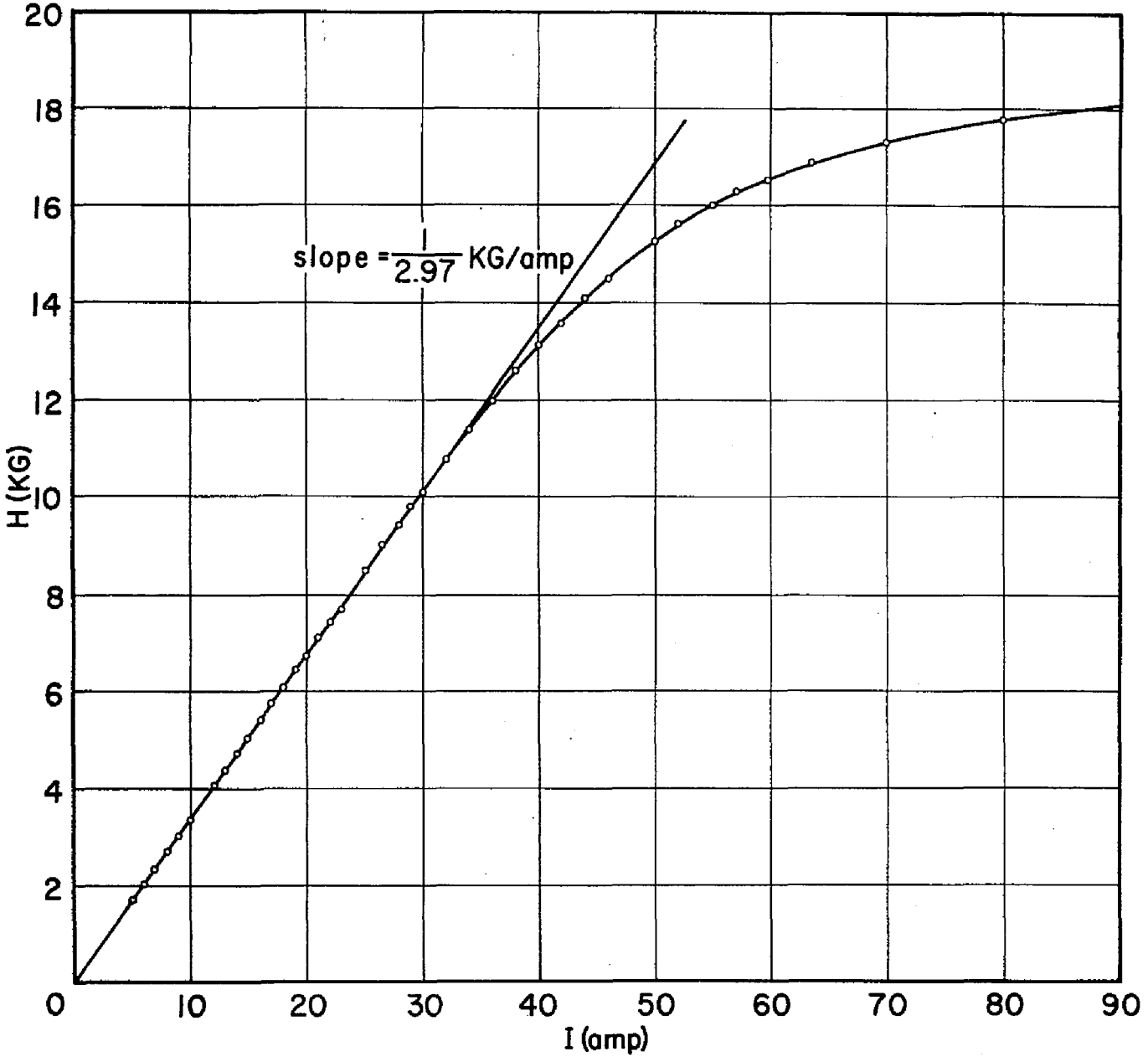
20
18
16
14
12
10
8
6
4
2
0
H (KG)
slope = 1/2.97 KG/amp
10
20
30
40
50
60
70
80
90
I (amp)

Fig. 5

Measuring Circuits

The electric current leads were connected directly to each end of the crystal with the bismuth solder. The circuit for maintaining the crystal current consisted simply of a 12 volt battery in series with a resistance box, a 1 ohm standard resistor, and the crystal. The current was measured by noting the difference in potential across the standard resistor with a Rhodes voltmeter-potentiometer.

The electric potential leads of Advance number 40 resistance wire were placed in contact with the crystal by soldering them to the thermal leads of the thermometers. They were then taken out of the system in the manner previously indicated and connected directly to a Rubicon microvolt potentiometer (Model 2768, Minneapolis-Honeywell Reg. Co., Philadelphia). Voltages were determined by feeding the off-balance of the potentiometer through a Liston-Becker dc breaker amplifier (Liston-Becker Instrument Co., Inc., Stamford, Conn.), then through a voltage divider, and into a Brown recorder (Minneapolis-Honeywell Co., Minneapolis, Minn.). Special care was taken in this voltage measuring circuit to avoid any spurious electric grounds, as well as thermal fluctuations which would produce unwanted potentials. This recording circuit was identical with that shown in the lower part of the Fig. 6.

In setting up the thermometer circuit we were careful to choose resistance thermometers of similar temperature characteristics (see Fig. 7). This was done in order that a pair of thermometers (either the longitudinal or the transverse pair) could easily be employed in a

bridge circuit for continuous measurement of the temperature difference with increasing magnetic field as described by Zebouni.[34] It was later found that at the crystal temperatures used this arrangement was not necessary. A point by point measurement of thermometer temperature was sufficient. This being the case, the circuit for the later measurements was somewhat simplified. Fig. 6 shows the circuit that was used. The variable resistance (90-100 kiloohms) was adjusted so that identical currents passed through each thermometer. The voltage across each of the two resistors could then be measured with a K-2 potentiometer. The microvolt potentiometer which was used in the early experiments but later found to be unnecessary was inserted in the diagonal of the bridge as shown.

The heater current circuit (not shown) consisted of a series arrangement of the heater, a variable resistance box, a milliammeter, and a 12 volt battery. The voltage across the heater was measured with a Rhodes voltmeter-potentiometer.

The key signal circuit, a telegraph key with a 45 volt battery which energized an RC circuit, was used in all experiments involving magnetic field sweeps. Its purpose was to superimpose small voltage "pips" on the recorder sheet corresponding to specific values of magnet current.

---

[34] N. H. Zebouni, op.cit.

THERMOMETER CIRCUIT

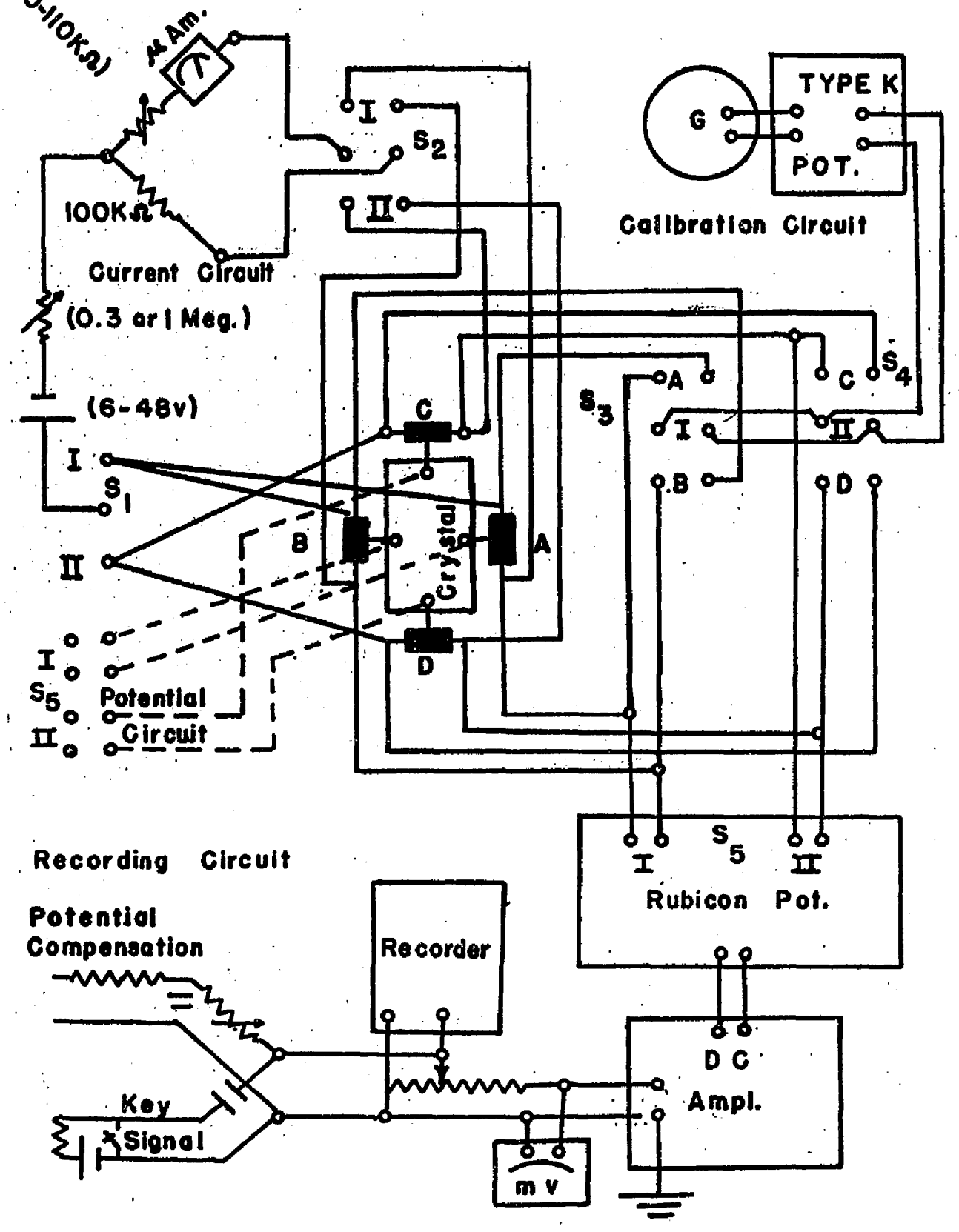

Fig. 6

CHAPTER III

EXPERIMENTAL PROCEDURE

General Preparations

Much of the general preparation for an experiment at liquid helium temperatures has become quite routine in this laboratory. For this reason, detailed consideration will be made only of those processes which are peculiar to the measurements of the effects put forth in Chapter I.

In all of the experiments, the crystal assembly was pre-cooled to temperatures near that of liquid nitrogen for a period of four hours or longer. This process involved evacuating the interspace in the double wall of the helium dewar, sealing off that vacuum with the stopcock (see Fig. 3), and filling the outer dewar with liquid nitrogen. After this, the previously evacuated helium chamber was filled with helium gas to a pressure slightly more than atmospheric. The helium gas served to exchange heat between the crystal assembly and the liquid nitrogen.

Crystal Alignment

The orientation of the bismuth crystal with respect to the magnetic field was determined by visual means. Usually, in experiments of this type, the crystal orientation can be learned by a simple study of the magnitude of one of the transport effects for different orientations

of the magnetic field.[35,36] This could not be done for bismuth since the maxima and minima of the transport effects with respect to crystal orientation are not sufficiently sharp.

The upper surface of the helium chamber cap, which was rigidly fixed with respect to the crystal, was marked with a straight line, with orientation parallel to the trigonal axis of the crystal. The orientation of this line was believed to be accurate within 0.2 degrees. After the suspension system had been placed in position for the experiment, a front silvered glass mirror was placed on the cap with the orientation of the mark. Visual alignment of the magnet was then performed with the aid of the mirror. A careful orientation study of the galvanomagnetic effects later showed that the alignment of the crystal in the high field magnet was approximately 1.7 degrees from the desired orientation. It is felt that alignment of the crystal in the lower field magnets had about the same degree of accuracy.

The Galvanomagnetic Effects

For the measurement of the galvanomagnetic effects the crystal chamber was not sealed vacuum tight. Instead, an opening of one or two millimeters was left to connect the crystal chamber with the surrounding liquid helium bath. The outer can would have been removed completely had it not been for the possibility of injury to the delicate crystal assembly while inserting or removing it from the helium dewar.

---

[35] N. H. Zebouni, op.cit.

[36] C. J. Bergeron, op.cit.

The galvanomagnetic measurements were thus made with the crystal in direct contact with liquid helium to insure isothermal conditions.

After the liquid helium had been transferred into the system, the circuits involving the crystal were checked for continuity. (Due to the radical temperature change in one instance, contact was lost between a voltage lead and the crystal at the point where the voltage lead was soldered to the thermal lead.) Then the recorder trace was calibrated by manually varying the output of the microvolt potentiometer. The "high field" data was taken by allowing the recorder to establish a well defined zero value and then (with current in the crystal) turning on the magnetic field and sweeping it steadily over its range. Voltage "pips" were superimposed at the magnet current values corresponding to the smallest divisions on the scale of the voltmeter used to monitor the current. At the end of a sweep the field was turned off, and the recorder was again allowed to establish its zero value.

A few seeps were also taken in this same manner with the small magnet, although a point by point technique proved sufficient for the greater part of the intermediate field data. Likewise, the very low field data (using the Helmholtz coils) were taken at intervals of approximately 2 gauss.

For the orientation study referred to in Chapter I, a number of sweeps with the high field magnet were performed. For these sweeps the magnetic field was positioned at intervals of approximately 6 degrees over a range of nearly 70 degrees in either direction from the trigonal axis orientation.

All data, with the exception of the orientation study, was taken with the magnetic field oriented parallel to the trigonal axis of the crystal. In order to compensate for possible misalignment of the probes, data was taken for both positive and negative values of the magnetic field. The analysis of this will be given in Chapter IV.

The Thermoelectric Power and Ettingshausen-Nernst Effect

The techniques for measurement of these thermomagnetic potentials were essentially the same as for the galvanomagnetic effects with a few exceptions: The crystal chamber was sealed vacuum tight and maintained at a pressure of about 2×10^{-6} millimeters of mercury. The zero value on the recorder trace was obtained with the heater current off, although this procedure was overlooked in some of the earlier sweeps. A part of a later experimental run was used to obtain measurements to correct this deficiency. The temperature of the crystal was measured with the carbon resistance thermometers.

The Thermometer Calibration

A special experimental run was entirely devoted to an accurate calibration of the four thermometers. A steady (less than 1 per cent variation) current of a few microamperes was passed through the resistors. Then, corresponding to various temperatures of the thermometers, the voltage across each of them in turn was measured with a K-2 type potentiometer. This calibration curve is shown in Fig. 7. The temperature of the thermometers was obtained by noting the vapor pressure of the liquid helium with mercury and oil manometers. This pressure was converted to temperature by the "1958 He^4 Scale of Temperatures."[37]

---

[37]Nat. Bureau of Std., Monograph 10 (1960).

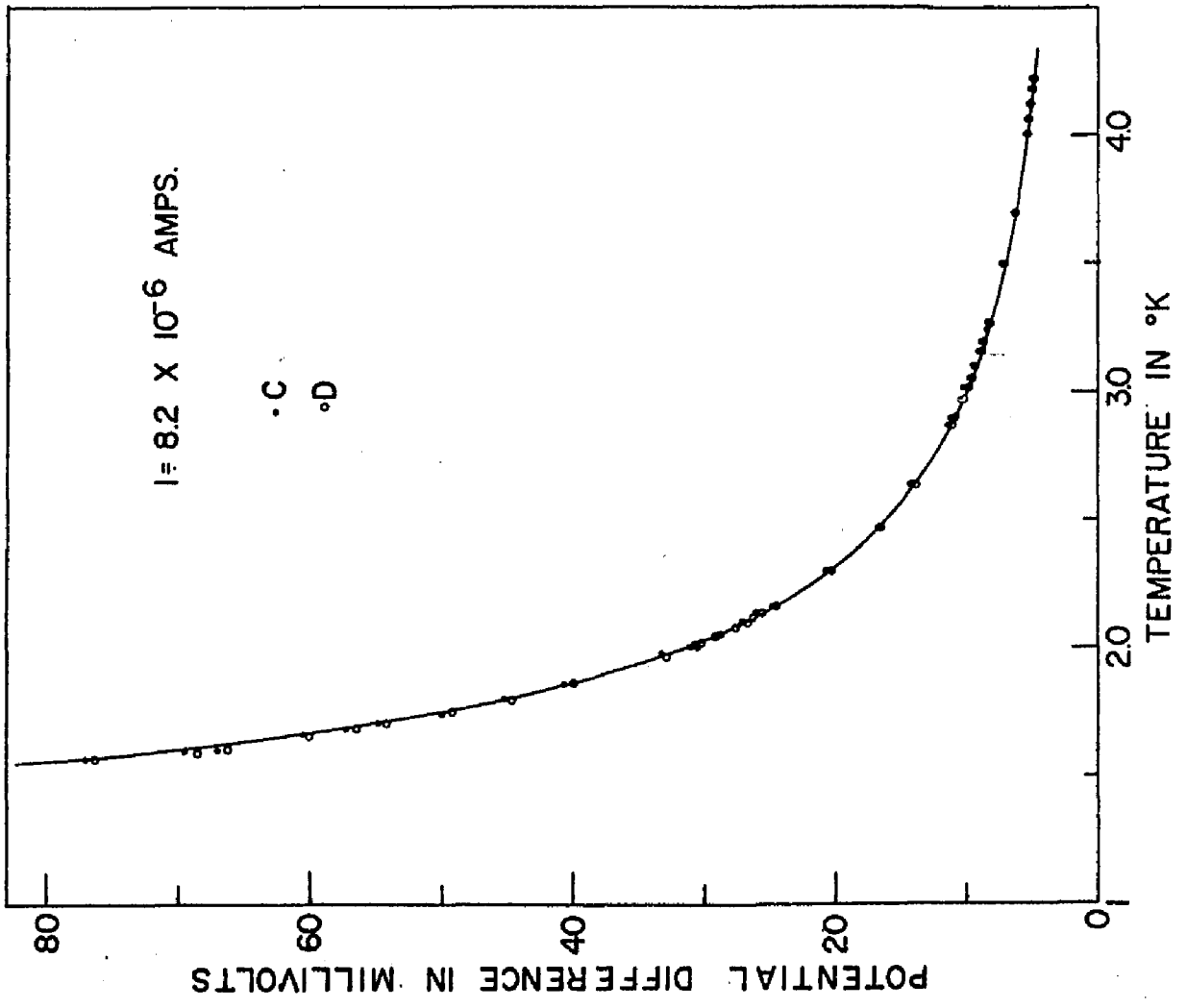
I= 8.2 X 10⁻⁶ AMPS.
C
D
80
60
40
20
0
POTENTIAL DIFFERENCE IN MILLIVOLTS
4.0
3.0
2.0
TEMPERATURE IN °K

Fig. 7

The Thermal Effects

As mentioned in Chapter II, an attempt was made to obtain a record of the temperature differences between each set of the two paired thermometers for a continuous sweep of the magnetic field. No oscillations in either effect were observed at the temperatures investigated. This being the case, the bridge circuit, which was designed to feed its unbalance to the input of the microvolt potentiometer, was not used for the later experiments. The thermal conductivity was measured simply by passing a known heat current through the crystal and observing the difference in temperature developed between the longitudinal thermometers. A repeat of the experiment was necessary to obtain this data when erratic results were detected in the analysis of the first run. The trouble seemingly stemmed from a deterioration in the heater contact to the crystal, after aging and repeated temperature cycling between room temperature and liquid helium temperature. The faulty contact was repaired, and the second run produced coherent results. Data was taken at four different temperatures in the range 4.2°K to 2°K. For greater precision, the slope of the thermometer calibration curve was accurately determined in the region of each of the four points by allowing the temperature of the helium bath to slowly decrease and determining the temperature at several points in each of the four regions of interest. This calibration was done with the heater off. Because the temperature of the crystal was slowly changing while the measurements of temperature difference were being made, greater accuracy was obtained by alternating temperature

measurements between the longitudinal thermometers and taking the measurements at equally spaced intervals of time.

Measurement of the thermal conductivity were not needed for different values of magnetic field as it was found that at zero field the electron contribution to the conductivity was less than one-half of one per cent of the total. No measurable temperature difference in the transverse thermometers (Righi-Leduc effect) was detected.

CHAPTER IV

RESULTS AND CONCLUSIONS

The Fermi Hole Ellipsoid

The method for obtaining the eccentricity of the Fermi ellipsoid is drawn from Eq. (30) of Chapter I. It is seen from this that the extremal area of intersection of the ellipsoid with a plane perpendicular to the magnetic field can be determined simply by measuring the period of the oscillatory Hall effect or magnetoresistance. That is,

$$S_m(\zeta_o) = \frac{eh}{c} \frac{1}{\Delta(1/H)} \tag{38}$$

To study the proposed ellipsoidal Fermi surface then, one must measure $\Delta(1/H)$ for various orientations of the field H with respect to the axes of the bismuth crystal. Recall from Chapter I that the major axis of the ellipsoid is assumed to be oriented along the trigonal axis of the crystal. Most investigators have assumed that the ellipsoid is circular in cross section when viewed along the trigonal axis. That is to say, the Fermi surface is taken to be that of a prolate spheroid lying along the trigonal axis. This circular symmetry is implied from a) the quadratic dependence of the ellipsoid in the x-z and y-z planes coupled with b) the requirement of three-fold symmetry in the x-y plane. There is some evidence from the work

of Friedman and Koenig[38] that the cross section is not circular. It is, however, not well established. The argument presented here is for the prolate spheroid model.

The measurements of the period were made at various orientations in the plane containing the trigonal axis and one binary axis (the 3-2 plane). This geometry is shown in Fig. 8. In the figure, ψ is the angle between the trigonal axis and the magnetic field, a and b are the semi-minor axes, and c is the semi-major axis of the proposed ellipsoid. The shaded area is $S_m(\zeta_o)$, the extremal area of intersection of the ellipsoid and the plane perpendicular to the magnetic field H. The variable r is the semi-major axis of the elliptical surface $S_m(\zeta_o)$. For the case $\psi = 0$, it is seen that $r = b$. Notice that the ellipsoid is shown with momentum coordinates. These coincide in direction with the space coordinates shown at the right in the figure.

For this orientation study the sweeps were taken at 1.8°K in order to obtain more pronounced oscillations. The periods were obtained from magnetic field sweeps for both the magnetoresistance and the Hall effect. The Hall effect measurements were used for values of ψ within the range of about $\pm$ 30 degrees. Then for larger values of ψ (where the transverse voltages were becoming increasingly harder to detect) the sweeps were taken of the magnetoresistance. A determination of the periodicity can be had by plotting the resistivity element ρ_{ij} in function of the inverse magnetic field 1/H.

---

[38] Friedman, A. N., and Koenig, S. H., I.B.M. Jour. 4, 158 (1960).

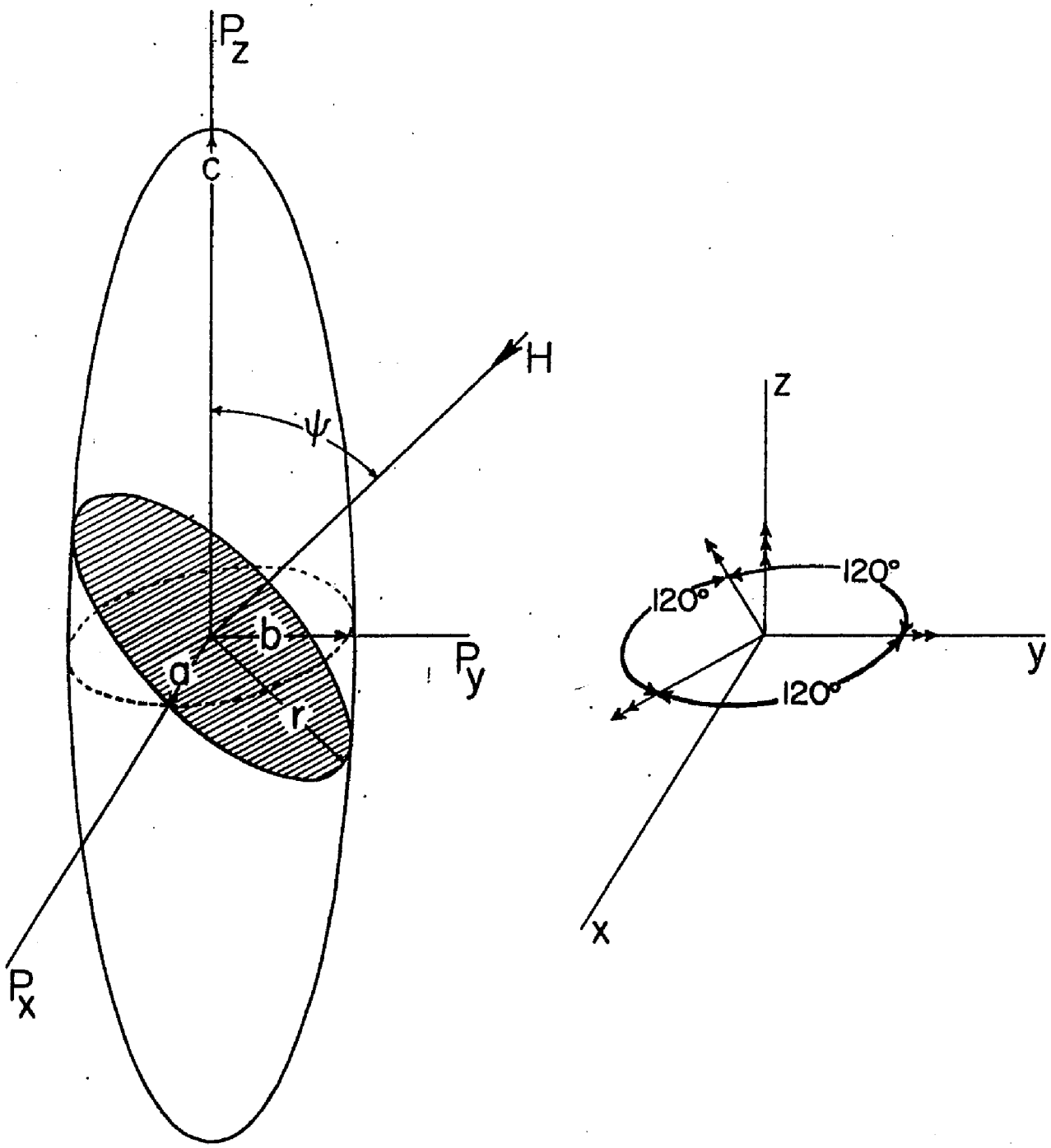

Fig. 8

This periodicity is illustrated in Fig. 9 where the Hall resistivity ρ_{21} is given for 2.1°K. This procedure for period analysis is, however, quite unnecessary as one needs only to examine the curves in the vicinity of the resistivity maxima (and/or minima) to arrive at the period. This simpler procedure was followed: The raw voltage data were taken directly from the recorder trace and examined for maxima and/or minima. Then, for each value of ψ, the values of 1/H corresponding to successive maxima were plotted against successive integers. The slope of the resulting curve (a straight line) gives the value of the period. Three of these plots corresponding to three different values of ψ are given in Fig. 10. Data of the period determination by this method for all values of ψ investigated are listed in Appendix 2. It can be observed in Fig. 10 that for larger values of ψ a certain difficulty arises in the analysis: the oscillations observed on the recorder trace are due not only to the hole ellipsoid under investigation, but also the presence of other ellipsoids (those of Schoenberg). Notice that the presence of this longer period superimposed upon the period due to the hole ellipsoid causes a periodic error in the exact determination of the maxima and minima corresponding to the hole ellipsoid. A simple consideration shows that this periodic error is just the period of the intervening ellipsoid. With this consideration, we simply draw the median line of the periodically oscillating points to determine the true slope of the curve corresponding to the hole ellipsoid (see Fig. 10, $\psi = 63.6°$).

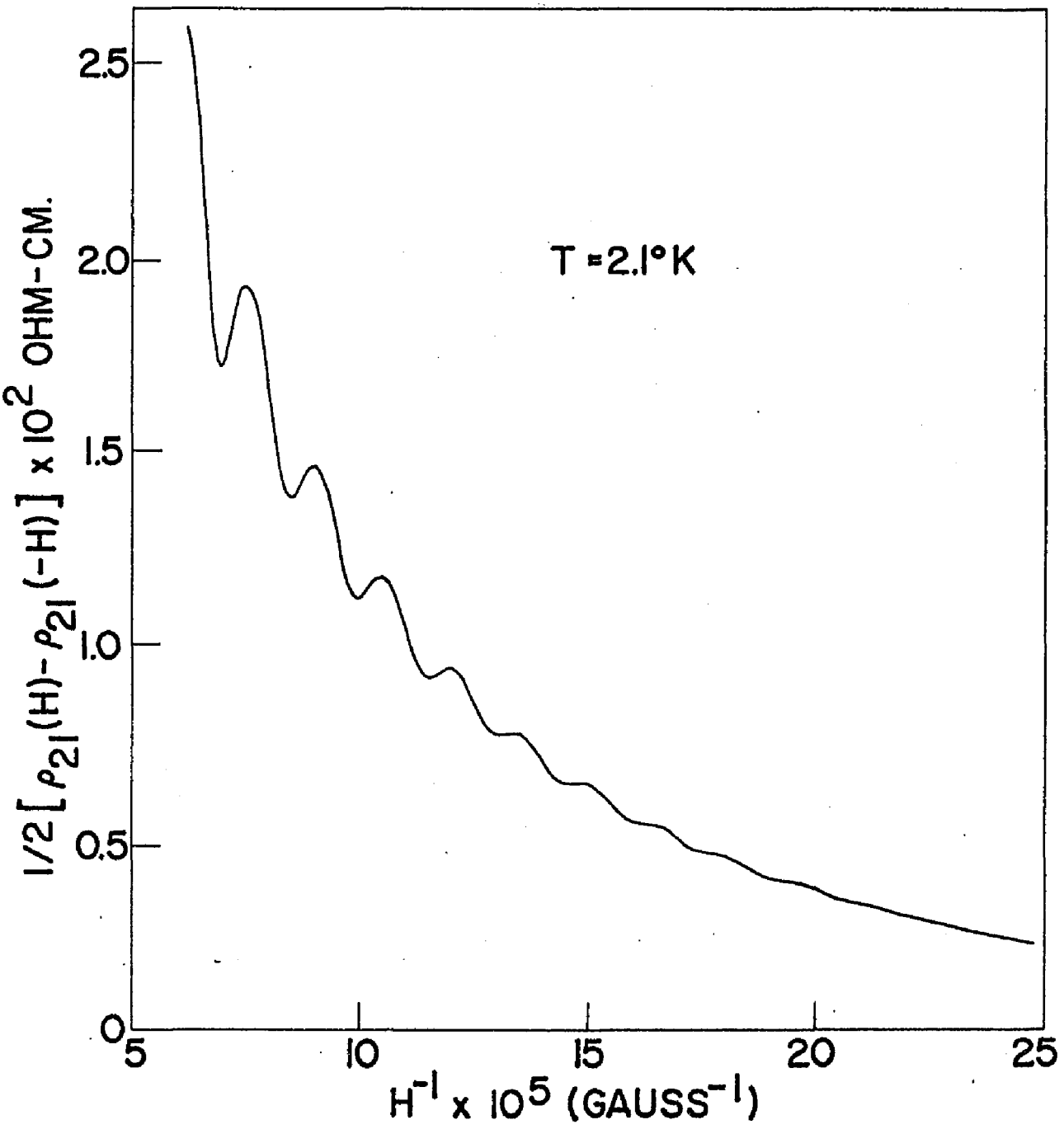
T = 2.1°K
1/2 [ρ21(H) - ρ21(-H)] x 10^2 OHM-CM.
H^-1 x 10^5 (GAUSS^-1)
0
0.5
1.0
1.5
2.0
2.5
5
10
15
20
25

Fig. 9

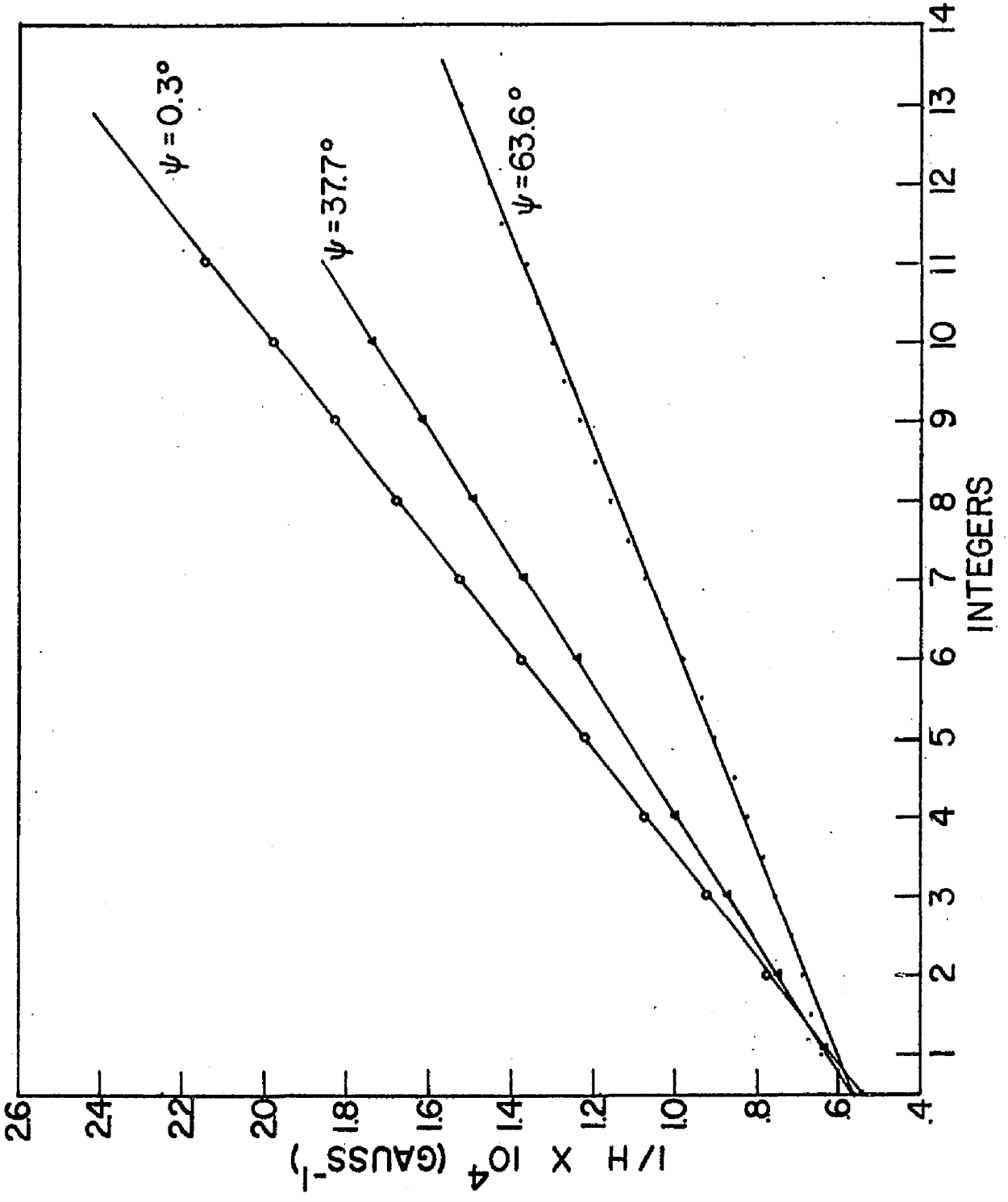
ψ = 0.3°
ψ = 37.7°
ψ = 63.6°
INTEGERS
1/H X 10⁴ (GAUSS⁻¹)
1
2
3
4
5
6
7
8
9
10
11
12
13
14
.4
.6
.8
1.0
1.2
1.4
1.6
1.8
2.0
2.2
2.4
2.6

Fig. 10

A simple trigonometric consideration of the ellipsoid in combination with Eq. (38) yields a linear dependence of the square of the period on the square of cosine ψ. Specifically, it is seen that

$$\Delta^2\left(\frac{1}{H}\right) = \left(\frac{eh}{\pi ac}\right)^2 \left[\left(\frac{1}{a^2} - \frac{1}{c^2}\right) \cos^2\psi + \frac{1}{c^2}\right] \quad . \tag{39}$$

A plot of the data obtained from the field sweeps for both positive and negative values of ψ is given in Fig. 11. The linearity of the curve indicates that the Fermi surface is indeed an ellipsoid. There is some evidence from the work of Brandt, et al.[39] that there is a departure of the Fermi surface from that of an ellipsoid for values of $|\psi| > 75^\circ$. This departure was not mentioned in a later publication concerning presumably the same experimental data.[40] This was not examined by our technique. The experimental points in Fig. 11 were adjusted to correct for misalignment of the magnet with respect to the trigonal axis. An adjustment of 1.7° was found to give the best fit of the points to the straight line. The intercept of the curve gives $\Delta(1/H) = 1.52 \times 10^{-5}$ gauss^{-1} for the period with the magnetic field along the trigonal axis ($\psi = 0$). Both intercepts were examined using Eq. (38) to find the extreme cross sectional areas of the ellipsoid in momentum space. These values are listed in Table I along with other parameters pertaining to the ellipsoid. The volume of the ellipsoid is given by

$$V = \frac{4}{3}\pi a^2 c \tag{40}$$

---

[39] Brandt, N. B., Dubrovskaya, A. E., and Kytin, G. A., JETP (USSR) 37, 572 (1959).

[40] Brandt, N. B., op. cit.

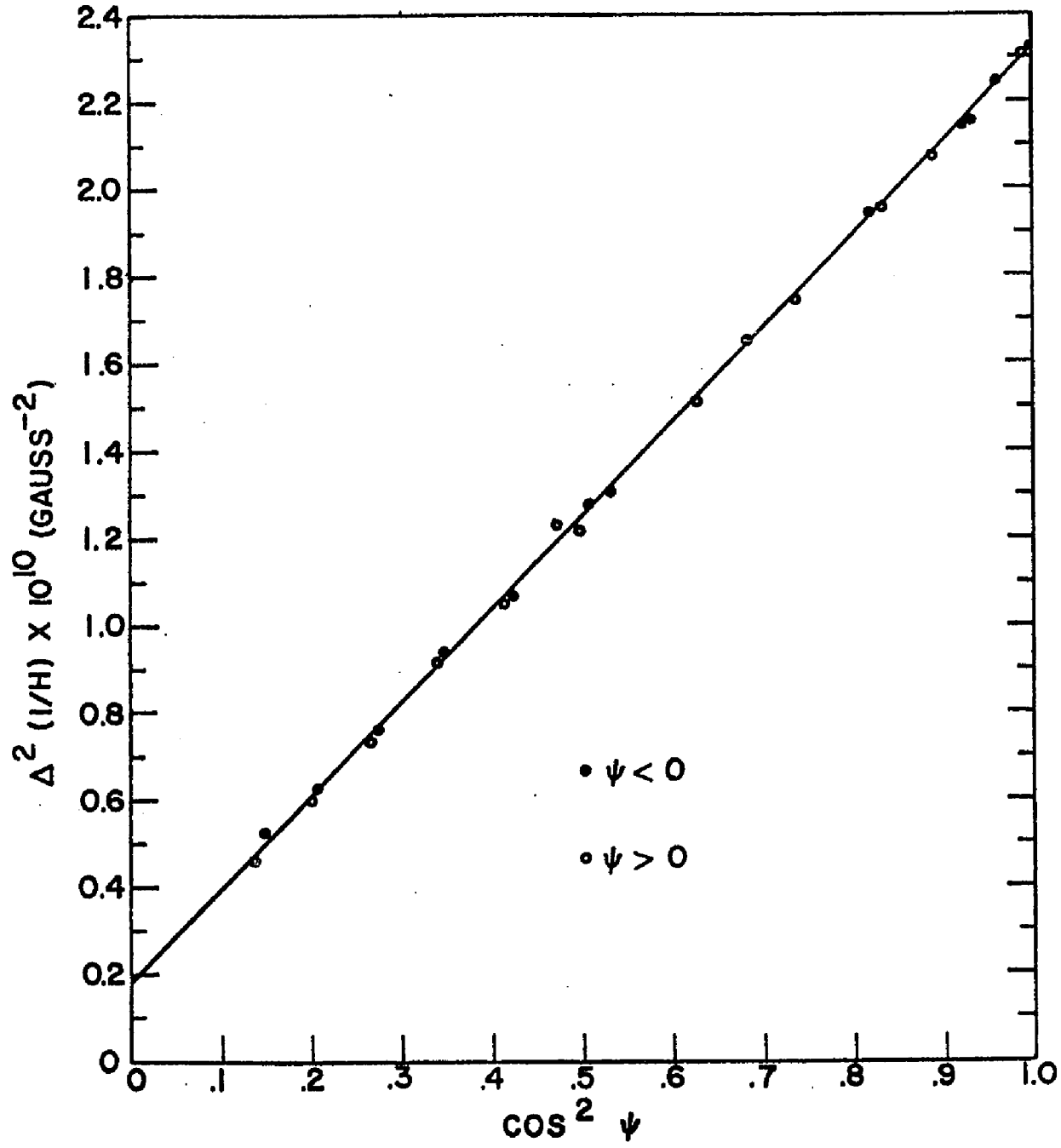
2.4
2.2
2.0
1.8
1.6
1.4
1.2
1.0
0.8
0.6
0.4
0.2
0
Δ^2 (I/H) X 10^{10} (GAUSS^{-2})
0
.1
.2
.3
.4
.5
.6
.7
.8
.9
1.0
cos^2 ψ
• $\psi < 0$
∘ $\psi > 0$

Fig. 11

and is found to be $V = 4.97 \times 10^{-62}$ $gm^3cm^3sec^{-3}$. The number of states (holes) per unit volume per ellipsoidal pocket was computed from the density of states relation[41]

$$n^H = 2\frac{V}{h^3} = 0.343 \times 10^{18} \text{ holes/cm}^3 \tag{41}$$

where h is Planck's constant, and the factor of 2 arises from the fact that the carriers are Fermions. The number of holes per atom per pocket is

$$n^H \frac{M}{A_o \rho} = 1.21 \times 10^{-5} \text{ holes/atom} \tag{42}$$

where ρ is the density of bismuth, M is the atomic weight, and A_o is Avogadro's number. For the effective masses of the holes, one can write

$$\frac{1}{\pi} S_{\perp}(\zeta) = p_x p_z = p_x \sqrt{2m_{\parallel}\zeta} \tag{43}$$

$$\frac{1}{\pi} S_{\parallel}(\zeta) = p_x p_y = p_x \sqrt{2m_{\perp}\zeta}$$

where the parallel ($\parallel$) and perpendicular ($\perp$) directions are taken with respect to the major axes of the ellipsoid. It follows that the relations

$$\frac{S^2_{\perp}(\zeta)}{S^2_{\parallel}(\zeta)} = \frac{m_{\parallel}}{m_{\perp}} = \frac{\Delta^2_{\parallel}\left(\frac{1}{H}\right)}{\Delta^2_{\perp}\left(\frac{1}{H}\right)} \tag{44}$$

exist between the periods, the extremal cross sectional areas of the ellipsoid, and the effective masses.

In order to determine the other parameters of the hole ellipsoid, one must look further at the theory of the oscillatory phenomena.

---

[41] Dekker, A. J., Solid State Physics, Prentice-Hall, Inc., 1957.

Lifshitz and Kosevich[42] have related the oscillatory part of the galvanomagnetic effects to the oscillations of the magnetic moment (de Haas-van Alphen effect) through the magnitude of the classical mobility tensor. The results allow us to write very approximately (we are using only the first term of a highly convergent infinite series) for the oscillatory part of the resistivity tensor

$$\Delta\rho^{ij} \propto H^{1/2} T e^{-\frac{2\pi^2 kT}{\beta^* H}} \sin\left(\frac{2\pi\zeta_o}{\beta^* H} + \delta\right) \tag{45}$$

if for the temperatures and fields under consideration the hyperbolic sine can be replaced by the exponential term, see above. In Eq. (45), k is Boltzmann's constant, ζ_o is the Fermi energy, β^* is the effective double Bohr magneton

$$\beta^* = \frac{e\hbar}{m^* c} ,$$

and δ is a phase factor which will be considered in greater detail later in this chapter. Inspection of Eq. (45) gives the expression

$$\Delta\left(\frac{1}{H}\right) = \frac{\beta^*}{\zeta_o} \tag{46}$$

for the period of oscillation. The amplitude of the oscillations is reduced if account is taken of a possible broadening of the energy levels due to collisions or other causes. Dingle[43] has shown that the effect of the broadening that would correspond to a collision time t_o is as if the temperature T were increased by an amount x where

$$x = \frac{h}{\pi k t_o} \tag{47}$$

---

[43] Dingle, R. B., Proc. Roy. Soc. (London) A211, 500 (1952).

Reynolds, et al.,[44] have determined a value of β^* for bismuth using the above considerations, and arrived at the value

$$\beta^* = 3.0 \times 10^{-19} \text{ erg/gauss}$$

for the trigonal axis orientation. This analysis was done by studying the temperature dependence of the amplitude of the oscillations for several different temperatures and fields. A Dingle temperature of $x = 0.5$ degree was used. Our own analysis to determine the value of m^* (and thus β^*) is given later in this chapter in the section concerned with the further analysis of the oscillatory phenomena. Our analysis is somewhat simpler (and possibly more accurate) as we retain the hyperbolic sine rather than replacing it by the exponential and examine the variation of the oscillation amplitude with temperature for fixed values of magnetic field. The Fermi energy was calculated from Eq. (46) using the experimentally determined values of $\Delta(1/H)$ and $m_\perp$. The value of $m_{||}$ is determined with Eq. (44). Table I gives the values of various parameters for the hole ellipsoid as determined in this work. Results on the same ellipsoid by other investigators using various techniques are also listed for comparison. It is seen that the agreement is quite good in all cases. The recent work of Brandt[45] in determining these parameters from extremely low temperature de Haas-van Alphen studies affords us a rather complete list of parameters for comparison. The values of $m_\perp$ and ζ_o obtained by Reynolds, et al.[46] are essentially the same as those obtained in the present investigation.

---

[44] Reynolds, et al., op.cit.

[45] Brandt, N. B., op.cit.

[46] Reynolds, et al., op.cit.

Table I

Data From Various Measurements on the Fermi Hole Ellipsoid

	Present Work	de Haas-van Alphen Effect BRANDT	Cyclotron Resonance GALT et al.	Anamolous Skin Effect SMITH	Hall Effect REYNOLDS et al.
$S_\perp$ $(\times 10^{42} gm^2 cm^2/sec^2)$	6.97	6.75	---	---	---
$S_\parallel$ $(\times 10^{42} gm^2 cm^2/sec^2)$	25.02	25.75	---	---	---
$S_\parallel/S_\perp$	3.59	3.81	---	---	---
n^H $(\times 10^{-18} cm^{-3})$	0.343	0.34	---	---	---
ζ_o^H $(\times 10^{14}$ ergs)	1.9	2.5	---	---	2.0
$m_\perp^H/m_o$	0.065	0.05	0.068	---	0.062
$m_\parallel^H/m_o$	0.84	0.7	0.92	---	---
$m_\parallel^H/m_\perp^H$	12.9	14.0	13.5	12.8	---

Analysis of the Energy Bands with Sondheimer-Wilson Theory

The quasi-classical expressions for the electric current density $\vec{J}$ and the heat current density $\vec{w^*}$ are given by[47]

$$\vec{J} = e\int \vec{v} f dE \tag{48}$$

and

$$\vec{w^*} = e\int \vec{v} E f dE \tag{49}$$

where $\vec{v}$ is the group velocity of the electrons, E is the energy of the electrons, and f is the distribution function of the electrons. In equilibrium the f is simply the Fermi distribution function, but in general one must write

$$f = f_o + f_1$$

where f_1 is a perturbation term which depends upon the electric field $\vec{E}$ and the negative temperature gradient $\vec{G}$. $\vec{J}$ and $\vec{w^*}$ are related to the $\vec{E}$ and $\vec{G}$ by Eq. (7).

In the Sondheimer-Wilson approach we consider the effect of a number of bands or "pockets" of carriers. The energy surfaces of the pockets are assumed to be quadratic in momentum space. The anisotropy of the pockets will be considered later in this discussion. An analysis of the experimental data has led to the assumption of the existence of three different bands of electrons and two bands of holes (including the hole ellipsoid we have just discussed in the preceeding section). For the five bands, then, the expressions for the quantities of interest are

---

[47] Wilson, A. H., op.cit.

$$\sigma_{11} = \frac{e^2}{3\pi^2\hbar^4}\left[i_1^{(1)} + i_1^{(2)} + i_1^{(3)} + i_1^{(4)} + i_1^{(5)}\right] \tag{50}$$

$$\sigma_{12} = -\frac{e^2}{3\pi^2\hbar^4}\left[i_4^{(1)} + i_4^{(2)} - i_4^{(3)} + i_4^{(4)} - i_4^{(5)}\right] \tag{51}$$

$$\epsilon''_{11} = \frac{e}{3\pi^2\hbar^4}\frac{1}{T}\left[i_2^{(1)} + i_2^{(2)} - i_2^{(3)} + i_2^{(4)} - i_2^{(5)}\right] \tag{52}$$

$$\epsilon''_{12} = \frac{e}{3\pi^2\hbar^4}\frac{1}{T}\left[-i_5^{(1)} - i_5^{(2)} - i_5^{(3)} - i_5^{(4)} - i_5^{(5)}\right] \tag{53}$$

where the superscripts on the i's refer to the different bands. The expressions for the $i^{(\beta)}$ are

$$i_1^{(\beta)} = -(2m_\beta)^{3/2}\frac{m_\beta}{\hbar}\int_0^\infty \frac{E^{3/2}}{\tau_\beta\left[\alpha^2 + \left(\frac{m_\beta}{h\tau_\beta}\right)^2\right]}\frac{\partial f}{\partial E}\,dE \tag{54}$$

$$i_4^{(\beta)} = -(2m_\beta)^{3/2}\alpha\int_0^\infty \frac{E^{3/2}}{\left[\alpha^2 + \left(\frac{m_\beta}{h\tau_\beta}\right)^2\right]}\frac{\partial f}{\partial E}\,dE \tag{55}$$

$$i_2^{(\beta)} = -(2m_\beta)^{3/2}\frac{m_\beta}{\hbar}\int_0^\infty \frac{E^{3/2}(E-\zeta_\beta)}{\tau_\beta\left[\alpha^2 + \left(\frac{m_\beta}{h\tau_\beta}\right)^2\right]}\frac{\partial f}{\partial E}\,dE \tag{56}$$

$$i_5^{(\beta)} = -(2m_\beta)^{3/2}\alpha\int_0^\infty \frac{E^{3/2}(E-\zeta_\beta)}{\left[\alpha^2 + \left(\frac{m_\beta}{h\tau_\beta}\right)^2\right]}\frac{\partial f}{\partial E}\,dE. \tag{57}$$

In the above expressions

$$\alpha = \frac{eH}{hc}.$$

The distribution functions f for the $i^{(3)}$ and $i^{(5)}$ are for holes. For convenience, we also use the previously defined quantity (see Eq. 34)

$$H_\beta = \frac{cm_\beta}{e\tau_\beta} .$$

In the solution of the σ_{ij} we use the first order approximation of placing f equal to the Fermi distribution step function and obtain

$$\sigma_{12} = ecH\left[- \frac{n_1}{H_1^2 + H^2} - \frac{n_2}{H_2^2 + H^2} + \frac{n_3}{H_3^2 + H^2} - \frac{n_4}{H_4^2 + H^2} + \frac{n_5}{H_5^2 + H^2} \right] \tag{58}$$

$$\sigma_{11} = ec\left[\frac{H_1 n_1}{H_1^2 + H^2} + \frac{H_2 n_2}{H_2^2 + H^2} + \frac{H_3 n_3}{H_3^2 + H^2} + \frac{H_4 n_4}{H_4^2 + H^2} + \frac{H_5 n_5}{H_5^2 + H^2} \right] \tag{59}$$

where we have assumed that τ is independent of E. These solutions have been discussed in Chapter I. For the solutions of the ϵ''_{ij}, the integration gives zero in the first order approximation of replacing the distribution function by the step function. We then turn to the second order approximation for the Fermi distribution function noting the relation

$$- \int_o^\infty \phi(E) \frac{\partial f_o}{\partial E} dE = \phi(\zeta_\beta) + \frac{\pi^2}{6} k^2 T^2 \frac{d^2\phi}{dE^2}\Big|_{E = \zeta_\beta} \tag{60}$$

The integration gives

$$\epsilon''_{12} = - \frac{\pi^2 k^2 cT}{2}\left[\frac{H}{H_1^2 + H^2}\frac{n_1}{\zeta_1} + \frac{H}{H_2^2 + H^2}\frac{n_2}{\zeta_2} + \frac{H}{H_3^2 + H^2}\frac{n_3}{\zeta_3} + \frac{H}{H_4^2 + H^2}\frac{n_4}{\zeta_4} + \frac{H}{H_5^2 + H^2}\frac{n_5}{\zeta_5} \right] \tag{61}$$

$$\epsilon''_{11} = \frac{\pi^2 k^2 cT}{2}\left[\frac{H_1}{H_1^2 + H^2}\frac{n_1}{\zeta_1} + \frac{H_2}{H_2^2 + H^2}\frac{n_2}{\zeta_2} - \frac{H_3}{H_3^2 + H^2}\frac{n_3}{\zeta_3} + \frac{H_4}{H_4^2 + H^2}\frac{n_4}{\zeta_4} - \frac{H_5}{H_5^2 + H^2}\frac{n_5}{\zeta_5} \right] \tag{62}$$

if we again assume that the time of relaxation τ is independent of the energy E. In general, we must take

$$\tau = g\mathcal{E}^{\mu} \tag{63}$$

Then, for $\mu \neq 0$--and there is indication that it lies in the range $-\frac{1}{2} < \mu < 0$[48]--the expression for ϵ''_{12} is

$$\epsilon''_{12} = -\frac{\pi^2 k^2 cT}{2} \sum_{\beta=1}^{5} \frac{H}{H_\beta^2 + H^2} \frac{n_\beta}{\zeta_\beta} \left(1 + \frac{4}{3}\mu_\beta \frac{H_\beta^2}{H_\beta^2 + H^2}\right) \tag{64}$$

The corresponding expression for ϵ''_{11} is somewhat more difficult to obtain but will have characteristics similar to Eq. (62). In the preceeding equations one should note that Eq. (33) applies to each band.

The five bands which have been presented have energy surfaces (in momentum space) which are not isotropic and present different effective masses in different directions. In the preceeding equations, an average mobility has been assumed for each band. The anisotrppic effects can be made compatible with this presentation by taking different effective number of carriers in different directions for each band. It can be shown that for a set of three or six ellipsoids (the Shoenberg electron ellipsoids) symmetrically distributed in momentum space, one can write

$$\sigma_{11} = ec \sum_{\beta} \frac{a_\beta n_\beta H_\beta}{H^2 + H_\beta^2} \tag{65}$$

and

$$\sigma_{12} = c \sum_{\beta} \frac{e_\beta n_\beta H}{H_\beta^2 + H^2} \tag{66}$$

---

[48] Ibid.

where the a_β is a "weighting" factor.[49,50] Note that the expression for σ_{12} is not altered. We repeat that the factor a_β enters into the expression to account for the quadratic energy surfaces lying in the basal plane (1-2 plane) of the crystal in which the measurements are made. The m_β given in the Sondheimer-Wilson theory represent the effective cyclotron masses of the various bands and cannot be used directly to obtain the average mobilities in the basal plane if the energy surfaces are anisotropic. Note that for the hole ellipsoid (β=3) described in the previous section, the cross section of the Fermi surface in the basal plane is circular, implying that for this pocket, $a_3 = 1$. In general, all pockets which are not circular in the basal plane must be "weighted" with the a_β in order to obtain the correct expressions for their contributions to the conductivities. For these measurements on bismuth, we quote the results for Galt, et al., with a = 10.65, Shoenberg with a = 10.17, Azbel and Kamer with a = 8.96[51] and Abeles and Meiboom with a = 3.22 for the electron pocket of three or six ellipsoids.

In the analysis of the experimental data for the several bands, we must satisfy the conditions[52]

$$\frac{2}{\pi}\int_0^\infty \sigma_{11}\,dH = ec\left[a_1n_1 + a_2n_2 + a_3n_3 + a_4n_4 + a_5n_5\right] \qquad (67)$$

and

---

[49] Abeles, B., and Meiboom, S., Phys. Rev. 101, 544 (1956).

[50] Galt, et al., op.cit.

[51] Ibid.

[52] McClure, J. W., Phys. Rev. 112, 715 (1958).

$$\frac{2}{\pi}\int_0^{\infty}\frac{\sigma_{12}}{H}dH = ec\left[\frac{n_1}{H_1}+\frac{n_2}{H_2}-\frac{n_3}{H_3}+\frac{n_4}{H_4}-\frac{n_5}{H_5}\right] \quad . \tag{68}$$

From the experimental data we obtain

$$\sum_{\beta=1}^{5} a_\beta n_\beta = 2.12 \times 10^{18}/cm^3. \tag{69}$$

The bulk of experimental evidence points to the model with six electron ellipsoids and two hole ellipsoids. It would be extremely difficult for us to account for 0.68 holes/cm^3 (present data) and 0.78 electrons/cm^3 (Shoenberg[53])--or even for the 0.55 electrons/cm^3 as proposed by Galt, et al.[54]--if we take the value of a to be in the neighborhood of 10 as previously indicated and treat the electrons as a single band. Even in the case of three electron ellipsoids and one hole ellipsoid which has been discarded, we see that the sum of the effective number of electrons plus the number of holes is considerably greater than the $2.12 \times 10^{18}/cm^3$ which we find if $a \approx 10$. In the analysis, it seems that one should strive to a) maintain the sum of the electrons in the various pockets to be equal to the total number of electrons in the Shoenberg ellipsoids, and b) maintain the number of holes equal to the number of electrons. Furthermore, in the analysis, we strive to have the proposed model fit the experimental curve in the following characteristics: 1) the residual conductivity at H = 0,

$$\sigma_{11}(\text{residual}) = ec\sum_{\beta}\frac{a_\beta n_\beta}{H_\beta}, \tag{70}$$

2) the slope of the σ_{12} curve at the origin,

---

[53] Shoenberg, op.cit.

[54] Galt, et al., op.cit.

$$\left.\frac{d\sigma_{12}}{dH}\right|_{H=0} = \frac{n_1}{H_1^2} + \frac{n_2}{H_2^2} - \frac{n_3}{H_3^2} + \frac{n_4}{H_4^2} - \frac{n_5}{H_5^2}, \tag{71}$$

and 3) the point at which the sign reversal in the Hall effect takes place.

The results of our analysis (curve fitting) of the bands is to be taken as nothing more than an indication of the true nature of the band structure. Better precision and calculating devices would be necessary to obtain a satisfactory fit to the experimental data. The calculations indicate that a high degree of precision in the determination of the H_β is necessary for acceptible results; otherwise, there is a great deal of imprecision in the determination of the various parameters. An approximate set of bands has been obtained by setting the parameters $a_\beta = 1$. This approximation is not completely unreasonable for the approach we are taking since the Shoenberg ellipsoids are not taken as one pocket but rather are broken down into three. The velocity modulation due to the anisotropy is then not nearly so great as in the case of the single electron band. The set of bands is as follows: there are three bands of electrons with

$$\begin{aligned} H_1 &= 24 \text{ gauss}, \quad n_1 = 0.18 \times 10^{18}/\text{cm}^3 \\ H_2 &= 125 \text{ gauss}, \quad n_2 = 0.39 \times 10^{18}/\text{cm}^3 \\ H_4 &= 400 \text{ gauss}, \quad n_4 = 0.35 \times 10^{18}/\text{cm}^3 \end{aligned} \tag{72}$$

and two bands of holes with

$$\begin{aligned} H_3 &= 250 \text{ gauss}, \quad n_3 = 0.68 \times 10^{18}/\text{cm}^3 \\ H_5 &= 2500 \text{ gauss}, \quad n_5 = 0.45 \times 10^{18}/\text{cm}^3. \end{aligned} \tag{73}$$

There is no apparent reason why, if there are indeed three discrete bands of electrons, they would not have been detected by the de Haas-van Alphen studies. We do note, however, that the total number of electrons here is approximately that expected by the six ellipsoid model. Also, the sum of n_1 and n_2 is approximately the number of electrons found by cyclotron resonance studies ($n_e = 0.55 \times 10^{18}/cm^3$).[55] It is suggested that there is a possible explanation for these descrepancies. We consider the three Shoenberg electron ellipsoidal pockets and for this argument suppose that there is strong electron-electron interaction between the electrons of the different ellipsoids. The representation of this set of three ellipsoids in the basal plane is also a representation of the orbits in velocity space. The three ellipsoids are shown superimposed upon one another in Fig. 12. Consider two different electrons arriving at the point A on two different ellipsoidal paths as shown in the figure. The conditions for a collision with exchange of momentum are very favorable since the values of $|v|$, $|p|$ and ζ are the same for each of the electrons. If they do exchange momentum, their respective orbits will be modified and will result in the form shown in the figure. Of course, many combinations are possible. In the figure, only the main orbital systems are shown and labeled (1), (1'), and (4). The initial elliptical orbit is labeled (2). The time required for a complete cycle on one

---

[55] Ibid.

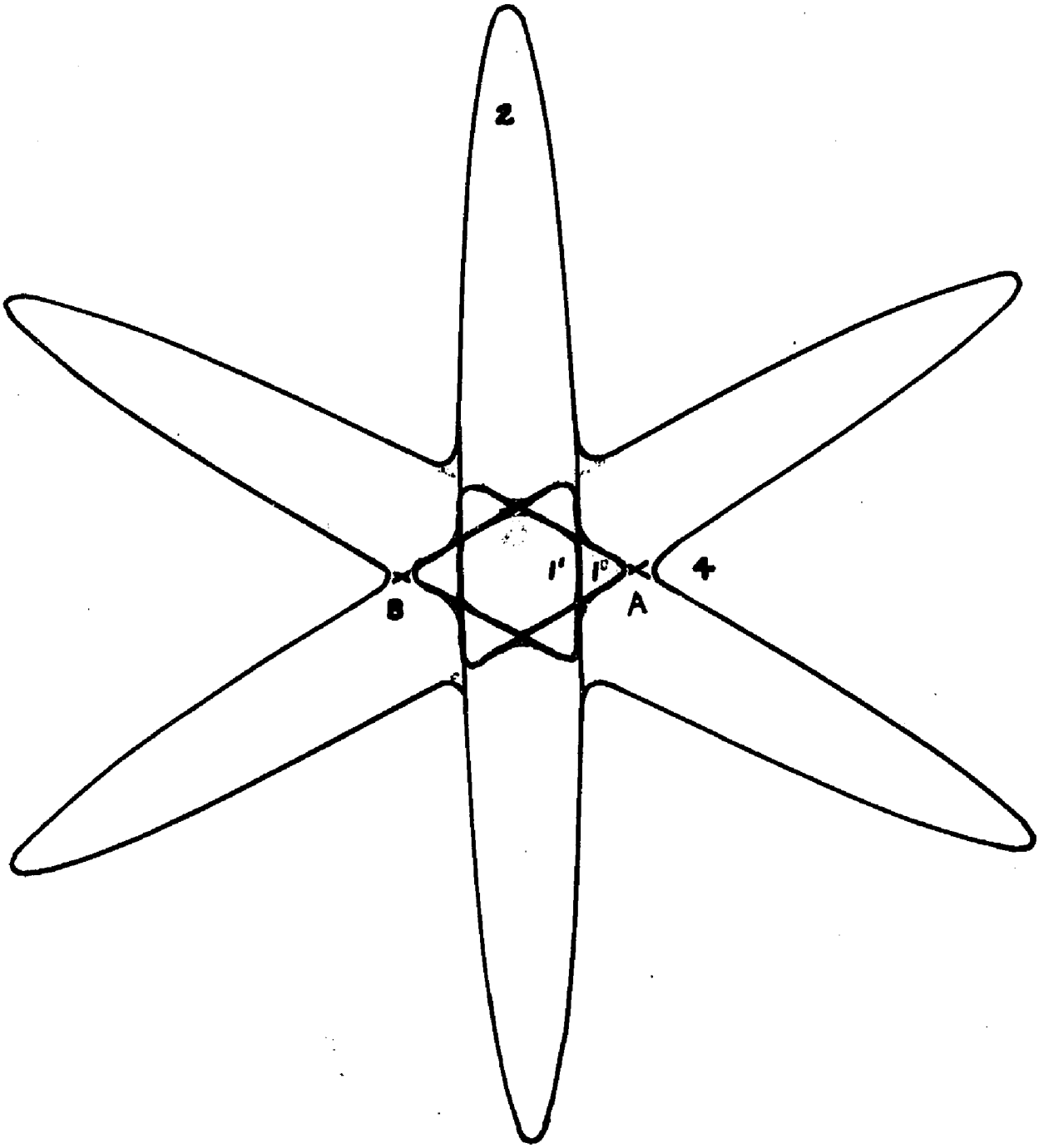

Fig. 12

of the main orbits shown in the figure is obtained quite simply since the ratio of major to minor axis for the ellipse is known (10:1). We then have for the orbit time

$$T_1 : T_{1'} : T_2 : T_4 \propto H_1 : H_{1'} : H_2 : H_4 \propto 1 : 1 : \bar{6} : 1\bar{6}$$

where we have the approximate values

$H_1 = 25$ gauss $\qquad H_2 = 150$ gauss

$H_{1'} = 25$ gauss $\qquad H_4 = 400$ gauss

Under the same assumption it should be expected that $n_4 \approx 8n_1$ which is not the case. Nevertheless this picture of decomposed orbits is only a crude picture as the condition $|v|\ |p|\ \xi$ identical for two interacting electrons is also satisfied for other points than A. Let's say that it may represent an averaging probability, explain the splitting of the H_j of the Shoenberg ellipsoids into three, and explain also the low value for the a_j corresponding to it.

It is seen that band number three represents the band composed of the two hole ellipsoids of the previous section. In addition, it will be necessary (as will be pointed out in a following section) to have one or more bands of reasonably high saturation field values to account for the pronounced oscillations at high fields. Band number five serves this purpose. The experimental values for the σ_{ij} at 4.2°K for the range of fields from zero to 16 kilogauss are shown in Fig. 13.

Concerning the ϵ''_{ij}, it may be seen from Eqs. (61) and (62) that ϵ''_{12} is expected to be negative for all values of magnetic field while ϵ''_{11} may be positive or negative depending upon the relative magnitudes of the terms. This is in agreement with experimental measurements.

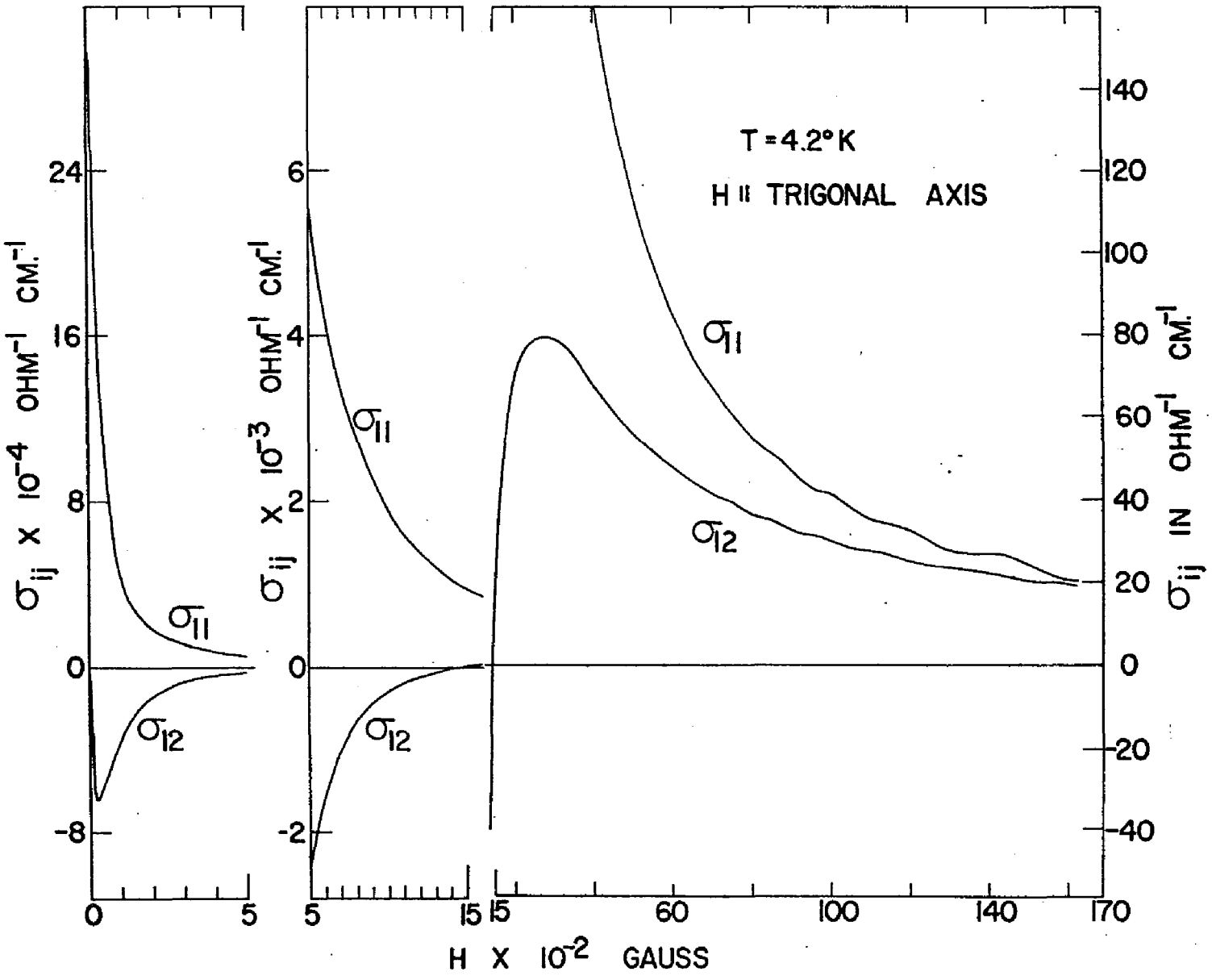
T = 4.2° K
H ∥ TRIGONAL AXIS
σ11
σ12
σij x 10-4 OHM-1 CM.-1
σij x 10-3 OHM-1 CM.-1
σij IN OHM-1 CM.-1
H X 10-2 GAUSS
24
16
8
0
-8
6
4
2
0
-2
140
120
100
80
60
40
20
0
-20
-40
0
5
15
60
100
140
170

Fig. 13

Experimental data show that the sign of ϵ''_{11} reverses from positive to negative at H = 152 gauss. This is compatible with the positioning of the "densely" populated hole pocket with H_3 = 250 gauss. Other general characteristics of the ϵ''_{ij} curves (the positions of the minima, high field oscillations, 1/H dependence of the ϵ''_{12}, etc.) agree qualitatively with the proposed band structure. We will discuss some of these points in further detail. The data for the ϵ''_{ij} for 4.3°K and values of magnetic field ranging from 0 to 16 kilogauss is shown in Fig. 14.

We digress briefly from the analysis of the data to consider the nature of the potentials which were measured. The experimental data presented for the thermoelectric power are in fact the effects produced by the bismuth-copper thermocouple formed by the bismuth crystal and the copper leads. One must, therefore, consider the contribution of the copper to the effects. The kinetic equation by which this effect will be examined is Eq. (13) with $\hat{J} = 0$. The equation is then

$$\vec{E^*} = \vec{E} = \hat{\epsilon}\vec{G} \tag{74}$$

where the $\vec{E^*}$ has been equated to $\vec{E}$ due to the isothermal nature of the potentiometer. Zebouni[56] has demonstrated that, for our two dimensional case, the thermoelectric tensor due to the copper has the form

$$\hat{\epsilon}_B = \begin{bmatrix} \epsilon_B & 0 \\ 0 & \epsilon_B \end{bmatrix} \tag{75}$$

---

[56] Zebouni, N. H., op.cit.

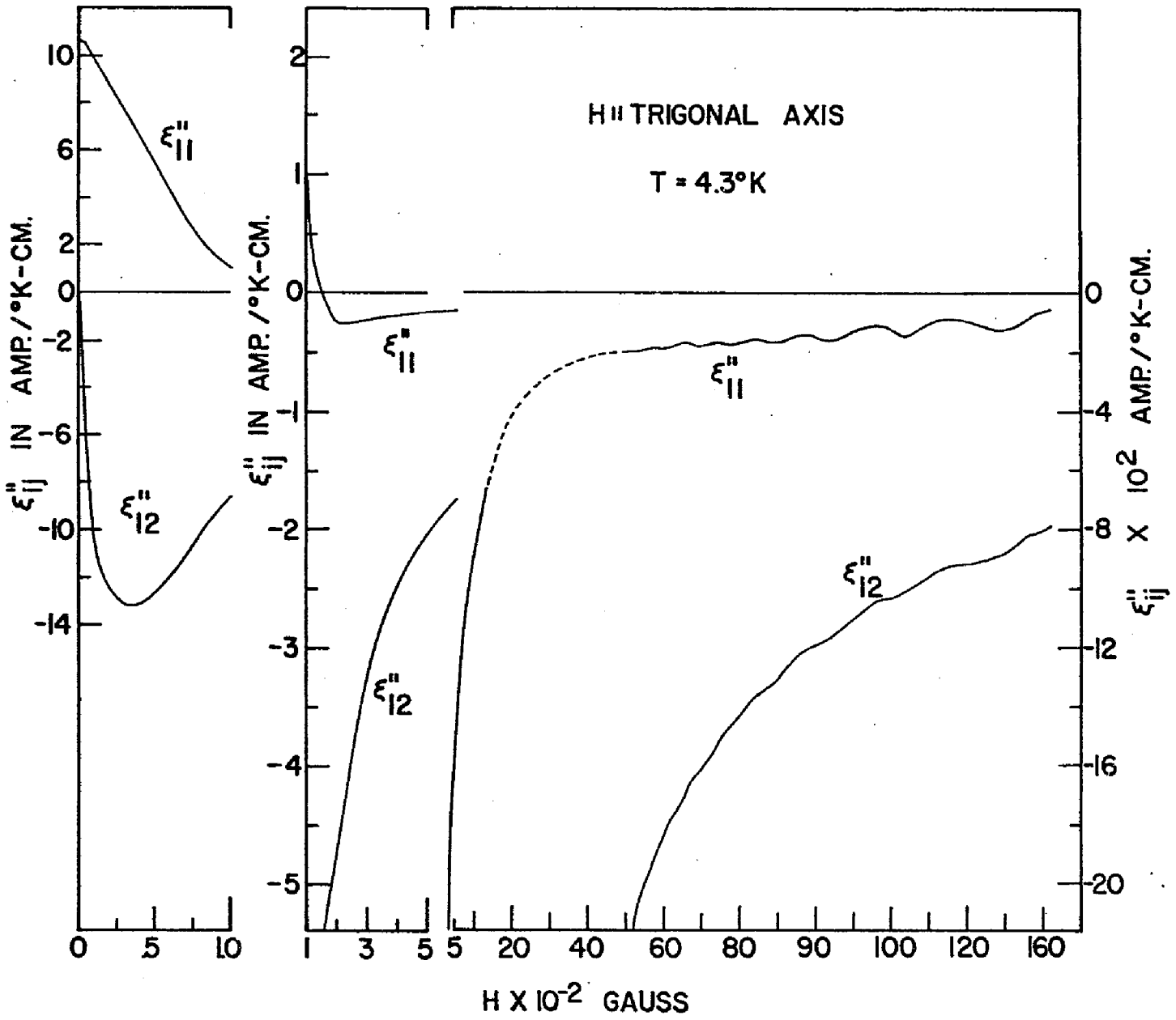
H ∥ TRIGONAL AXIS
T = 4.3°K
ϵ''_{11}
ϵ''_{12}
ϵ''_{ij} IN AMP./°K-CM.
ϵ''_{ij} X 10^2 AMP./°K-CM.
H X 10^{-2} GAUSS

Fig. 14

and is incorporated into Eq. (74) to give

$$\vec{E} = (\hat{\epsilon} - \hat{\epsilon}_B)\vec{G}. \tag{76}$$

The presence of the copper leads is then accurately described by the modified relation

$$\hat{\epsilon}' = \hat{\lambda}^{-1}(\hat{\epsilon} - \hat{\epsilon}_B) \tag{77}$$

The calculation of the important quantity ϵ'' is modified from the form of Eq. (27) to

$$\hat{\epsilon}'' = \hat{\sigma}\hat{\lambda}\hat{\epsilon}' + \hat{\sigma}\hat{\epsilon}_B. \tag{78}$$

An approximate value is given for ϵ_B for H = 0 in the paper of Blatt and Kropshot.[57] This data indicates the value of ϵ_B at zero field to be

$$\epsilon_B(0) \approx 0.6 \times 10^{-6} \text{ volt/deg.} \tag{79}$$

Since the conductivity and the thermoelectric coefficient of copper are essentially independent of H we may consider that this is the order of magnitude of the correction term for all values of magnetic field in the range we have taken. At a temperature of 4.3°K and zero magnetic field, our experimental data yields

$$\lambda_{11}\epsilon'_{11} = 34.56 \times 10^{-6} \text{ volt/deg.} \tag{80}$$

The correction term introduced by the copper is less than two per cent. In this discussion it should be kept in mind that the $\hat{\epsilon}''$ referred to has been computed using only the first term on the right in Eq. (78).

We consider now the nature of the band with large $H_\beta(\beta = 5)$. The known values of n and ζ for the Shoenberg electron ellipsoids and the two hole ellipsoids of this investigation cannot account for more

than one per cent of the measured values for ϵ''_{11} and ϵ''_{12}. The fifth band then should have such characteristics as to account for these large experimental values. Let us modify Eqs. (61) and (62) to their high field approximations where all the bands are asymptotic except number five. We have

$$\epsilon''_{11} \approx - \frac{\pi^2 k^2 cT}{3} \frac{H_5}{H_5^2 + H^2} \left| \frac{dn_5}{d\zeta} \right| \tag{81}$$

$$\epsilon''_{12} \approx - \frac{\pi^2 k^2 cT}{3} \frac{H}{H_5^2 + H^2} \left| \frac{dn_5}{d\zeta} \right| \tag{82}$$

where we have replaced the factor n_5/ζ_5 by its equivalent in terms of the density of states

$$\frac{n_5}{\zeta_5} = \frac{2}{3} \left| \frac{dn_5}{d\zeta} \right| \tag{83}$$

(see Eq. 33). Therefore, in this range of magnetic fields

$$\frac{\epsilon''_{12}}{\epsilon''_{11}} \approx \frac{H}{H_5} . \tag{84}$$

It is seen from the data that this proportionality is relatively well obeyed with $H_5 > 1300$ gauss. We must point out that the first correction term to ϵ''_{11} is negative and all the correction terms to ϵ''_{12} are positive; hence, the proportionality is not obeyed for fields less than about 1300 gauss.

Let us now examine the expression for the linear term in the specific heat

$$C = \Gamma T \tag{85}$$

where

$$\Gamma = \frac{\pi^2 k^2}{3} \left.\frac{dn}{d\zeta}\right|_{\zeta = \zeta_0} . \qquad (86)$$

It is seen that Eq. (82) can be written

$$\epsilon''_{12} = - \frac{cC}{H} , \quad H \gg 0 \qquad (87)$$

At large values of magnetic field, then, the ϵ''_{12} should vary inversely with H. The value of Γ has been determined by Kalinkina and Strekov[58] to be

$$\Gamma = 1.6 \times 10^{-5} \text{ cal/gm-atom deg}^2$$

In Eq. (85) Kalinkina and Strekov have supposed that the specific heat C is due to a Fermi distribution of carriers, and in this case Γ is constant. Eq. (85) holds only for temperatures near absolute zero. Otherwise, the specific heat of the carriers cannot be calculated simply by the product ΓT. The specific heat becomes smaller with increasing temperature. Our data shows that ϵ''_{12} is not proportional to T, and, in fact, the values at 2.1°K and 4.2°K are of the same order of magnitude. Table II gives a comparison of the experimental values of the monotonic part of ϵ''_{12} which we are considering here for various values of magnetic field to the values of ϵ''_{12} calculated from Eq. (87) using $C = \Gamma T$. (A closer approximation might be had by using Eq. (82) rather than the high field approximation for these computations.) The 1/H dependence is seen to be quite good.

---

[58] Kalinkina, I. N., and Strekov, P. G., op.cit.

Table II

A Comparison of the ϵ''_{12} Calculated from Specific Heat Data* to the Corresponding Experimental Quantities for Several High Field Values.

	$\epsilon''_{12} \times 10^{-2}$ amp/°K-cm			
H (kilogauss)	Experimental at 2.1°K	Calculated at 2.1°K	Experimental at 4.3°K	Calculated at 4.3°K
6	-15.0	-11.0	-18.43	-22.5
8	-12.0	- 8.25	-14.36	-16.9
10	-10.05	- 6.6	-11.95	-13.52
12	- 8.75	- 5.5	-10.31	-11.27
14	- 7.7	- 4.71	- 9.14	- 9.66
16	- 6.8	- 4.12	- 8.27	- 8.45

*Using Eq. (87) and the data of reference 58.

Analysis of the Oscillatory Conductivities

The experimentally measurable quantities for the galvanomagnetic effects are seen from Eq. (13) of Chapter I by setting the isothermal condition $\vec{G} = 0$, $\vec{w^*} = 0$. Then, remembering the conditions given in Eqs. (9) and (10), we have for the two dimensional resistivity tensor

$$\hat{\rho} = \begin{bmatrix} \rho_{11} & -\rho_{21} \\ \rho_{21} & \rho_{11} \end{bmatrix} = [\rho_{ij}] \quad . \tag{88}$$

The conductivities are then computed from the experimentally observed values of the $[\rho_{ij}]$ by the well known expression

$$[\sigma_{ij}] = \frac{[\rho_{ji}]}{|\rho_{ij}|} \tag{89}$$

where $[D_{ji}]$ is the adjoint matrix of the $[\rho_{ij}]$, and $|\rho_{ij}|$ is the determinant of the resistivity tensor $[\rho_{ij}]$. For our specific case, the conductivity tensor elements are given by

$$\sigma_{11} = \frac{\rho_{11}}{\rho_{11}^2 + \rho_{21}^2} \quad ; \qquad \sigma_{12} = \frac{\rho_{21}}{\rho_{11}^2 + \rho_{21}^2} \quad . \tag{90}$$

The experimental determination of the ρ_{ij} in function of the magnetic field H for the two temperatures of 4.2°K and 2.1°K is shown in Fig. 15. These values have been determined by the method mentioned in the preceeding chapter: that is,

$$\rho_{21} = \frac{1}{2}\left[\rho_{21}(H) - \rho_{21}(-H)\right] \tag{91}$$

and

$$\rho_{11} = \frac{1}{2}\left[\rho_{11}(H) + \rho_{11}(-H)\right] . \tag{92}$$

Since the ρ_{21} is an odd function of the field and the ρ_{11} is an even function of the field. The effect of misalignment of the probes wherein part of the ρ_{11} is superimposed upon the ρ_{21} (or vise-versa) is shown in the case of the Hall resistivity determination at 2.1°K in Fig. 16 (the lower curve).

Lifshitz and Kosevich[59] have shown that the oscillatory part of the conductivity tensor is mostly due to oscillations in the number of carriers (which is a function of both energy ζ and magnetic field H) is

$$n(H,\zeta) = n(0,\zeta) + h^{-3} \sum_{\beta} F^{\beta}(H,\zeta) = \sum_{\beta} n_o^{\beta} + h^{-3} \sum_{\beta} F^{\beta}(H,\zeta). \tag{93}$$

In this expression, the quantity F is defined by

---

[59] Lifshitz, I. M., and Kosevich, L. M., op.cit.

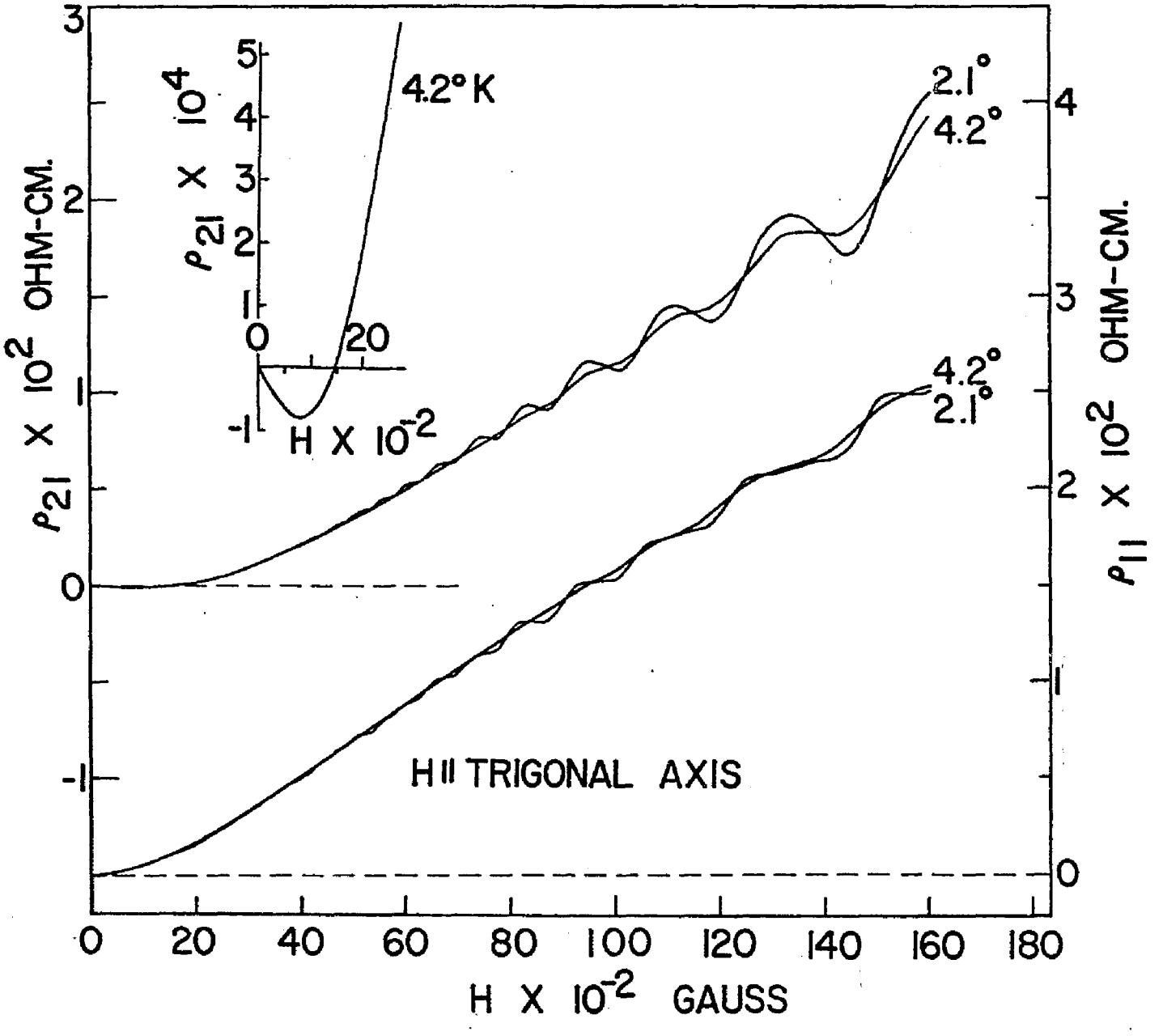
ρ_{21} X 10^2 OHM-CM.
ρ_{11} X 10^2 OHM-CM.
ρ_{21} X 10^4
4.2° K
H X 10^{-2}
2.1°
4.2°
4.2°
2.1°
H II TRIGONAL AXIS
H X 10^{-2} GAUSS

Fig. 15

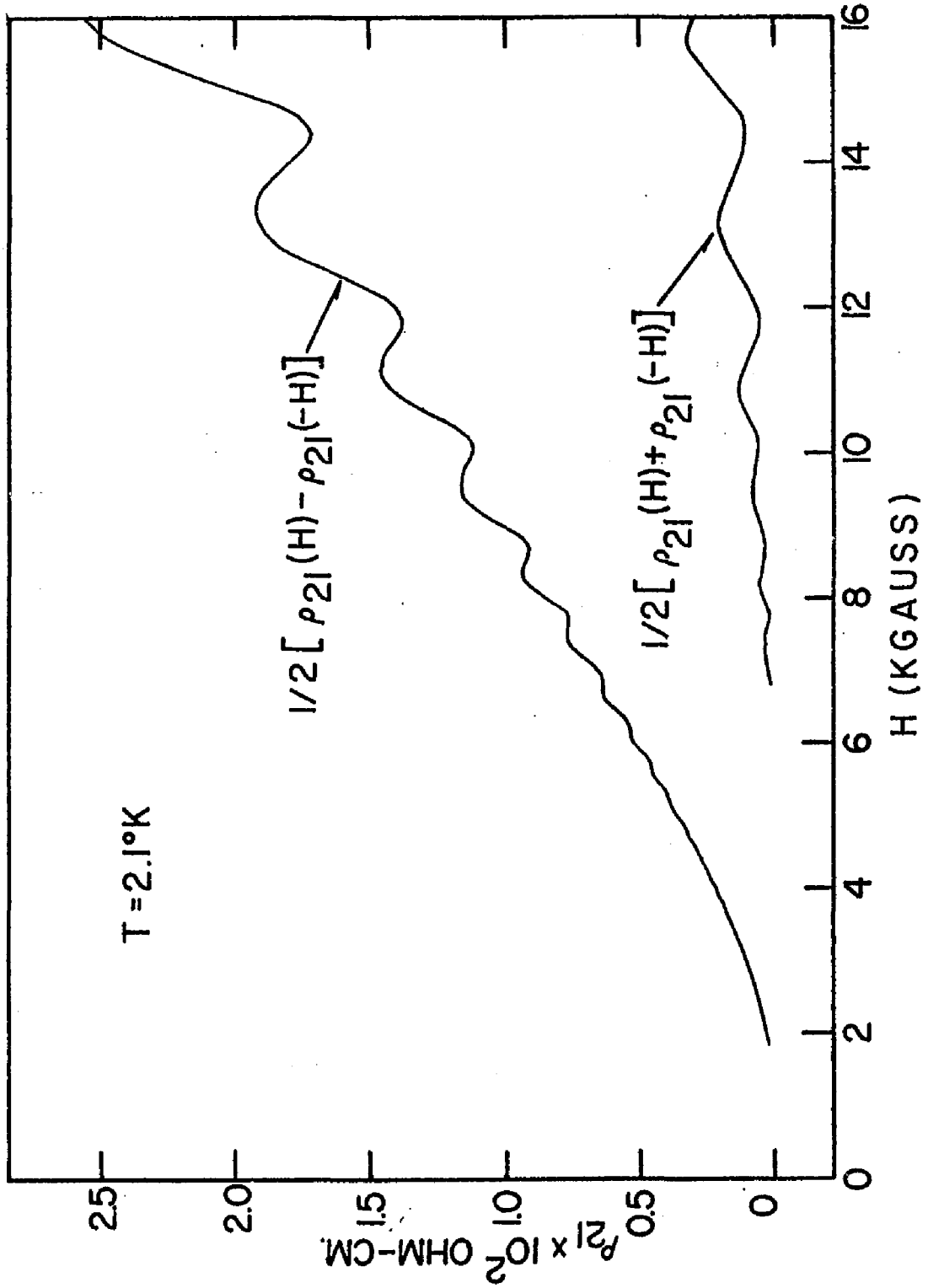
T = 2.1°K
1/2 [ρ21 (H) − ρ21 (−H)]
1/2 [ρ21 (H) + ρ21 (−H)]
ρ21 x 10² OHM-CM.
H (KGAUSS)
0
0.5
1.0
1.5
2.0
2.5
2
4
6
8
10
12
14
16

Fig. 16

$$F^{\beta}(H,\zeta) = \sum_{\kappa=1}^{\infty} A_{\kappa}^{\beta}(H,\zeta)\ \exp\left[2\pi i\kappa\left(\frac{S_m^{\beta_c}}{ehH} - \gamma^{\beta}\right) - i\left(\frac{\pi}{2} \mp \frac{\pi}{4}\right)\right] \tag{94}$$

where

$$A_{\kappa}^{\beta} = 4\left(\frac{ehH}{\kappa c}\right)^{3/2} \frac{m^*(\zeta_{\beta}, p_z^m)\kappa\lambda^{\beta}\sinh \kappa\lambda^{\beta}}{dS_m/d\zeta\ \left|d^2S(\zeta,p_z)/dp_z^2\right|_m^{1/2}} \cdot \tag{95}$$

The superscript (or subscript) β refers to the band, κ is an integer ranging from 1 to ∞ (in the Poisson summation) and the subscript (or superscript) m indicates that the quantity is to be evaluated at the extreme cross sectional area of the bands (pockets) which is perpendicular to the magnetic field H. The γ is the fraction (less than unity) which appears in the expression for the energy of the states in the presence of a magnetic field; it has the value of $+\frac{1}{2}$ for free electrons. The momentum directed parallel to the field H is represented by p_z. The m^* refers to the effective mass and, for this formula, is to be taken as a positive quantity; it is related to the extremal cross sectional area of the pocket by the expression

$$\frac{dS_m}{d\zeta} = \pm\ 2\pi m^* \tag{96}$$

where the plus sign is taken for pockets of electrons and the negative sign is taken for pockets of holes. ζ is the Fermi energy. The quantity λ is given by

$$\lambda = \frac{2\pi^2 kT}{\hbar\omega^*} \tag{97}$$

where

$$\omega^* = \frac{eH}{m^*c}$$

and k is Boltzmann's constant. Note that in this presentation e, the electronic charge, is taken as positive. It is easily shown that

$$\left| \frac{\partial^2 S(\zeta, p_z)}{\partial p_z^2} \right| = \frac{2\pi}{R^2} \tag{98}$$

for the case of an ellipsoid of revolution with the axis of revolution parallel to H. In Eq. (98), R is the ratio of major to minor axis of the ellipsoid. In the expression for the F^{β}, $-\frac{\pi}{4}$ is to be inserted when the extremal cross sectional area perpendicular to the field represents a maximum ($\partial^2 S(\zeta, p_z)/\partial p_z^2 > 0$), and $+\frac{\pi}{4}$ corresponds to a minimal area. This expression of Lifshitz and Kosevich for the number of carriers as a function of energy and magnetic field relies on the assumption that the number of states is very large; or, in terms of the extremal cross sectional area

$$S_m^{\beta} \gg \frac{ehH}{c}$$

It follows in the Lifshitz-Kosevich presentation that the oscillatory part of the conductivity tensor (which is related to the oscillations in the de Haas-van Alphen effect through the classical mobility tensor) is, for $i,j \neq z,z$

$$\tilde{\sigma}_{ij} = \sum_{\beta} q_{m\beta}^{ij} h^{-3} F^{\beta}(H,\zeta) \tag{99}$$

where $q_{m\beta}^{ij}(\zeta,H)$ is the "classical mobility tensor" of the carriers at the extremal cross section of the βth band. The q_m^{ij} are related to the average mobilities of the carriers $\overline{q^{ij}}$ by the distribution function but usually can be expressed as

$$q_m^{ij} \approx \overline{q^{ij}} \quad \text{more explictly} \quad q_m^{ij} = \overline{q^{ij}} + \frac{p^2(\zeta_o)}{2m^*} \frac{\partial \overline{q^{ij}}}{\partial \zeta_o}$$

Since in the experiments described in the section on the Fermi hole ellipsoid a single type of oscillation appears, we consider the

case for one fixed value of β ($\beta = 3$). We will from this point omit the β superscript assuming that the oscillations arise from a single band. Then, the oscillations due to the two ellipsoidal pockets of holes are given by

$$\tilde{\sigma}^{ij} = q_m^{ij}\, h^{-3}\, F(H,\zeta). \tag{100}$$

If we first take the case of a fixed value of ζ, $\zeta = \zeta_o$, the expression for the oscillatory tensor element becomes

$$_o\tilde{\sigma}^{ij} = q_m^{ij}(\zeta_o,H)h^{-3}\, F(\zeta_o,H). \tag{101}$$

For high magnetic fields, we have for the two tensor components under consideration*

$$q_m^{11} \approx \overline{q^{11}} = \frac{ecH_3}{H^2} \tag{102}$$

and

$$q_m^{12} \approx \overline{q^{12}} = \pm \frac{ec}{H} \tag{103}$$

where the sign is positive for electrons and negative for holes. We then write

$$_o\tilde{\sigma}_{i2} = \frac{ec}{H} \sum_\kappa 8\left(\frac{ehH}{h\kappa c}\right)^{3/2} \frac{R}{(2\pi)^{3/2}} \frac{\kappa\lambda}{\sinh \kappa\lambda} \exp 2\pi i\kappa\left(\frac{S_m c}{ehH} - \gamma\right) - i\left(\frac{\pi}{2} - \frac{\pi}{4}\right). \tag{104}$$

The extra factor of two appears since there are two ellipsoids of holes. A similar expression can be written for the $_o\tilde{\sigma}_{11}$ by replacing $-\frac{ec}{H}$ in Eq. (104) by ecH_3/H^2.

It has been shown by Lifshitz[60] that the oscillation of the Fermi energy $\zeta = \zeta(H)$ must also be considered. This behavior, which is neglected in the de Haas-van Alphen theory, plays a more fundamental

---

*See the preceeding section.

[60] Lifshitz, I., Soviet Physics JETP 5, 1227 (1957).

role in the transport phenomena because of the larger magnitude of the σ^{ij}. That is, a second term will appear in the oscillatory part of the σ^{ij} as the condition affecting the system is not $\zeta = \zeta_o$ but rather

$$\sum_\beta n_\beta = n = \text{constant.} \tag{105}$$

This condition is better stated by

$$n_E - n_H = \text{constant},$$

where n_E is the total number of electrons and n_H is the total number of holes. This condition yields for the additional term

$$_c\tilde{\sigma}^{ij} = - h^{-3} \frac{\sum_\beta \frac{\partial n_o^\beta q_\beta^{ij}}{\partial \zeta_o}}{\sum_\beta \frac{\partial n_o^\beta}{\partial \zeta_o}} F(H,\zeta_o) \tag{106}$$

$$= - h^{-3} \left[\frac{\sum_\beta q_\beta^{ij} \frac{\partial n_o^\beta}{\partial \zeta_o}}{\sum_\beta \frac{\partial n_o^\beta}{\partial \zeta_o}} + \frac{\sum_\beta n_o^\beta \frac{\partial q_\beta^{ij}}{\partial \zeta_o}}{\sum_\beta \frac{\partial n_o^\beta}{\partial \zeta_o}} \right] F(H,\zeta_o)$$

in which n_o^β should be taken as positive for electrons and negative for holes. In the expression, the first term represents the contribution due to the rearrangement of the carriers in the different bands. The second term accounts for the possible change of mobility as the Fermi energy changes with magnetic field. For simplicity of argument, we examine the case of the transverse effect, $_c\tilde{\sigma}^{12}$. At very high magnetic fields, where all bands obey asymptotic conditions, it is seen that for

each value of β the q_β^{12} can be found by Eq. (103). It follows that $\partial q_\beta^{12}/\partial \zeta_o \approx 0$. Thus, it is seen that for high fields (asymptotic conditions), the first term of Eq. (106) will cancel the ${}_o\tilde{\sigma}^{12}$ leaving for the total oscillatory part of the σ_{12} only the very small contribution of the second term in Eq. (106)--no oscillations should appear. Experimentally, we find that there <u>are</u> pronounced oscillations in the high field range. This is shown in Figs. 13 and 17. This implies simply that some band (or bands) in bismuth has not reached its asymptotic value in the range of fields used in the experiments. From the presentation of the previous section, it is seen that the low mobility hole band ($\beta = 5$) is that which enhances these high field oscillations. Let us write the expression for the total oscillation in σ_{12} for the high fields assuming that all bands have reached asymptotic conditions except band number five. The expression is

$$\tilde{\sigma}^{12} = {}_o\tilde{\sigma}^{12} + {}_c\tilde{\sigma}^{12}$$

$$= h^{-3}\left[{}_{81}q^{12}\, F^{(3)} - \frac{\sum_\beta q_\beta^{12} \dfrac{\partial n_o^\beta}{\partial \zeta_o}}{\sum_\beta \dfrac{\partial n_o^\beta}{\partial \zeta_o}} F^{(3)} - \frac{\sum_\beta n_o^\beta \dfrac{\partial q_\beta^{12}}{\partial \zeta_o}}{\sum_\beta \dfrac{\partial n_o^\beta}{\partial \zeta_o}} F^{(3)} \right] \tag{107}$$

$$= -\frac{ec}{H}\left[1 - \frac{\left|\dfrac{\partial n^{(1)}}{\partial \zeta}\right| + \left|\dfrac{\partial n^{(2)}}{\partial \zeta}\right| + \left|\dfrac{\partial n^{(3)}}{\partial \zeta}\right| + \left|\dfrac{\partial n^{(4)}}{\partial \zeta}\right| + \dfrac{H^2}{H^2 + H_5^2}\dfrac{\partial n^{(5)}}{\partial \zeta}}{\left|\dfrac{\partial n^{(1)}}{\partial \zeta}\right| + \left|\dfrac{\partial n^{(2)}}{\partial \zeta}\right| + \left|\dfrac{\partial n^{(3)}}{\partial \zeta}\right| + \left|\dfrac{\partial n^{(4)}}{\partial \zeta}\right| + \left|\dfrac{\partial n^{(5)}}{\partial \zeta}\right|} \right] h^{-3} F^{(3)}$$

The small contribution of the $\partial q_\beta^{12}/\partial \zeta_o$ has been neglected. The absolute value signs are used for convenience since a) the coefficients would

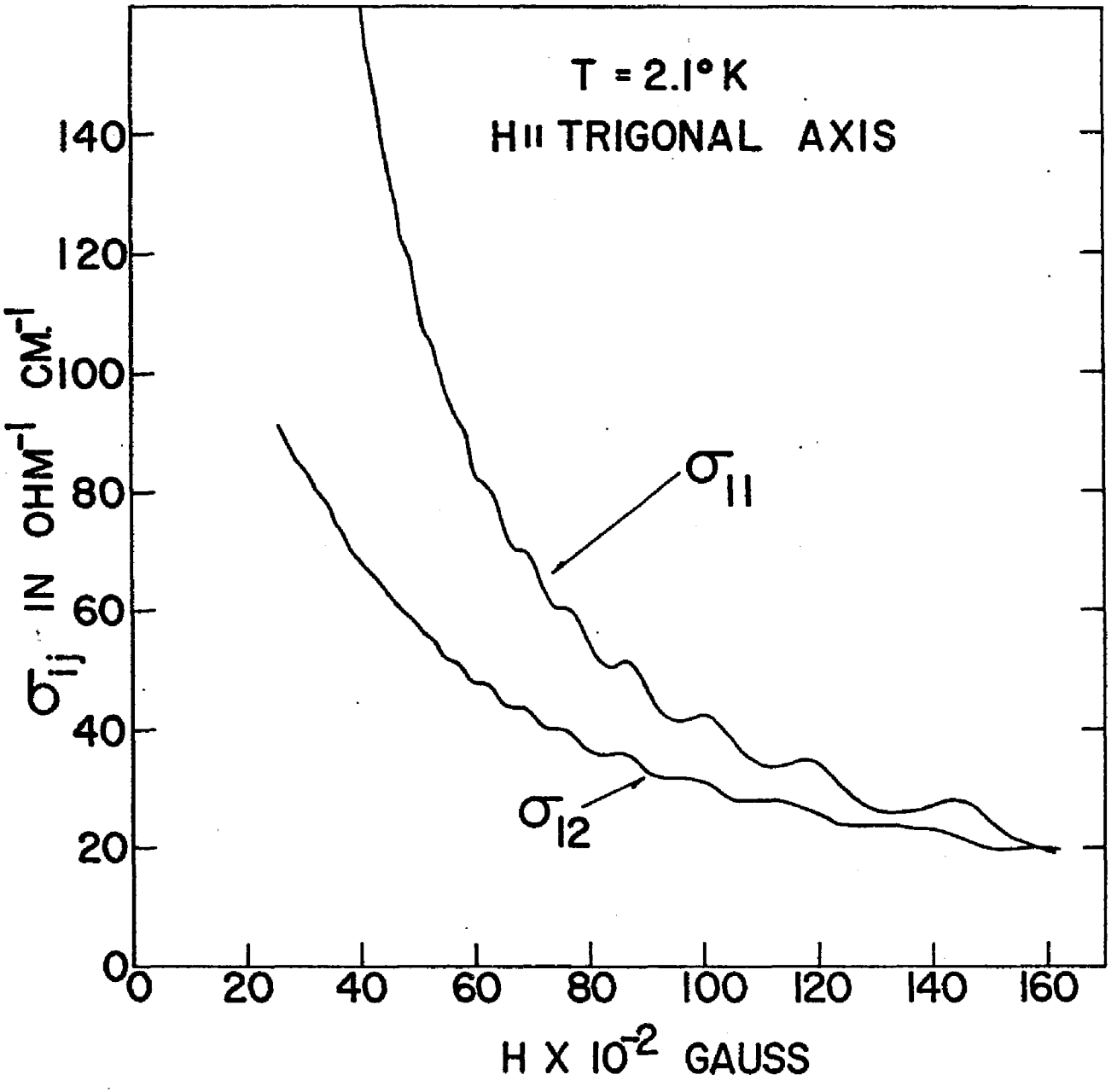
T = 2.1° K
H∥ TRIGONAL AXIS
σ11
σ12
σij IN OHM-1 CM-1
H X 10-2 GAUSS
0
20
40
60
80
100
120
140
160

Fig. 17

be positive for electrons and negative for holes and b) $\partial n/\partial \zeta > 0$ for electrons and $\partial n/\partial \zeta < 0$ for holes. After rearranging the expression we can write

$$\tilde{\sigma}^{12} = -\frac{ec}{H}\left[\frac{\dfrac{H_5^2}{H^2+H_5^2}\left|\dfrac{\partial n^{(5)}}{\partial \zeta}\right|}{\left|\dfrac{\partial n}{\partial \zeta}\right|}\right] h^{-3} F^{(3)} \tag{108}$$

$$= {}_o\tilde{\sigma}^{12}\left[\frac{H_5^2}{H_5^2+H^2}\right]\frac{\left|\partial n^{(5)}/\partial \zeta\right|}{\left|\partial n/\partial \zeta\right|}$$

Note that

$${}_o\tilde{\sigma}^{12} = \sum_\kappa {}_\kappa\tilde{\sigma}^{12} = \sum_\kappa \frac{h^{-3}ec}{H} F_\kappa \quad . \tag{109}$$

We can use the first term in the series ($\kappa = 1$) since most of the oscillation is seen to occur in the fundamental. Then, using Eq. (104), and taking the value of λ as determined in Table III and R = 3.6 the theoretical value of ${}_{o1}\tilde{\sigma}^{12}$ can be computed and compared to the experimentally determined $\tilde{\sigma}^{12}$ (see Table III). The results for three different high field values at 2.1°K are as follows:

$${}_{o1}\tilde{\sigma}^{12} / \tilde{\sigma}_{12} = 7.66, \quad H = 10 \text{ kilogauss}$$

$${}_{o1}\tilde{\sigma}^{12} / \tilde{\sigma}_{12} = 9.50, \quad H = 12 \text{ kilogauss}$$

$${}_{o1}\tilde{\sigma}^{12} / \tilde{\sigma}_{12} = 10.50, \quad H = 14 \text{ kilogauss}$$

where ${}_{o1}\tilde{\sigma}^{12} = .110\, H^{1/2}\lambda/\sinh\lambda$ in mho/cm if H is in gauss. If we take the approximation

$$\left|\partial n^{(5)}/\partial \zeta\right| \approx \partial n/\partial \zeta$$

we can solve for H_5 in each of the three cases using Eq. (108). The

results are given in Table V. These values are in reasonably good agreement with the H_5 proposed in Eq. (73).

Let us turn to an examination of the temperature dependence of the σ oscillations at high fields. In the approximation of Eg. (108) it is seen that the $F^{(3)}$ is the only temperature dependent quantity. It can be written more explicitly as

$$F^{(3)} = 4R\left(\frac{ehH}{e\pi c}\right)^{3/2} \sum_{\kappa} \frac{1}{\kappa^{3/2}} \frac{-\kappa\lambda}{\sinh \kappa\lambda} \exp\left[2\pi i\kappa \left(\frac{cS_m}{ehH} - \gamma\right) - i\frac{\pi}{4}\right] \qquad (110)$$

where λ is determined by (see Eq. 97)

$$\lambda = \frac{2\pi^2 kTm^*c}{\hbar eH} \qquad (111)$$

The approach we now take is to examine the amplitude of the oscillations for the two temperatures 4.2°K and 2.1°K with a fixed value of magnetic field. It should be pointed out that a degree of accuracy is lost in determining these amplitudes since the σ^{ij} is determined by computation from the ρ^{ij}, and then $\tilde{\sigma}^{ij}$ is determined graphically from the gross term. The $\tilde{\sigma}^{ij}$ are shown in Fig. 18. For the present consideration we neglect the harmonic terms, i.e. we take only the values corresponding to $\kappa = 1$. Also, the possibility of a Dingle temperature is not considered. For the two temperatures, 4.2°K and 2.1°K, we have

$$\left|\tilde{\sigma}^{12}\right|_{2.1^\circ} / \left|\tilde{\sigma}^{12}\right|_{4.2^\circ} = \frac{1}{2}\frac{\sinh 2\lambda}{\sinh \lambda}$$

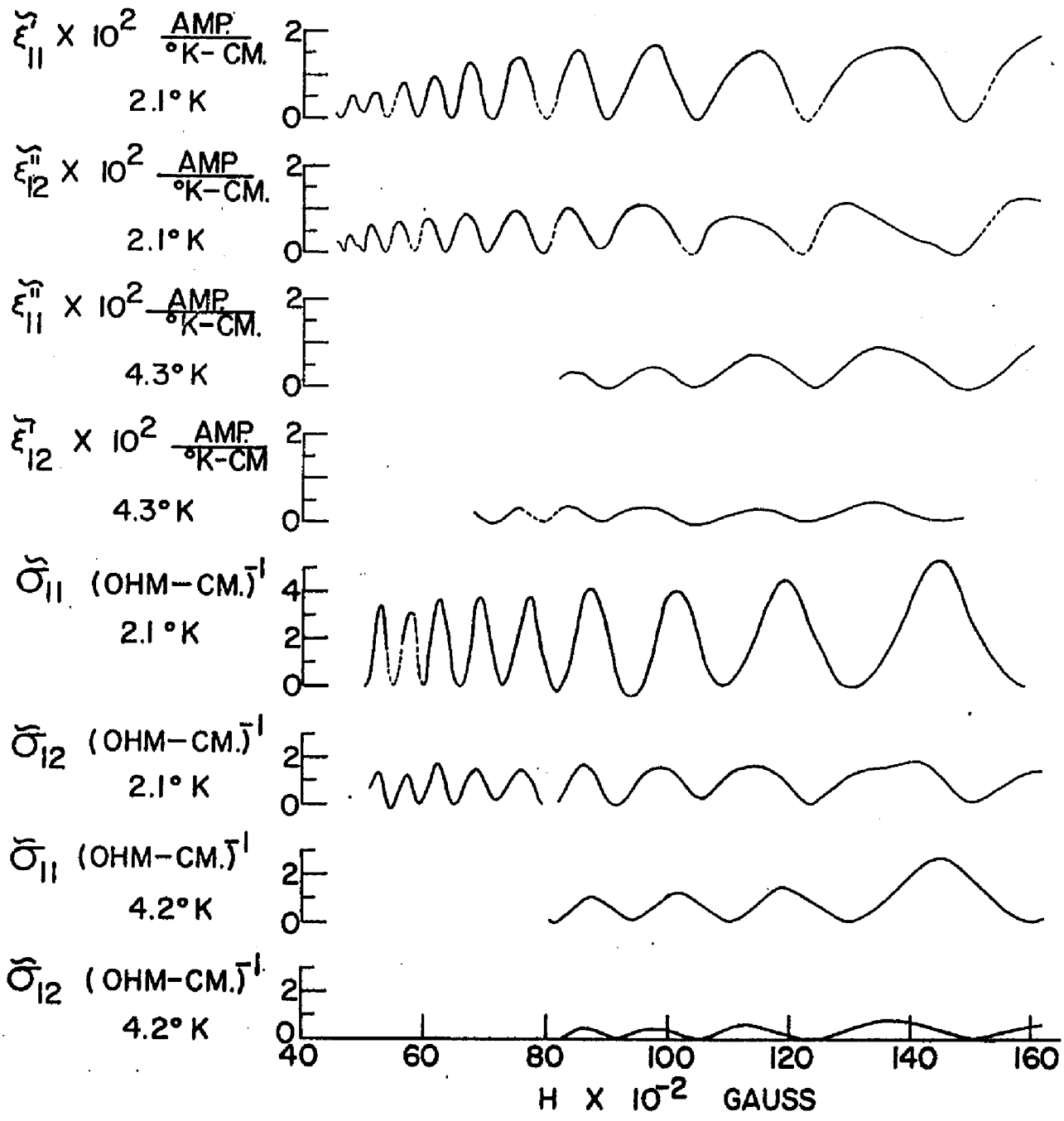
$\tilde{\xi}'_{11} \times 10^2$ AMP. °K-CM.
2.1° K
$\tilde{\xi}''_{12} \times 10^2$ AMP. °K-CM.
2.1° K
$\tilde{\xi}''_{11} \times 10^2$ AMP. °K-CM.
4.3° K
$\tilde{\xi}'_{12} \times 10^2$ AMP. °K-CM
4.3° K
$\tilde{\sigma}_{11}$ (OHM-CM.)$^{-1}$
2.1° K
$\tilde{\sigma}_{12}$ (OHM-CM.)$^{-1}$
2.1° K
$\tilde{\sigma}_{11}$ (OHM-CM.)$^{-1}$
4.2° K
$\tilde{\sigma}_{12}$ (OHM-CM.)$^{-1}$
4.2° K
2
0
4
40
60
80
100
120
140
160
H X 10^{-2} GAUSS

Fig. 18

From this relation, λ is obtained for three different values of magnetic field. Then, from Eq. (111) we compute the effective mass in the plane perpendicular to the magnetic field. The results are given in Table III.

Table III

A Comparison of Oscillation Amplitudes in the σ^{12} at 4.2°K and 2.1°K

H (kilogauss)	$2\lvert\tilde{\sigma}^{12}\rvert_{2.1^\circ}$ (mho/cm)	$2\lvert\tilde{\sigma}^{12}\rvert_{4.2^\circ}$ (mho/cm)	$\frac{\sinh 2\lambda}{\sinh \lambda}$	$\lambda_{2.1^\circ}$	$\frac{2\pi^2 kTm^*c}{\hbar e}$ (kilogauss)	$\frac{m^*}{m_o}$
10	1.58	0.42	7.50	1.996	19.96	0.0647
12	1.65	0.62	5.32	1.636	19.63	0.0636
14	1.8	0.80	4.50	1.45	20.3	0.0658

The temperature dependence of the $\tilde{\sigma}_{11}$ is the same as that of the $\tilde{\sigma}_{12}$ which has just been analyzed. Therefore, we can use a similar analysis on the $\tilde{\sigma}_{11}$ to obtain the value of the effective mass of these holes in the plane perpendicular to the magnetic field. These results are given in Table IV.

Table IV

A Comparison of Oscillation Amplitudes in the σ^{11} at 4.2°K and 2.1°K.

H (kilogauss)	$\frac{\sinh 2\lambda}{\sinh \lambda}$	$\lambda_{2.1^\circ}$	$\frac{2\pi^2 kTm^*c}{\hbar e}$ (kilogauss)	$\frac{m^*}{m_o}$	Average $\frac{m^*}{m_o}$
10	7.56	2.005	20.05	0.065	0.0648
12	6.12	1.784	21.41	0.0694	0.0665
14	4.33	1.408	19.71	0.0639	0.0648

The last column in Table IV gives the average value of m^*/m_o for the two different considerations ($\tilde{\sigma}^{12}$ and $\tilde{\sigma}^{11}$). The average value of m^*/m_o (which for this orientation of magnetic field is designated $m_\perp/m_o$) is used to compute the Fermi energy of the low mobility hole ellipsoid discussed in the initial section of this chapter.

We examine the magnitude of the $\tilde{\sigma}_{11}$ at high fields by comparing it to the corresponding expression for $\tilde{\sigma}_{12}$ given by Eq. (108). Under the same simplifying assumptions, i.e., we take $\mu = 0$, and neglect the influence of all other bands, we can write

$$\tilde{\sigma}_{11} = - q_5^{11} h^{-3} F(3).$$

This gives (see Eqs. 101, 102, and 103)

$$\tilde{\sigma}_{11} = o\tilde{\sigma}_{12} \frac{a_5 H_5 H}{H_5^2 + H^2} \tag{113}$$

where a_5 is the weighting factor described in the previous section. It is seen, then, that in this approximation the ratio of the amplitudes of the oscillatory parts of the σ^{ij} are

$$\tilde{\sigma}_{11}/\tilde{\sigma}_{12} = \frac{a_5 H}{H_5} \tag{114}$$

The experimental determination of the quantity $a_5 H_5$ can be obtained by solving Eq. (113) by successive approximation, and the determination of the quantity H_5/a_5 is made through Eq. (114). Table V summarizes the results obtained at 2.1°K.

Table V

Determination of Quantities H_5/a_5, $H_5 a_5$, H_5 and a_5 by comparing Oscillation Amplitudes of Hall Conductivity, Magnetoconductivity and $|_{o1}\sigma^{12}|$ Theoretical

H (kilogauss)	$2\tilde{\sigma}_{11}$ (mho/cm)	$2\tilde{\sigma}_{12}$ (mho/cm)	$2\,|_{o1}\tilde{\sigma}^{12}|$ (mho/cm)	H_5/a_5 (gauss)	$a_5 H_5$ (gauss)	H_5 (gauss)	a_5
10	4.35	1.58	12.1	3630	4150	3880	1.07
12	4.5	1.65	15.7	3670	4600	4110	1.12
14	5.2	1.8	18.9	3460	5950	4540	1.31

As pointed out already it may be seen that H_5 is in reasonably good agreement with the H_5 proposed in Eq. (73), and the a_5 values are in the neighborhood of unity. Data at 4.2°K yield to results in similar agreement.

An analysis of the σ^{ij} oscillations shown in Fig. 18 shows that the $\tilde{\sigma}^{11}$ and the $\tilde{\sigma}^{12}$ are not in phase, the phase difference being approximately 0.3π radians. The phase for the oscillations as predicted by the Lifshitz-Kosevich theory falls in between the two we have measured for the $\tilde{\sigma}^{11}$ and $\tilde{\sigma}^{12}$; it is within 0.1π of the phase of the experimentally determined $\tilde{\sigma}^{11}$. The harmonic content of the oscillations as predicted by the Lifshitz-Kosevich is shown in the two upper blocks of Fig. 19. The harmonic content of the experimentally determined $\tilde{\sigma}^{11}$ is in agreement with that expected from the theory in both amplitudes and phases of the harmonics. The experimentally determined $\tilde{\sigma}^{12}$ on the other hand has a considerably larger harmonic content than expected from the theory. The periods and phases of the $\tilde{\sigma}^{ij}$ are given in Table VII of the following section.

The Oscillations in the ϵ''_{ij}

As has been indicated previously, the ϵ''_{ij} are calculated from the experimental ϵ'_{ij} of Eqs. (25) and (26) by using the relation

$$\hat{\epsilon}'' = \hat{\sigma}\hat{\lambda}\hat{\epsilon}'$$

Specifically, for our geometry with the magnetic field oriented parallel to the trigonal axis of the crystal the tensor elements are given by

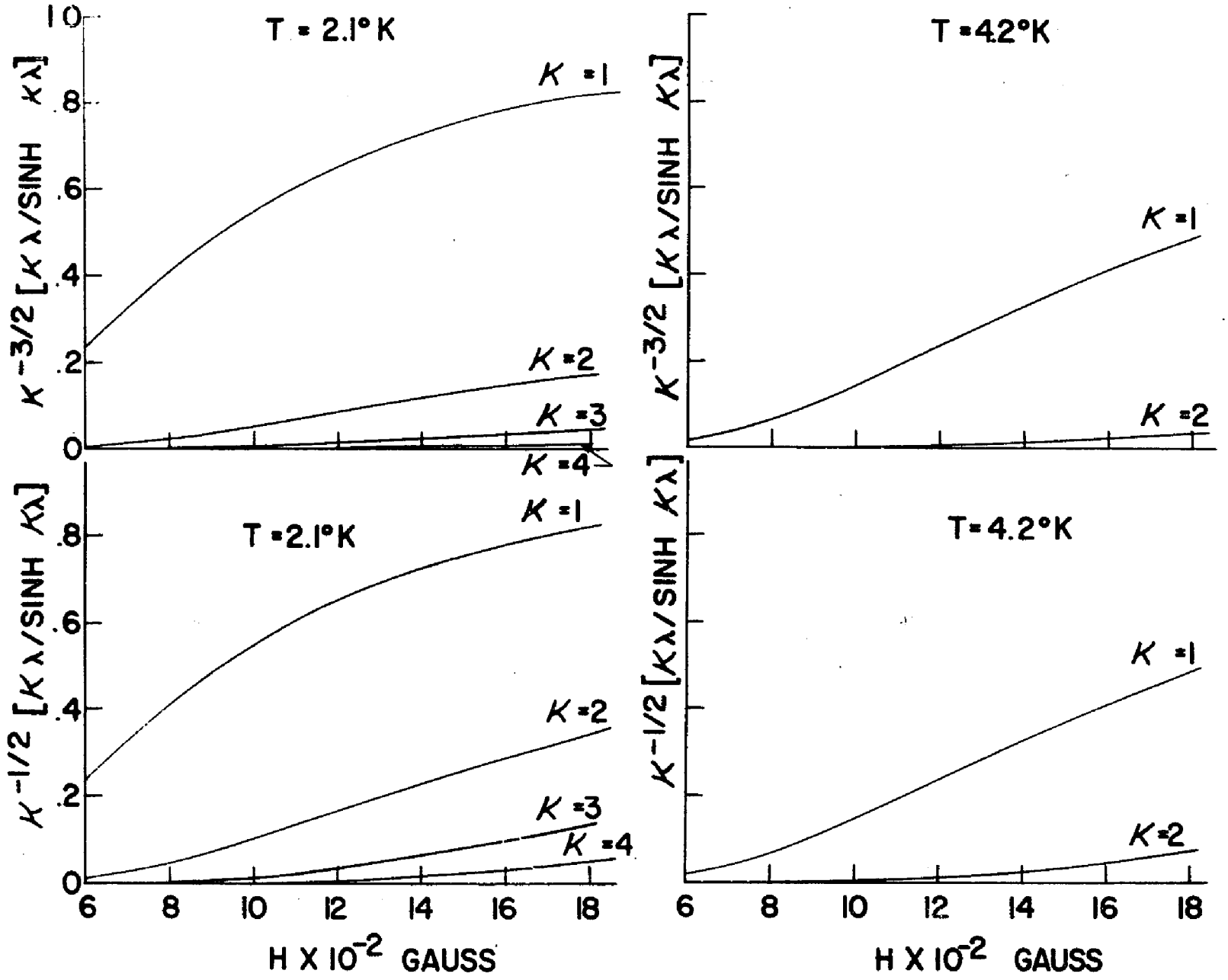
T = 2.1° K
T = 4.2° K
T = 2.1° K
T = 4.2° K
K = 1
K = 2
K = 3
K = 4
$K^{-3/2}[K\lambda/\sinh K\lambda]$
$K^{-1/2}[K\lambda/\sinh K\lambda]$
H X 10^{-2} GAUSS
H X 10^{-2} GAUSS

Fig. 19

$$\epsilon''_{11} = \epsilon''_{22} = \lambda_1 \left[\sigma_{11}\epsilon'_{11} - \sigma_{12}\epsilon'_{12}\right]$$
$$\epsilon''_{12} = -\epsilon''_{21} = \lambda_1 \left[\sigma_{11}\epsilon'_{12} + \sigma_{12}\epsilon'_{11}\right] \tag{115}$$

The experimental determination of the ϵ'_{ij} is given in Fig. 20. The experimental values of the ϵ''_{ij} are seen in Fig. 14 and 21.

In order to obtain an expression for the oscillations in the ϵ''_{12} which occur at high magnetic fields, we consider the asymptotic expression which may be obtained from Eq. (61),

$$\epsilon''_{12} = -\frac{\pi^2 k^2 c\ddot{T}}{3H} \frac{\partial n}{\partial \zeta} \quad . \tag{116}$$

We have used Eq. (83) to express the quantity in terms of the density of states. If we suppose Eq. (116) valid in the quantum case, the oscillations will arise from the variation of the carrier density $\partial n/\partial \zeta$. To obtain an expression for this, we turn to the theory of Lifshitz and Kosevich and their expression for the carrier concentration given in Eq. (93). Since the oscillations are seen to arise from the ellipsoidal hole pocket which has previously been described, we take the derivative of the carrier density n with respect to ζ for the single band ($\beta = 3$). Neglecting the small variation in A_k with energy ζ, we write for the oscillatory part of ${}_o\epsilon''_{12}$

$$\tilde{{}_o\epsilon''_{12}} = -\frac{\pi^2 k^2 cT}{3H} \frac{\partial \tilde{n}^{(3)}}{\partial \zeta} \tag{117}$$
$$= -\frac{\pi^2 k^2 cT}{3H} h^{-3} \frac{\partial}{\partial \zeta} F^{(3)}(H,\zeta).$$

This gives, in terms of ${}_{o\kappa}\tilde{\sigma}^{12}$

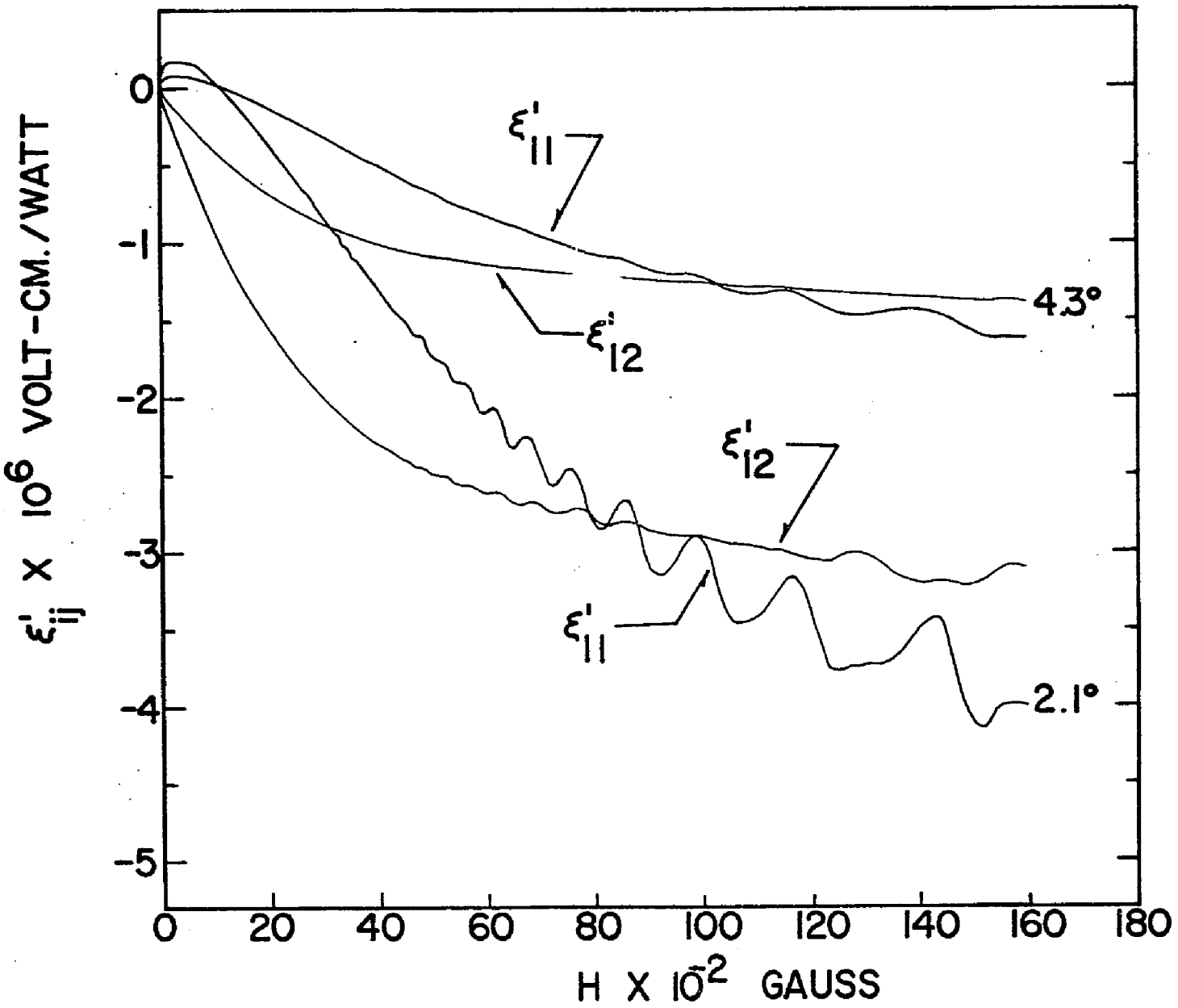
ε'_{ij} X 10^6 VOLT-CM./WATT
0
-1
-2
-3
-4
-5
ε'_{11}
ε'_{12}
4.3°
ε'_{12}
ε'_{11}
2.1°
0
20
40
60
80
100
120
140
160
180
H X 10^2 GAUSS

Fig. 20

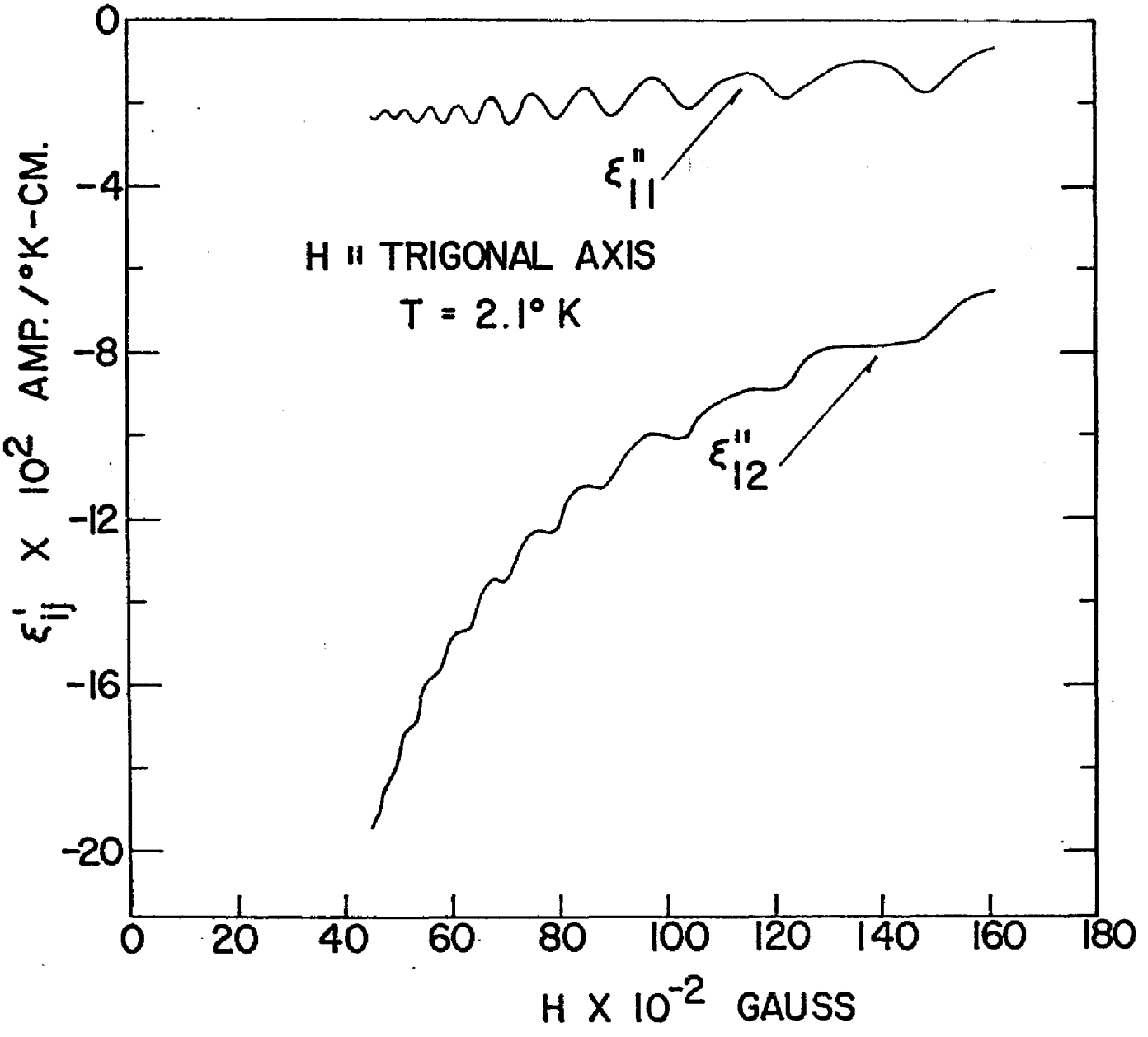
0
-4
-8
-12
-16
-20
ϵ'_{ij} X 10^2 AMP./°K-CM.
ϵ''_{11}
H = TRIGONAL AXIS
T = 2.1° K
ϵ''_{12}
0
20
40
60
80
100
120
140
160
180
H X 10^{-2} GAUSS

Fig. 21

$$ {}_{o}\tilde{\epsilon}^{jj}_{12} = \frac{4\pi^4 k^2 cm^*}{3e^2 h} \, i\frac{T}{H} \sum_{\kappa} \kappa \, {}_{o\kappa}\tilde{\sigma}^{12} $$

$$ = .86i \, \frac{T}{H} \sum_{\kappa} \kappa \, {}_{o\kappa}\tilde{\sigma}^{12} \qquad (118) $$

In Eq. (118), H is in gauss, ${}_{o}\tilde{\epsilon}^{jj}_{12}$ is in amperes/^{o}K-cm, and ${}_{o}\tilde{\sigma}^{12}$ is in mho/cm. It should be noted that the form of Eq. (116) is in agreement with the expression for ${}_{o}\tilde{\epsilon}^{jj}_{12}$ given by Bychkov, et al.[61] The corresponding expression for $\tilde{\epsilon}^{jj}_{11}$ is inherently more difficult to obtain as may be seen if one considers the companion equations from which the $\tilde{\epsilon}^{jj}_{12}$ is derived. It will not be considered here. Eq. (118) is written for $\kappa = 1$ as

$$ 2 \; {}_{o1}\tilde{\epsilon}^{jj}_{12} = .189 \; T \, H^{-1/2} \, \frac{\lambda}{\sinh \lambda} $$

in order that the values predicted by the theory may be calculated to compare with the experimental quantities of Fig. 18. Table VI gives the comparison of the experimental values with those expected from the theory we have presented

---

[61] Bychkov, Yu. A., Gurevich, L. E., and Nedlin, G. M., Soviet Physics JETP 10, 377 (1960).

Table VI

Comparison of the Experimentally Determined ϵ''_{12} to the Values Predicted by a Modified Lifshitz-Kosevich Theory.

	$T = 2.1^{\circ}K$		$T = 4.3^{\circ}K$	
	$2\lvert\tilde{\epsilon}''_{12}\rvert \times 10^2 \frac{amp}{^{\circ}K\text{-}cm}$		$2\lvert\tilde{\epsilon}''_{12}\rvert \times 10^2 \frac{amp}{^{\circ}K\text{-}cm}$	
H (kilogauss)	Predicted Value	Experimental Value	Predicted Value	Experimental Value
6	.12	.70	.018	---
8	.18	1.00	.06	.33
10	.22	1.05	.12	.35
12	.235	1.05	.175	.35
14	.24	1.20	.225	.50
16	.245	1.35	.265	---

The data of Table VI shows that, for $2.1^{\circ}K$, the expected magnetic field dependence is followed quite well by the experimental data. However, the experimental values differ by a factor of $\bar{5}$ from those expected from this simplified theory. At $4.3^{\circ}K$, the values of $\tilde{\epsilon}''_{12}$ predicted by the theory differ from experimental values by a lesser margin, the field dependence is nevertheless not as good as that at $2.1^{\circ}K$. It may also be noted that the predicted temperature variation is not satisfied.

An examination of the periods and relative phases of the oscillations in the $\tilde{\epsilon}''_{ij}$ (and also the $\tilde{\sigma}_{ij}$) yields the values given in Table VII.

Table VII

The Periods and Relative Phases* of the Oscillatory Effects

	$\tilde{\sigma}_{12}$	$\tilde{\sigma}_{11}$	$\tilde{\epsilon}_{12}$	$\tilde{\epsilon}_{11}$
$\Delta(\frac{1}{H})$ ($\times 10^{-5}$ gauss^{-1})	1.506	1.476	1.506	1.474
Phase (in radians)	0	-0.3π	0.5π	0.2π

*The phase is taken with respect to the phase of $\tilde{\sigma}_{12}$ which is $+ 0.2\pi$ with respect to that predicted by the Lifshitz-Kosevich theory.

It is seen that the period of oscillation of the $\tilde{\epsilon}''_{12}$ is the same as that for $\tilde{\sigma}_{12}$, but shifted in phase by $\pi/2$. This is in excellent agreement with the prediction of Eq. (118). The $\tilde{\epsilon}''_{11}$ and $\tilde{\sigma}_{11}$ also differ in phase by $\pi/2$, this in accord with the predictions of the theory of Zil'berman.[62]

The effects of the harmonics are more prominent for the $\tilde{\epsilon}''_{ij}$ than for the $\tilde{\sigma}_{ij}$. Note that the expression derived for $\tilde{\epsilon}''_{12}$ (Eq. 118) contains the harmonic terms

$$\frac{1}{\kappa^{1/2}} \frac{\kappa\lambda}{\sinh \kappa\lambda}$$

to be summed over κ, rather than the

$$\frac{1}{\kappa^{3/2}} \frac{\kappa\lambda}{\sinh \kappa\lambda}$$

of the $\tilde{\sigma}_{12}$ expression. This is seen by comparing the two lower blocks of Fig. 19 (which correspond to the ϵ''_{ij}) to the harmonic components of the $\tilde{\sigma}_{ij}$ given in the two upper blocks. This is borne out in the data for the ϵ'_{ij} (Fig. 20).

---

[62] Zil'berman, G. E., op. cit.

The Thermal Conductivity

Bismuth is a semi-metal with, as has been shown in the study of the galvanomagnetic effects, a carrier concentration of only about 10^{-5} per atom (see Eq. 42). This being the case, it is expected that almost all of the heat current will be carried by phonons. The thermal resistivity arises from a) scattering of the lattice waves by crystal boundaries, dislocations, and point imperfections, b) interaction between the phonons and electrons, c) scattering by impurities (which places an upper limit on the thermal conductivity), and d) anharmonic interactions between the phonons (Umklapp processes). These processes, which are listed with their increasing order of importance for increasing temperature, cause the thermal conductivity to deviate from the simple T^3 law which will be discussed presently.

A measure of the contribution of the electrons to the heat flow may be had by applying the Wiedermann-Franz law

$$\frac{\lambda_e}{\sigma} = L_n T. \tag{119}$$

L_n is the Lorenz number and is given by $L_n = 2.45 \times 10^{-8}$ volt^2 degree^{-2}. For a temperature of 4°K we obtain $\lambda_e = 3.18 \times 10^{-2}$ watt/deg-cm. It is seen by comparing this value with the thermal conductivity measured for the bismuth crystal (in Fig. 22) that the electron contribution to the total thermal conductivity is only a small fraction of one per cent. Measurements of the thermal conductivity with and without an external magnetic field served to substantuate this. Thus, we are justified in using the close approximation that all of the heat conductivity is due to the lattice.

It may be noted that in the absence of electric current $\vec{J}$, the flux of heat $\vec{w}^*$ is identical to the previously defined heat flux $\vec{w}$; this is seen from Eq. (6) by setting $\vec{J} = 0$. For our experimental study we have restricted the heat current to the 1-direction. The effects then are characterized by the relation

$$w_1^* = w_1 = \lambda_{11} G_1 + \lambda_{12} G_2$$

for our two dimensional case. Over the temperature range studied, no transverse effect was detected although several experimental attempts were made. This being the case, the thermal effects are described by

$$w_1 = \lambda_{11} G_1,$$

or

$$\lambda_{11} \approx \lambda_1 = \frac{w_1}{G_1} = \gamma^{-1} \quad ; \quad \lambda_{12} \approx 0. \tag{120}$$

The 1 subscript is used to denote thermal conductivity or resistivity due to the lattice.

The measured values for the thermal conductivity over the temperatures range under consideration are shown in Fig. 22. Shown in the same plot are experimental values reported by White and Woods[63] on a zone refined sample of bismuth containing three crystals. Also, the results obtained by Shalyt[64] on a cylindrical single crystal are shown for purposes of comparison. The theoretical T^3 dependence of the λ_1 at low temperature is shown by the dashed line (it is adjusted to fit our data for the lower temperatures).

---

[63] White, G. K., and Woods, S. B., Canad. J. Phys. 36, 342 (1958).

[64] Shalyt, S., J. Phys. USSR 8, 315 (1944).

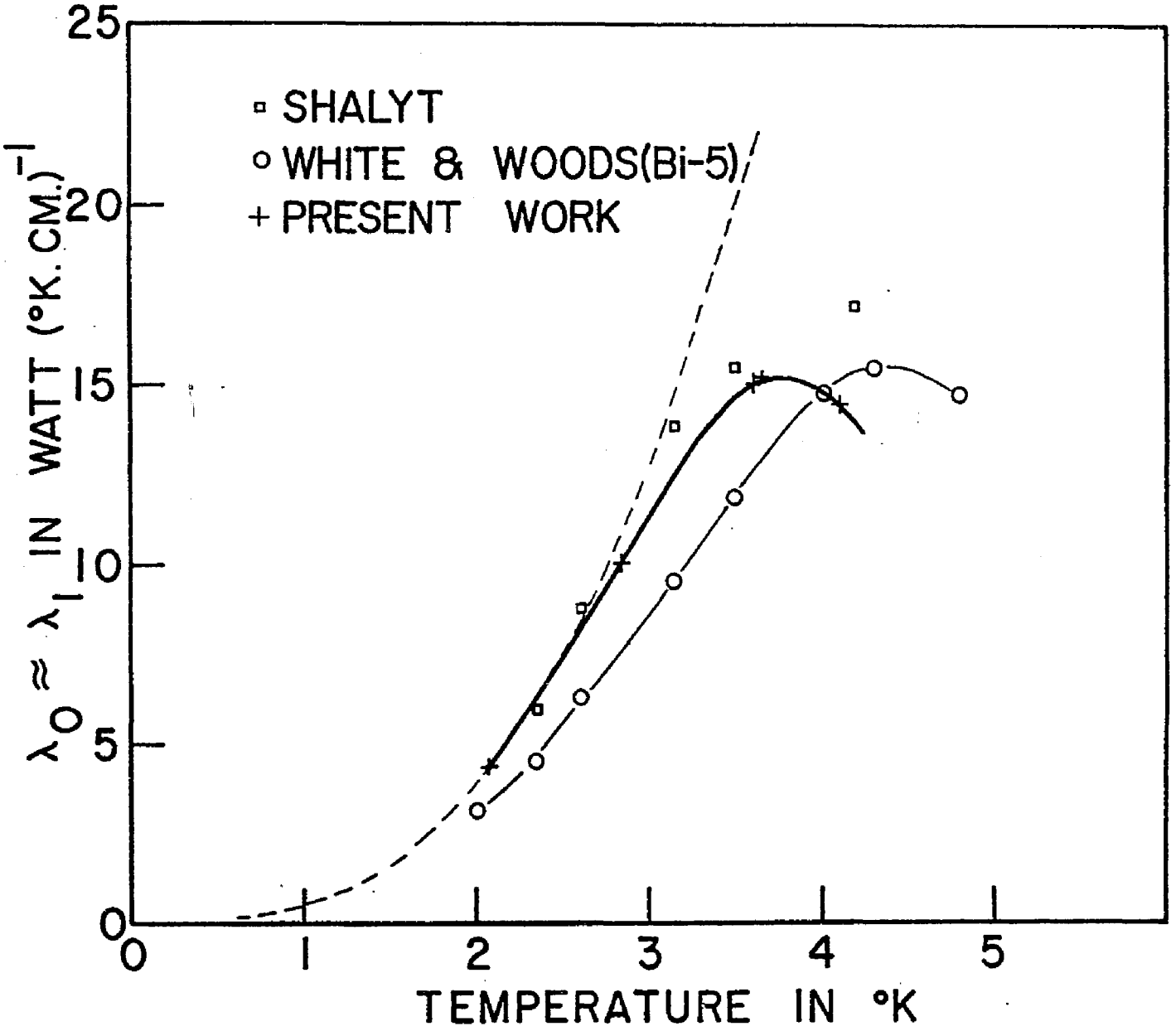
SHALYT
WHITE & WOODS(Bi-5)
PRESENT WORK
$\lambda_0 \approx \lambda_1$ IN WATT (°K. CM.)$^{-1}$
TEMPERATURE IN °K
0
5
10
15
20
25
0
1
2
3
4
5

Fig. 22

A simple theory of the lattice conductivity[65] gives

$$\lambda_l = \frac{1}{3} Cv\delta \tag{121}$$

where v is the average velocity of sound in the medium, δ is the mean free path of the phonons, and C is the specific heat given by

$$C = \frac{12\pi^4}{5} Nk \left(\frac{T}{\Theta}\right)^3 \tag{122}$$

for very low temperatures. N is the number of atoms per unit volume, k is Boltzmann's constant, and Θ is the Debye characteristic temperature. We can have an approximation for the velocity v in Eq. (121) by using a velocity calculated by taking an average value of the transverse and longitudinal velocities of propagation in the expression for the Debye frequency ν_D. Specifically, the approximate relation

$$\nu_D = \frac{k\Theta}{h} \approx v\left(\frac{3N}{4\pi}\right)^{1/3} \tag{123}$$

yields the expression for the average velocity

$$v = \frac{k\Theta}{\hbar(6\pi^2 N)^{1/3}} = 1.29 \times 10^5 \text{ cm/sec}$$

using $\Theta = 117^\circ K$.[66] If we consider that the mean free path is established at these temperatures by scattering from the boundaries of the sample, δ can be approximated by the small dimension of the crystal (2.5 cm). Then, for a temperature of $2.07^\circ K$, we find the value $\lambda_l = 5.43$ watts/$^\circ$K-cm. This compares favorably with the experimentally determined value of $\lambda_l = 4.32$ watts/$^\circ$K-cm.

Concerning the thermal conductivity data given in Fig. 22, we remark that the experimental point at $4.3^\circ K$ is considerably lower than

---

[65] Kittel, C., Solid State Physics, John Wiley and Sons, New York, 2nd ed., 1956.

[66] Kalinkina, I. N., and Strekov, P. G., op.cit.

expected and may be due in part to experimental error. Recall that the thermometers described in Chapter 2 are rather insensitive in this temperature region. A higher value of λ_1 at 4.3°K would not only be in accord with the work of other investigations[67,68], but would also give a more appropriate temperature dependence in the ϵ''_{12} as will be seen in the next section of this chapter.

It is of interest to note that oscillations similar to those discussed in the previous sections have been observed in the thermal resisitivity of bismuth at a temperature of 1.604°K by Steele and Babiskin.[69] Their attempts to detect the oscillations at higher temperatures were unsuccessful. No such oscillations have been observed in the transverse (Righi-Leduc) effect in bismuth.

The Low Mobility Hole Pocket

In the experimental data presented in the previous sections, we have shown strong evidence for the existence of an additional band of holes of quite low mobility (the $\beta = 5$ band). At this point we will recall this evidence, and then present further evidence for the low mobility hole pocket. Additional parameters for this pocket will also be determined.

The characteristics of the fifth band have been determined in the following ways: 1) Analysis of the conductivities by

---

[67] White, G. K. and Woods, S. B., op.cit.

[68] Shalyt, S., op.cit.

[69] Steele, M. C., and Babiskin, J., Phys. Rev. 98, 359 (1955).

Sondheimer-Wilson theory has indicated a low mobility hole band with

$$H_5 \approx 2500 \text{ gauss}, \quad n_5 \approx 0.45 \times 10^{18} \text{cm}^{-3}.$$

2) The fifth band ($\beta = 5$) is needed to account for the experimentally measured values of ϵ''_{11} and ϵ''_{12} (see Eq. 84). The indication here is that

$$H_5 \geq 1300 \text{ gauss}.$$

3) A study of the oscillations in the σ^{12} at selected values of H using the Lifshitz-Kosevich theory has given

$$H_5 \approx 3880 \text{ gauss}$$

$$H_5 \approx 4110 \text{ gauss}$$

$$H_5 \approx 4540 \text{ gauss}.$$

4) A comparison of ${}_{o1}\tilde{\sigma}^{12}$ to $\tilde{\sigma}_{11}$ for different values of H (Eq. 113) gives

$$a_5 H_5 \sim 4150 \text{ gauss}$$

$$a_5 H_5 \sim 4600 \text{ gauss}$$

$$a_5 H_5 \sim 5950 \text{ gauss}.$$

Let us now turn to an anlysis of the temperature variation in the ϵ''_{12} in order to obtain additional parameters for this band. We evaluate the integral of Eq. (57) for the determination of the ϵ''_{12} with relation

$$-\int_o^\infty \phi(E) \frac{\partial f_o}{\partial E} dE = \phi(\zeta_5) + \frac{\pi^2}{6} k^2 T^2 \left.\frac{d^2\phi}{dE^2}\right|_{E=\zeta_5} + \frac{14\pi^2}{720} k^4 T^4 \left.\frac{d^4\phi}{dE^4}\right|_{E=\zeta_5} \qquad (124)$$

Note that this is the same as Eq. (60) with the addition of a second

correction term. It results that

$$\epsilon''_{12} = -\frac{\pi^2 k^2 cT}{2H}\left(\frac{n_5}{\zeta_5}\right)_o\left[1 - \frac{7}{120}\pi^2\left(\frac{T}{T_5}\right)^2\right] \tag{125}$$

if ζ_5 is considered to be constant. If n_5 is held constant we obtain

$$\epsilon''_{12} = -\frac{\pi^2 k^2 cT}{2H}\left(\frac{n_5}{\zeta_5}\right)_o\left[1 - \frac{\pi^2}{10}\left(\frac{T}{T_5}\right)^2\right] \tag{126}$$

The condition $\sum_\beta n^{(\beta)} =$ constant will yield a more complex expression with the factor α included in the expression as

$$\epsilon''_{12} = -\frac{\pi^2 k^2 cT}{2H}\left(\frac{n_5}{\zeta_5}\right)_{T=0}\left[1 - \alpha\frac{\pi^2}{10}\left(\frac{T}{T_5}\right)^2\right] \tag{127}$$

We will take the approximation that $\alpha = 1$. In the preceeding equations, T_5 is the Fermi temperature for the band under consideration, defined by

$$\zeta_5)_o = kT_5 \tag{128}$$

If we express the above consideration in terms of the density of states, we have

$$\frac{\partial n_5}{\partial \zeta_5})_T = \frac{\partial n_5}{\partial \zeta_5})_o\left[1 - \frac{\pi^2}{10}\left(\frac{T}{T_5}\right)^2\right]. \tag{129}$$

The density of states as a function of temperature calculated from the experimental data at 8000 gauss is shown in Fig. 23. The straight line is the value for Γ = constant as given by Kalinkina and Strekov from specific heat measurements.[70] The extrapolation of the curve for the present data to zero indicates a Fermi temperature for the

---

[70] Kalinkina, I. N., and Strekov, P. G., op.cit.

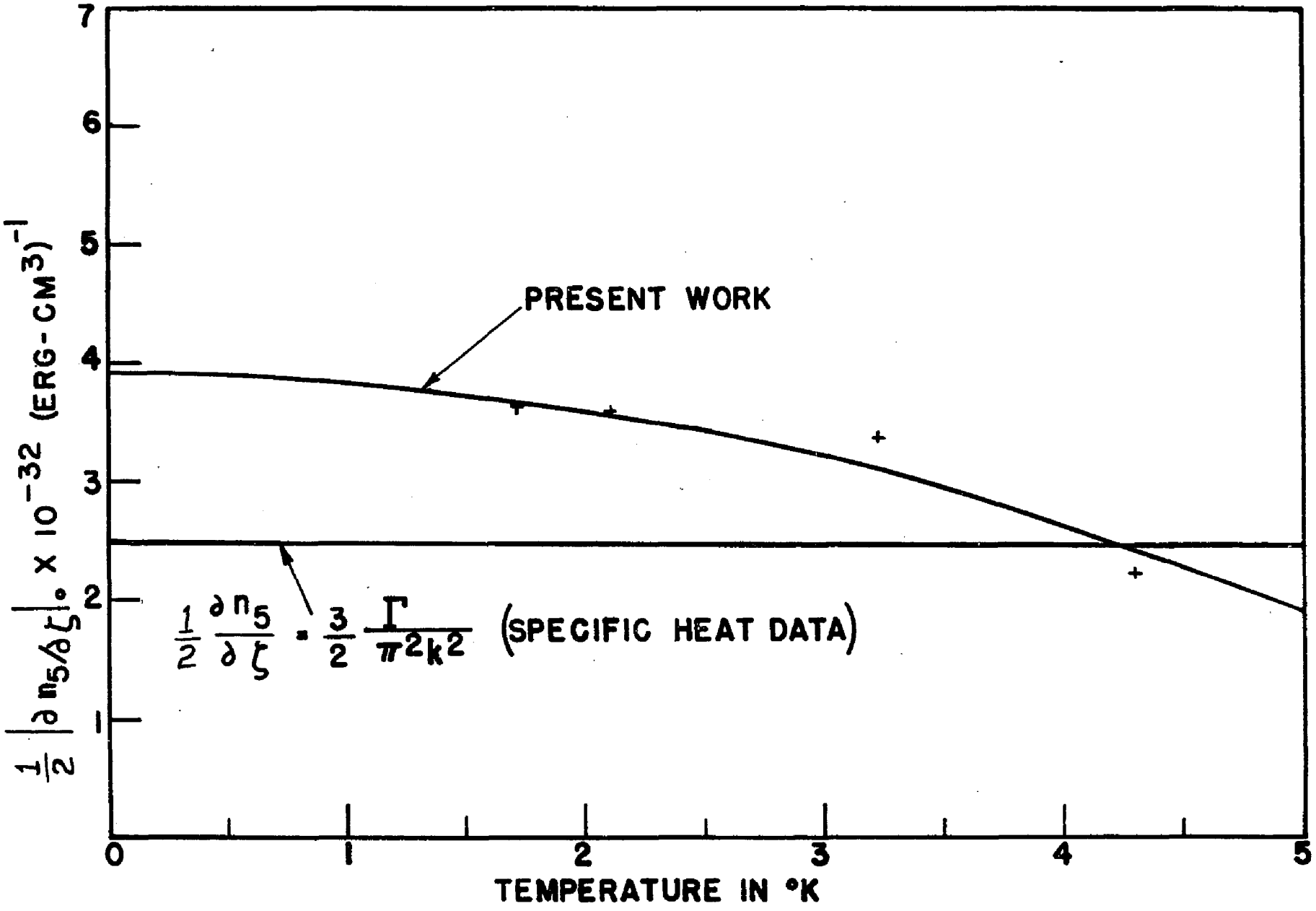
7
6
5
4
3
2
1
0
1
2
3
4
5
PRESENT WORK
$\frac{1}{2}\frac{\partial n_5}{\partial \zeta} = \frac{3}{2}\frac{\Gamma}{\pi^2 k^2}$ (SPECIFIC HEAT DATA)
$\frac{1}{2}\left|\partial n_5/\partial \zeta\right|_0 \times 10^{-32}$ (ERG-CM^3)$^{-1}$
TEMPERATURE IN °K

Fig. 23

fifth pocket of $T_5 = 7^{\circ}K$. The spread of the experimental points which leads to inaccuracy in the determination of the Fermi temperature is probably due to error in the measurement of the thermal conductivity at the higher temperatures. It seems likely (as was mentioned in the previous section) that the experimental point at $4.3^{\circ}K$ should be somewhat greater, and the Fermi temperature lies in the range

$$7^{\circ}K < T_5 < 14^{\circ}K.$$

Taking the value of $|dn_5/d\zeta|_o = 7 \times 10^{32}(\text{erg-cm}^{-3})^{-1}$, we determine the value of n_5 (see Eq. 83). For quadratic bands, the effective mass is computed from (see Eq. 33)

$$m^* = \frac{\hbar^2}{2\zeta_5} (3\pi^2 \frac{n_5}{p})^{2/3} \tag{130}$$

where in the expression we have allowed for the possibility of the band being composed of p pockets. Table VIII shows the values we have obtained for these parameters of the fifth band using successively the values of $7^{\circ}K$ and $14^{\circ}K$ for the Fermi temperature.

Table VIII

Parameters of the Low Mobility Hole Band

T_5 ($^{\circ}K$)	ζ_5 (ergs per electron)	n_5 (cm^{-3})	m^*/m_o p = 1	p = 2	p = 3	p = 6
7	$\sim 10^{-15}$	$\sim 0.5 \times 10^{18}$	3.67	2.30	1.76	1.11
14	$\sim 2 \times 10^{-5}$	$\sim 10^{18}$	2.91	1.83	1.40	0.88

The above results for the effective mass are computed under the assumption that the pockets are spherical. Another effective mass

for this pocket, the cyclotron effective mass, may be obtained--at least in order of magnitude--by comparing the saturation field H_5 we have obtained to the known cyclotron mobilities of the Shoenberg electron pocket and the low mobility hole pocket. We make the comparison by assuming that the relaxation time for each pocket is approximately the same. The parameters are a) $H_2 \approx 120$ gauss, $m_2 \approx 0.08\ m_o$, for the Shoenberg electrons,[71] and b) $H_3 \approx 250$ gauss, $m_3 \approx 0.065\ m_o$, for the low mobility hole ellipsoid. We obtain (see Eq. 34)

$$m^* \sim 0.65\ m_o$$

by comparison with the low mobility holes, and

$$m^* \sim 1.65\ m_o$$

by comparison with the Shoenberg electrons. These results are not conclusive, but do indicate that m_5^* is in the neighborhood of the mass of the free electron m_o.

In conclusion, we can make some remarks concerning the general nature of the low mobility hole pocket. Since it has been seen that $a_5 \approx 1$, we might suppose that the low mobility hole ellipsoid has an axis of symmetry along the trigonal axis, as is the case for the high mobility ellipsoid we have previously discussed. The number of pockets, then, is quite possibly equal to two. The cyclotron mass would enable us to determine the cross sectional area perpendicular to the trigonal axis S_m, and a comparison with the effective mass of Table VIII which depends upon the volume of the ellipsoid would enable us to know the eccentricity of the pocket.

---

[71] Galt, J. K., et al., op. cit.

These calculations are not given as the precision of the parameters we have presented are such that only a vague picture of the ellipsoid is possible. It may be noted that, taking $T_5 = 14^{o}K$, and the cyclotron mass $m_5 = m_o$, the expected period of oscillation associated with this band with the magnetic field parallel to the trigonal axis is $\Delta(\frac{1}{H}) \approx 0.9 \times 10^{-5}$ gauss^{-1}. Since these oscillations are much smaller than those from the high mobility hole pocket ($\beta = 3$), it would be extremely difficult to identify them in the experimental data.

APPENDIX Ia

Important Quantities Relating to the Bismuth Crystal.

a) Crystal structure of bismuth: Rhombohedral (trigonal)

$a = b = c = 4.74$ angstroms; $\alpha = \beta = \gamma = 57^{o}41'$

b) Atomic volume: 21.3 cm^3/mole

c) Crystal size: 24.3 mm x 6.9 mm x 2.5 mm

d) Probe distances: transverse--6.6 mm, longitudinal--17.0 mm

e) Resistivity ratio

$$\frac{|\rho_o|_{293^{o}K}}{|\rho_o|_{o^{o}K}} = \frac{121.95 \times 10^{-6} \text{ ohm-cm}}{2.96 \times 10^{-6} \text{ ohm-cm}} = 41.2$$

APPENDIX Ib

The Resistivity of the Crystal at Liquid Helium Temperatures

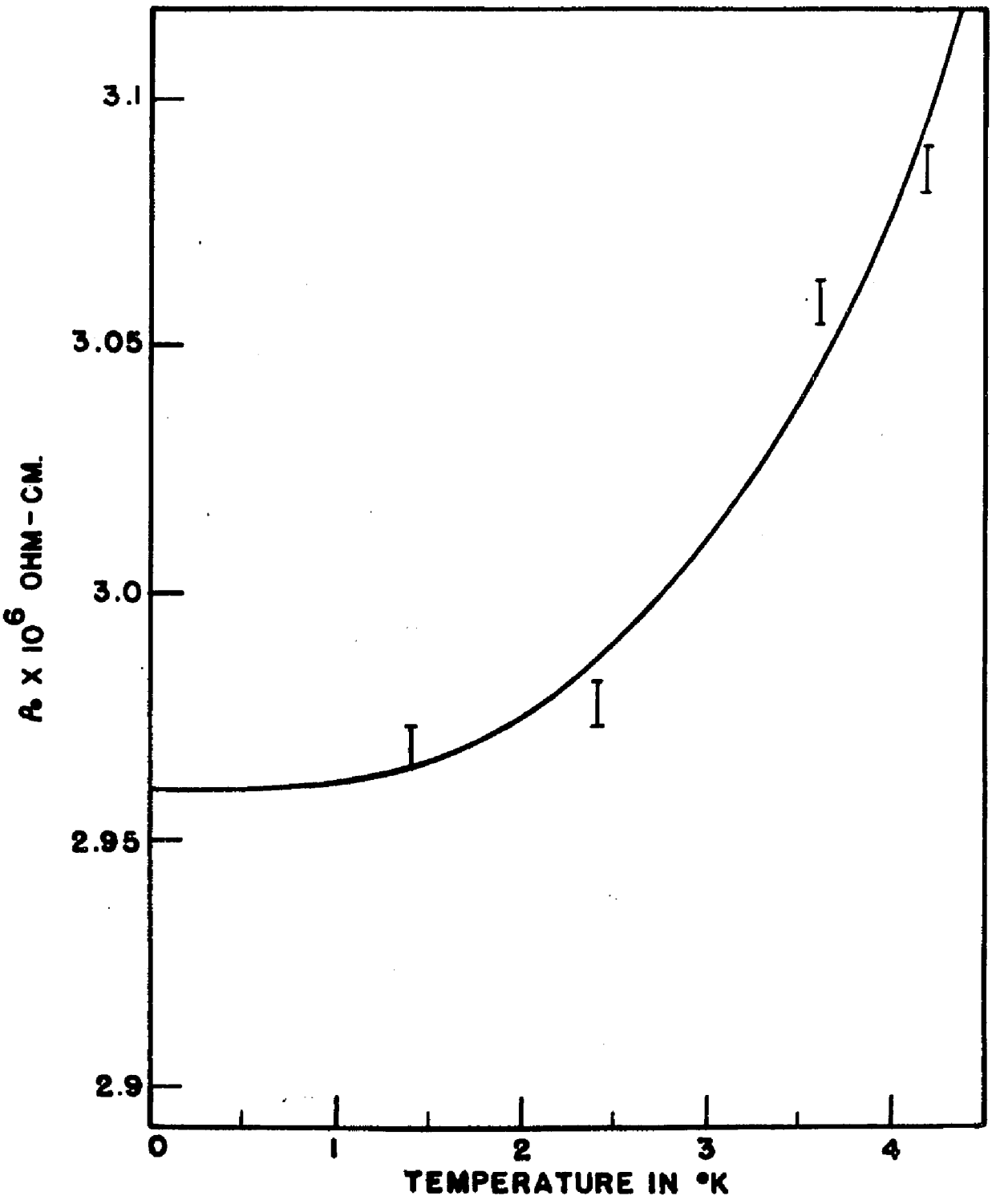

APPENDIX II

Data for the calibration curve of the high field magnet:

I (amperes)	H (gauss)	I (amperes)	H (gauss)
5.0	1684	15.0	5051
5.25	1768	15.25	5135
5.5	1852	15.5	5219
5.75	1936	15.75	5303
6.0	2020	16.0	5387
6.25	2104	16.25	5471
6.5	2189	16.5	5556
6.75	2273	16.75	5640
7.0	2357	17.0	5724
7.25	2441	17.25	5808
7.5	2525	17.5	5892
7.75	2609	17.75	5976
8.0	2694	18.0	6061
8.25	2778	18.25	6145
8.5	2862	18.5	6229
8.75	2946	18.75	6313
9.0	3030	19.0	6397
9.25	3114	19.25	6481
9.5	3199	19.5	6566
9.75	3283	19.75	6650
10.0	3367	20.0	6734
10.25	3451	20.25	6818
10.5	3535	20.5	6902
10.75	3620	20.75	6987
11.0	3704	21.0	7071
11.25	3788	21.25	7155
11.5	3872	21.5	7239
11.75	3956	21.75	7323
12.0	4040	22.0	7407
12.25	4125	22.25	7491
12.5	4209	22.5	7576
12.75	4293	22.75	7660
13.0	4377	23.0	7744
13.25	4461	23.25	7828
13.5	4545	23.5	7912
13.75	4630	23.75	7997
14.0	4714	24.0	8081
14.25	4798	24.25	8165
14.5	4882	24.5	8249
14.75	4966	24.75	8333

I (amperes)	H (gauss)	I (amperes)	H (gauss)
25.0	8418	37.0	12300
25.25	8502	37.5	12450
25.5	8586	38.0	12600
25.75	8670	38.5	12730
26.0	8754	39.0	12860
26.25	8838	39.5	13000
26.5	8923	40.0	13150
26.75	9007	40.5	13280
27.0	9091	41.0	13400
27.25	9175	41.5	13530
27.5	9259	42.0	13660
27.75	9343	42.5	13770
28.0	9428	43.0	13880
28.25	9512	43.5	13990
28.5	9596	44.0	14100
28.75	9680	44.5	14200
29.0	9764	45.0	14300
29.25	9848	45.5	14400
29.5	9933	46.0	14490
29.75	10017	46.5	14600
30.0	10101	47.0	14700
30.5	10269	47.5	14790
31.0	10438	48.0	14870
31.5	10606	48.5	14960
32.0	10779	49.0	15060
32.5	10943	49.5	15160
33.0	11111	50.0	15250
33.5	11250	51.0	15420
34.0	11400	52.0	15580
34.5	11560	53.0	15740
35.0	11700	54.0	15870
35.5	11850	55.0	16000
36.0	12020	56.0	16120
36.5	12160	57.0	16230

APPENDIX III

Numerical data for the hole ellipsoid:

ψ	$\cos^2\psi$	$\Delta(1/H)$ $\times 10^5 \text{gauss}^{-1}$	$\Delta^2(1/H)$ $\times 10^{10}\text{gauss}^{-2}$	$S_m(\zeta)$ $\times 10^{42}\frac{\text{gm}^2\text{cm}^2}{\text{sec}^2}$
0.3	1.0000	1.524	2.322	6.967
6.2	.9884	1.520	2.310	6.986
15.2	.9312	1.470	2.161	7.223
19.7	.8864	1.440	2.074	7.374
24.2	.8319	1.400	1.960	7.584
30.95	.7355	1.320	1.742	8.044
37.7	.6260	1.230	1.513	8.633
45.3	.4948	1.105	1.221	9.609
46.7	.4703	1.110	1.232	9.966
50.1	.4115	1.025	1.051	10.360
54.6	.3356	.958	.918	11.083
59.1	.2637	.860	.739	12.346
63.6	.1977	.776	.602	13.682
68.1	.1391	.680	.462	15.614
-11.8	.9582	1.500	2.250	7.079
-16.3	.9212	.465	2.146	7.249
-25.3	.8174	1.395	1.946	7.611
-34.3	.6824	1.285	1.651	8.263
-43.3	.5297	1.145	1.311	9.273
-44.7	.5052	1.130	1.277	9.396
-49.5	.4219	1.035	1.071	10.259
-54.0	.3455	.970	.941	10.946
-58.5	.2730	.873	.762	12.163
-63.0	.2061	.790	.624	13.441
-67.5	.1465	.726	.527	14.625

APPENDIX IVa

Numerical data for the ρ_{ij}, σ_{ij}, ϵ'_{ij}, and ϵ''_{ij} at 2.1°K:

H	ρ_{11} x10^{4}ohm-cm	ρ_{21} x10^{4}ohm-cm	σ_{11} mho/cm	σ_{12} mho/cm	ϵ'_{11} x10^{6}volt-cm/watt	ϵ'_{21} x10^{6}volt-cm/watt	ϵ''_{11} x10^{4}amp/°K-cm	ϵ''_{12} x10^{4}amp/°K-cm
2694	28.36	7.61	328.93	88.26	- 68.23	-189.55	-267.25	-3199.73
2862	31.35	9.09	294.24	85.32	- 76.08	-196.37	-263.64	-3007.95
3030	34.29	10.80	265.31	83.56	- 84.30	-202.66	-254.17	-2845.96
3199	37.23	12.39	241.82	80.48	- 92.16	-208.40	-258.07	-2705.58
3367	40.31	14.43	219.90	78.72	-100.37	-214.05	-244.39	-2572.66
3535		16.14			-108.23	-218.81		
3704	46.79	18.30	185.37	72.50	-115.38	-223.30	-243.26	-2328.61
3788	48.33	19.09	178.99	70.70	-120.38	-225.81	-261.20	-2289.79
3872	49.92	20.23	172.06	69.73	-123.95	-228.15	-253.60	-2241.63
3956	51.32	21.36	166.09	69.13	-125.73	-229.40	-235.12	-2189.85
4040	52.51	22.39	160.51	68.05	-131.45	-231.74	-249.39	-2159.36
4125	54.72	23.75	153.78	66.75	-134.31			
4209	55.84	24.66	149.86	66.18	-138.59			
4293	57.15	25.68	145.58	65.42				
4377	59.20	26.93	139.96	63.67				
4461	60.65	28.18	135.61	63.01		-240.53		
4545	61.95	29.20	132.08	62.25	-152.17	-241.25	-237.71	-1934.54
4630	63.77	30.45	127.70	60.98	-157.17	-244.12	-242.65	-1907.42
4714	65.64	31.93	123.20	59.93	-159.85	-245.56	-232.92	-1864.07
4798	66.62	32.84	120.76	59.53	-160.03	-245.92	-219.31	-1835.63
4882	67.92	33.75	118.08	58.67	-163.96	-247.17	-227.31	-1816.07
4966	69.98	35.45	113.72	57.61	-171.46	-249.33	-240.31	-1789.12
5051	72.26	37.16	109.45	56.28	-174.14	-250.94	-230.94	-1744.00
5135	73.38	38.30	107.10	55.90	-174.67	-251.12	-218.54	-1715.65
5219	74.22	38.86	105.75	55.37	-176.46	-251.48	-221.65	-1701.77
5303	75.57	39.66	103.75	54.45	-182.53	-253.10	-241.34	-1694.06

H	ρ_{11} x10^4ohm-cm	ρ_{21} x10^4ohm-cm	σ_{11} mho/cm	σ_{12} mho/cm	ϵ'_{11} x10^6volt-cm/watt	ϵ'_{21} x10^6volt-cm/watt	ϵ''_{11} x10^4amp/°K-cm	ϵ''_{12} x10^4amp/°K-cm
5387	77.91	41.48	100.01	53.24	-189.32	-255.79	-248.67	-1668.90
5471		43.30			-191.46	-257.40		
5556		44.77			-190.39	-257.40		
5640	82.34	45.57	92.97	51.45	-190.75	-257.04	-210.97	-1577.73
5724	83.46	46.14	91.77	50.73	-195.92	-258.30	-228.17	-1574.55
5808		47.16			-202.89	-260.10		
5802		49.55			-209.68	-262.43		
5976	90.22	51.70	83.44	47.82	-211.11	-263.33	-235.11	-1500.69
6061	90.83	52.84	82.26	47.85	-208.61	-263.42	-213.12	-1481.23
6145	90.92	53.18	81.95	47.93	-207.18	-262.79	-205.07	-1472.61
6229	91.62	53.75	81.20	47.64	-209.68	-263.15	-210.14	-1467.45
6313	93.67	54.55	79.72	46.43	-217.54	-265.30	-235.18	-1462.47
6397	96.61	56.82	76.91	45.23	-226.11	-267.01	-248.61	-1439.66
6481	99.50	59.32	74.15	44.21	-232.18	-268.71	-249.77	-1412.81
6566	101.37	61.59	72.05	43.78	-231.82	-269.61	-229.35	-1384.06
6650	102.26	63.30	70.70	43.76	-229.32	-269.43	-206.94	-1361.17
6734	102.40	63.75	70.38	43.82	-225.39	-270.51	-187.70	-1353.16
6818	102.54	63.64	70.40	43.70	-225.39	-268.35	-193.89	-1345.11
6902	103.33	63.86	70.03	43.28	-230.75	-269.07	-211.26	-1349.24
6987	105.34	64.89	68.82	42.39	-240.75	-271.05	-237.64	-1350.58
7071	108.18	67.05	66.78	41.39	-250.04	-273.20	-252.27	-1338.25
7155	111.07	70.11	64.38	40.64	-256.47	-274.82	-250.08	-1315.81
7239	113.13	72.95	62.43	40.26	-257.54	-275.89	-232.69	-1291.36
7323	114.39	75.23	61.03	40.13	-254.68	-276.25	-208.51	-1267.34
7407	114.95	76.48	60.30	40.12	σ249.86	-275.89	-187.11	-1247.74
7491	115.09	76.59	60.22	40.08	-246.47	-274.99	-178.87	-1237.27
7576	115.46	76.48	60.20	39.87	-244.68	-274.28	-177.49	-1229.30
7660	116.30	76.36	60.08	39.45	-248.61	-274.28	-192.69	-1230.22
7744	118.02	76.93	59.47	38.76	-256.11	-275.89	-212.27	-1232.40
7828		78.18			-264.69	-277.87		
7912		81.02			-276.47	-279.48		
7997	127.63				-282.55	-281.28		

H	ρ_{11} x10^4ohm-cm	ρ_{21} x10^4ohm-cm	σ_{11} mho/cm	σ_{12} mho/cm	ϵ'_{11} x10^6volt-cm/watt	ϵ'_{21} x10^6volt-cm/watt	ϵ''_{11} x10^4amp/°K-cm	ϵ''_{12} x10^4amp/°K-cm
8081	129.78				-285.05	-282.17		
8165	130.99	90.91	51.52	35.76	-285.40	-282.89	-214.78	-1159.77
8249	131.65	92.73	50.78	35.77	-280.40	-283.07	-192.52	-1142.19
8333	131.74	93.52	50.47	35.83	-276.47	-282.71	-179.01	-1131.39
8418	131.41	93.52	50.51	35.95	-271.47	-282.26	-166.89	-1124.02
8502	131.04	92.61	50.89	35.96	-267.19	-281.82	-161.98	-1120.85
8586	130.95	91.70	51.24	35.88	-266.11	-281.82	-164.91	-1122.65
8670	131.74	91.25	51.30	35.53	-268.97	-282.00	-176.81	-1124.24
8754	133.42	92.05	50.78	35.04	-277.90	-283.25	-196.01	-1128.81
8923	140.14	96.82	48.30	33.37	-300.41	-286.84	-231.10	-1117.58
9091	146.95	104.89	45.08	32.18	-313.62	-288.10	-227.82	-1080.14
9259	150.35	112.05	42.76	31.87	-315.05	-288.64	-200.01	-1047.50
9428	151.80	116.14	41.55	31.79	-310.05	-289.71	-171.89	-1024.71
9596	152.27				-301.48	-290.97		
9764	152.41	115.57	41.66	31.59	-292.37	-290.97	-139.85	- 999.51
9933	153.06	112.84	42.33	31.21	-290.76	-291.06	-150.91	-1001.22
10101	155.76	112.16	42.28	30.44	-300.76	-292.41	-178.49	-1007.09
10269		115.23			-320.77	-294.20		
10438	168.17	122.27	38.90	28.28	-338.98	-302.82	-216.30	- 999.98
10606	172.42	132.05	36.56	28.00	-347.02	-296.09	-205.74	- 961.24
10779	174.10	139.20	35.04	28.02	-346.31	-296.00	-179.80	- 939.42
10943	174.94	143.52	34.17	28.03	-342.91	-297.07	-158.62	- 924.86
11111	175.92	145.79	33.70	27.93	-338.63	-298.69	-143.66	- 913.66
11250	177.08	145.23	33.76	27.69	-331.12	-300.39	-133.92	- 903.74
11460	177.97	142.95	34.15	27.43	-322.55	-301.74	-128.18	- 896.42
11560	179.04	140.45	34.58	27.12	-316.84	-303.00	-128.06	- 892.49
11700	180.86	138.30	34.89	26.68	-316.48	-303.27	-138.10	- 890.35
11850	184.08	138.18	34.75	26.08	-325.05	-304.70	-156.64	- 892.25
12020	189.07	140.57	34.06	25.33	-341.13	-306.23	-180.85	- 892.46
12160		145.34				-307.21		
12300	201.29	153.07	31.48	23.94		-306.77		
12450	205.21				-375.06	-306.59		

H	ρ_{11} $\times 10^4$ ohm-cm	ρ_{21} $\times 10^4$ ohm-cm	σ_{11} mho/cm	σ_{12} mho/cm	ϵ'_{11} $\times 10^6$ volt-cm/watt	ϵ'_{21} $\times 10^6$ volt-cm/watt	ϵ''_{11} $\times 10^4$ amp/°K-cm	ϵ''_{12} $\times 10^4$ amp/°K-cm
12600	207.13	170.45	28.79	23.69	-369.35	-302.55	-162.18	- 817.04
12730	207.78	178.07	27.75	23.78	-374.35	-301.38	-150.72	- 807.99
12860	208.15	183.86	26.99	23.84	-374.35	-301.38	-136.59	- 798.25
13000	208.62	187.95	26.46	23.84	-372.92	-302.91	-123.86	- 791.24
13150	209.60	190.57	26.12	23.75	-372.56	-305.24	-116.18	- 787.17
13400	211.93	192.16	25.90	23.48	-371.67	-311.79	-107.82	- 786.28
13660	213.89	189.43	26.20	23.21	-365.59	-317.09	-103.96	- 785.86
13880	215.10	183.52	26.91	22.96	-355.41	-320.59	-103.11	- 785.48
14100	216.27	177.27	27.66	22.67	-346.84	-321.31	-108.04	- 783.86
14300	218.98	172.39	28.19	22.20	-342.56	-320.59	-118.98	- 778.81
14490	224.85	172.95	27.94	21.49	-358.99	-320.50	-147.06	- 780.20
14700	233.30	179.09	26.97	20.70	-381.13	-322.02	-169.04	- 775.76
14870	242.02	191.59	25.40	20.11	-403.10	-322.38	-175.81	- 762.57
15060	248.36	206.02	23.85	19.80	-413.64	-320.77	-164.57	- 741.26
15250	250.56				-412.92	-317.63		
15420	250.70	231.59	21.52	19.88	-405.24	-313.77	-116.22	- 693.10
15580	250.18	240.57	20.77	19.97	-399.71	-310.72	- 98.10	- 675.56
15740	250.09	248.07	20.16	19.99	-399.35	-310.00	- 86.65	- 666.05
15870	250.51	252.84	19.78	19.96	-402.03	-310.72	- 81.85	- 663.07
16000	251.49	256.36	19.50	19.88	-400.24	-312.69	- 74.37	- 657.70
16120	252.61	259.32	19.28	19.79	-399.35	-315.38	- 68.19	- 654.31

Note: The values of the ϵ''_{ij} were computed using $\lambda = 4.68$ watt/°K-cm.

APPENDIX IVb

Numerical data for the ρ_{ij}, σ_{ij}, ϵ'_{ij}, and ϵ''_{ij} at 4.3°K:

H gauss	$\times 10^4 \rho_{11}$ ohm-cm	$\times 10^4 \rho_{21}$ ohm-cm	σ_{11} $\times 10^{-4}$ mho/cm	σ_{12} $\times 10^{-4}$ mho/cm	ϵ'_{11} $\times 10^6$ volt-cm/watt	ϵ'_{12} $\times 10^6$ volt-cm/watt	ϵ''_{11} $\times 10^4$ amp/°K-cm	ϵ''_{12} $\times 10^4$ amp/°K-cm
0	3.24	0	30.83	0	2.56	0	106555	0
2	3.25	- .09	30.72	- .90	2.60	- .46	107203	-22221
4	3.29	- .21	30.29	- 1.93	2.66	- 1.08	105948	-51098
6	3.37	- .34	29.39	- 2.97	2.76	- 1.51	103464	-70970
8	3.46	- .47	28.38	- 3.86	2.90	- 1.90	1012100	-87886
10	3.59	- .61	27.07	- 4.60	3.08	- 2.21	98834	-104355
12	3.77	- .77	25.47	- 5.17	3.30	- 2.46	96300	-107622
14	3.96	- .92	23.96	- 5.57	3.50	- 2.66	93218	-112333
16	4.15	-1.09	22.54	- 5.92	3.75	- 2.88	91098	-117612
18	4.36	-1.28	21.10	- 6.19	4.06	- 3.08	89910	-121662
20	4.59	-1.49	19.74	- 6.40	4.34	- 3.26	87494	-124376
50			10.40	- 5.44	6.72	- 5.39	54770	-125037
100			4.40	- 3.49	8.19	- 8.08	10584	- 86576
150			2.64	- 2.15	8.71	-10.45	702	- 62519
200			1.81	- 1.42	8.81	-12.51	- 2444	- 47453
250			1.41	- .99	8.79	-14.40	- 2511	- 39150
300			1.12	- .69	8.65	-16.22	- 2025	- 32589
350			.91	- .51	8.47	-18.20	- 2120	- 28188
			mho/cm	mho/cm				
373	.90	- .50	8533	-4733	8.39	-18.26	- 2002.86	- 26395
547	1.74	- .68	4967	-1951	7.55	-25.14	- 1558.7	- 18846
721	2.84	- .80	3264	-913.5	6.08	-31.43	- 1196.5	- 14598
895	4.16	- .80	2321	-444.0	3.89	-38.01	- 1059.2	- 12143
1069	5.78	- .69	1705	-203.6	1.69	-43.70	- 812.03	- 10110
1243	7.57	- .47	1316	- 81.03	- .97	-49.38	- 847.40	- 8761
1417	9.57	.10	1045	- 10.81	-4.37	-54.47	- 696.06	- 7677
1591	11.63	.42	859.0	31.25	-6.93	-59.26	- 553.23	- 6901
1765	13.79	1.00	725.0	52.82	-9.84	-63.75	- 508.68	- 6309
1939	16.05	1.67	616.2	64.27	-13.24	-67.64	- 514.22	- 5740

H	ρ_{11} $\times 10^4$ ohm-cm	ρ_{21} $\times 10^4$ ohm-cm	σ_{11} mho/cm	σ_{12} mho/cm	ϵ'_{11} $\times 10^6$ volt-cm/watt	ϵ'_{21} $\times 10^6$ volt-cm/watt	ϵ''_{11} $\times 10^4$ amp/°K-cm	ϵ''_{12} $\times 10^4$ amp/°K-cm
3030	35.22	10.57	260.47	78.17	- 32.366	- 89.178	-197.01	-3495.91
3367	40.21	13.98	221.88	77.14	- 37.29	- 93.98	-138.24	-3203.46
3704	46.42	17.84	187.70	72.14	- 44.33	- 98.08	-168.09	-2916.92
4040	52.57	21.93	162.03	67.59	- 48.90	-101.82	-140.56	-2673.27
4377		26.14			- 55.58	-104.84		
4714		30.68			- 62.27	-107.51		
5051	71.33	35.23	112.70	55.66	- 67.19	-110.00	-195.70	-2178.60
5387	77.63	40.34	101.43	52.71	- 72.47	-112.14	-194.41	-2051.16
5724		45.46			- 77.04	-113.74		
6061	90.22	50.80	84.16	47.39	- 81.62	-115.17	-190.54	-1830.56
6397	96.19	56.14	77.55	45.26	- 86.19	-116.77	-180.89	-1749.03
6734	102.49	61.93	71.47	43.19	- 89.01	-117.84	-188.76	-1655.94
6902	105.34	64.43	69.09	42.26	- 92.17	-118.73	-182.39	-1633.10
7071	108.32	67.05	66.75	41.32	- 93.93	-119.62	-179.21	-1601.72
7239	111.45	70.34	64.17	40.50	- 96.39	-120.33	-177.16	-1569.35
7407	114.15	73.30	62.03	39.83	- 97.45	-120.68	-167.10	-1534.57
7576	116.95	75.80	60.21	39.03	- 99.559	-120.86	-172.52	-1506.97
7744		79.43			-102.37	-121.40		
7912		81.82			-104.13	-122.11		
8081		84.66			-105.89	-122.82		
8249	129.92	87.96	52.78	35.73	-106.60	-123.18	-165.29	-1391.85
8418	132.07	90.12	51.66	35.24	-106.95	-123.53	-157.98	-1370.53
8586	134.17	92.28	50.60	34.80	-108.35	-123.53	-159.77	-1352.85
8754	136.78	94.66	49.43	34.21	-110.82	-124.07	-166.55	-1339.78
8923	140.28				-113.63	-124.96		
9091	144.24	102.05	46.20	32.69	-115.74	-125.49	-168.14	-1293.48
9259	147.41	105.57	44.84	32.11	-117.15	-125.67	-164.35	-1268.60
9428	150.12	108.87	43.65	31.66	-117.50	-126.56	-151.57	-1248.05
9596	152.31				-117.15	-126.38		
9764	154.41	112.73	42.25	30.84	-117.15	-126.56	-141.18	-1209.56
9933	156.79	114.21	41.67	30.35	-118.21	-126.91	-144.91	-1198.31
10101	159.68	116.03	40.99	29.78	-120.67	-127.27	-155.97	-1189.32

H	ρ_{11} $\times 10^4$ ohm-cm	ρ_{21} $\times 10^4$ ohm-cm	σ_{11} mho/cm	σ_{12} mho/cm	ϵ'_{11} $\times 10^6$ volt-cm/watt	ϵ'_{21} $\times 10^6$ volt-cm/watt	ϵ''_{11} $\times 10^4$ amp/°K-cm	ϵ''_{12} $\times 10^4$ amp/°K-cm
10269		118.75			-123.13	-128.16		
10438	166.40	122.62	38.95	28.70	-125.94	-129.05	-162.19	-1166.52
10606		127.05			-128.06	-129.58		
10779	172.42	131.60	36.65	27.97	-129.46	-129.94	-149.82	-1131.75
10943	174.75	135.57	35.72	27.71	-129.81	-130.12	-139.24	-1113.21
11111	176.38	138.80	35.11	27.53	-129.46	-130.30	-129.37	-1098.74
11250	178.30	140.12	34.67	27.25	-128.41	-130.47	-121.08	-1083.05
11400	180.49	141.37	34.34	26.90	-128.41	-130.65	-120.85	-1071.89
11560	182.91	142.28	34.06	26.50	-128.41	-131.01	-115.16	-1054.53
11700	185.62	143.75	33.68	26.08	-129.46	-131.19	-126.70	-1052.19
11850	188.65	145.46	33.24	25.63	-131.22			
12020	191.92	148.30	32.63	25.21	-134.04	-132.61	-125.42	-1032.72
12160	195.46	152.05	31.87	24.80	-136.85			
12300	198.78	156.03	31.13	24.43	-138.96	-133.14	-144.77	-1017.89
12450	201.90	160.46	30.36	24.13	-141.42			
12600	204.05	165.01	29.63	23.96	-142.48	-133.86	-136.93	- 996.35
12730	205.96	170.01	28.87	23.84	-142.83			
12860	207.59	173.76	28.33	23.71	-143.53	-134.03	-119.84	- 971.99
13000	209.09	177.39	27.81	23.59	-142.83			
13150	210.44	179.66	27.49	23.47	-142.48	-134.75	-101.82	- 951.35
13400	212.91	182.85	27.03	23.22	-141.07	-134.92	- 91.94	- 934.48
13660	215.48	183.41	26.91	22.91	-140.37	-135.64	- 90.52	- 926.83
13880	218.23	182.73	26.94	22.56	-140.02	-136.17	- 94.54	- 921.52
14100	221.26	182.28	26.92	22.18	-140.72	-136.88	-101.60	- 918.88
14300	224.76	183.07	26.75	21.79	-141.78	-137.06	-108.82	- 911.87
14490	229.00	185.80	26.33	21.37	-144.24	-137.59	-115.87	- 905.19
14700	233.76	190.57	25.60	20.95	-148.11	-138.31	-122.65	- 898.74
14870	238.80	197.28	24.89	20.56	-151.98	-139.02	-124.75	- 888.98
15060	242.91	205.12	24.04	20.30	-154.44	-139.02	-120.27	- 874.56
15250	245.89	213.19	23.22	20.13	-157.26	-139.37	-114.14	- 864.18
15420	248.46	221.37	22.44	19.99	-157.96	-139.02	-103.28	- 847.38

H	ρ_{11} $\times 10^4$ ohm-cm	ρ_{21} $\times 10^4$ ohm-cm	σ_{11} mho/cm	σ_{12} mho/cm	ϵ'_{11} $\times 10^6$ volt-cm/watt	ϵ'_{21} $\times 10^6$ volt-cm/watt	ϵ''_{11} $\times 10^4$ amp/°K-cm	ϵ''_{12} $\times 10^4$ amp/°K-cm
15580	250.00	228.19	21.82	19.92	-157.96	-139.02	- 91.53	- 834.23
15740	251.40	235.35	21.20	19.85	-157.96	-139.02	- 79.62	- 821.03
15870	252.56	239.33	20.86	19.77	-157.61	-139.20	- 72.39	- 812.65
16000	253.73	242.96	20.56	19.69	-157.26	-139.55	- 65.58	- 805.29
16120	255.04	245.92	20.32	19.59	-156.90	-139.55	- 61.28	- 797.77
16230	256.48	248.19	20.14	19.48	-156.20	-139.73	- 57.05	- 790.68

Note: The values of the ϵ''_{ij} were computed using $\lambda = 13.5$ watt/°K-cm.

SELECTED BIBLIOGRAPHY

Abeles, B., and Meiboom, S., Phys. Rev. 101, 544 (1956).

Bergeron, C. J., Dissertation, Louisiana State University, 1961.

Blatt, F. J., and Kropshot, R. H., Phys. Rev. 118, 480 (1960).

Brandt, N. B., JETP(USSR) 38, 1355 (1960).

Callen, H. B., Phys. Rev. 85, 16 (1952).

Callen, H. B. Thermodynamics, John Wiley and Sons, Inc., New York, 1960.

Galt, J. K., Yager, W. A., Merritt, F. R., Celtin, B. B., and Brailsford, A. D., Phys. Rev. 114, 1396 (1959).

Heine, V., Proc. Roy. Soc. A69, 513 (1956).

Kahn, A. H. and Frederikse, H. P. R. in Solid State Physics 9, F. Seitz and D. Turnbull, editors, Academic Press, Inc., New York, 1959.

Kalinkina, I. N., and Strekov, P. G., Soviet Physics JETP 34, 426 (1958).

Kittel, C., Solid State Physics, John Wiley and Sons, Inc., New York, 2nd ed., 1956.

Lifshitz, I., Soviet Physics JETP 5, 1227 (1957).

Lifshitz, I., and Kosevich, L. M., Soviet Physics JETP 6, 67 (1958).

Reneker, Darrell H., Phys. Rev. 115, 303 (1959).

Reynolds, J. M., Hemstreet, H. W., Leinhardt, T. E., and Triantos, D. D., Phys. Rev. 96, 1203 (1959).

Schoenberg, D., Phil. Trans. A245, 1 (1952).

Smith, George E., Phys. Rev. 115, 1561 (1959).

Steele, M. C. and Babiskin, J., Phys. Rev. 98, 359 (1955).

White, G. K. and Woods, S. B., Canad. J. Phys. 36, 342 (1958).

Wilson, A. H., The Theory of Metals, Cambridge Univ. Press, 1954.

Zebouni, N. H., Dissertation, Louisiana State University, 1961.

Zil'berman, G. E., Soviet Physics JETP 2, 650 (1956).

VITA

Jimmy R. Sybert was born in Greenville, Texas, on December 25, 1934. In 1952 he entered North Texas State College and was graduated with honors from that institution in 1955 with the degree of Bachelor of Arts. In 1956 he received the degree of Master of Arts in Physics from the same institution. Upon graduation he joined the physics faculty at North Texas State College and remained in that position until he entered the Graduate School of Louisiana State University in September of 1958. In 1959 he received a fellowship from the Southern Fellowships Fund; and the following year was awarded a Faculty Fellowship from the National Science Foundation. He is now a candidate for the degree of Doctor of Philosophy in the Department of Physics and Astronomy of Louisiana State University.

EXAMINATION AND THESIS REPORT

Candidate: Jimmy R. Sybert

Major Field: Physics

Title of Thesis: Transport Phenomena in a Single Crystal of Bismuth at Liquid Helium Temperatures.

Approved:

Major Professor and Chairman

Dean of the Graduate School

EXAMINING COMMITTEE:

Date of Examination:

June 17, 1961